Dissertation zur Erlangung des Doktorgrades
der Fakultät für Chemie und Pharmazie
der Ludwig-Maximilians-Universität München

Revealing the role of TECPR1 in mammalian autophagy

Lisa Dempfle

aus

Radolfzell am Bodensee, Deutschland

2018

Erklärung

Diese Dissertation wurde im Sinne von § 7 der Promotionsordnung vom 28. November 2011 von Herrn Dr. Thomas Wollert betreut.

Eidesstattliche Versicherung

Diese Dissertation wurde eigenständig und ohne unerlaubte Hilfe erarbeitet.

München, 03.05.2018

……………………………………………
Lisa Dempfle

Dissertation eingereicht am 25.01.2018

1. Gutachter: PD Dr. Thomas Wollert

2. Gutachter: Hon.-Prof. Dr. Franz-Ulrich Hartl

Mündliche Prüfung am 13.04.2018

TABLE OF CONTENTS

LIST OF ABBREVIATIONS 1

SUMMARY 3

1 INTRODUCTION 5

1.1 Regulation and initiation of autophagy 6

1.2 The role of ubiquitin-like conjugation systems in autophagy 8

1.3 The role of ATG8 proteins in autophagy 9
Mammalian ATG8 homologs 10
Specific functions of the different mammalian ATG8 homologs 11
ATG8-interacting proteins 12

1.4 The role of the endocytic pathway in autophagy 13
The endocytic pathway 13
Autophagy and the endocytic pathway 14

1.5 The role of TECPR1 in autophagy 15

1.6 Aims of this study 17

2 MATERIALS AND METHODS 19

2.1 Reagents 19

2.2 Cloning 19
pMRFP-C1 21
PtdInsP-sensors 21
hATG8s and other ATG proteins 22
TECPR1 and TECPR1 constructs 24
WDR81 26

2.3 Recombinant expression and purification of proteins 27
TECPR1 and TECPR1 constructs 28
hATG8s and other ATG proteins 28
Protein methods and storage 28

2.4 Preparation of liposomes 29
Lipid mixes 29
Small unilamellar vesicles 29
Large unilamellar vesicles 30
Giant unilamellar vesicles 30

2.5 *In vitro* lipidation reaction 30
GUV experiments 30
Floatation assay 30

2.6 Cell culture 31
Transfection of cells 32
Generation of KO lines using CRISPR/Cas9 gene editing 33
Generation of stable cell lines 35
Immunofluorescence 35
Western blot 37
Co-Immunoprecipitation 37
Formation of aggregates and aggregate clearance assay 38
EGFR degradation assay 38

2.7 Confocal microscopy and image analysis 38
Statistical analysis 39

2.8 Electron microscopy of cells 39
Immunoelectron microscopy 39
Correlative light and electron microscopy 40

3 RESULTS 41

3.1 Conjugation of hATG8 proteins to membranes 41
Conjugation of hATG8 proteins to GUVs by ATG12–ATG5-TECPR1 41
In vivo hATG8 conjugation and puncta formation 42
Turnover of endogenous LC3B in wt and TECPR1$^{-\backslash-}$ cells 44

3.2 Subcellular localization of TECPR1 45

3.3 Interaction of TECPR1 with hATG8 proteins 47
Colocalization of TECPR1 with hATG8 proteins 47
Video microscopy of LC3C- and TECPR1-positive structures 50
Interaction of TECPR1 with LC3C and other hATG8 proteins 52
Tandem RFP-GFP-hATG8 reporter 55

3.4 Lipid-binding specificity of TECPR1 57
Binding of TECPR1 to phosphoinositides *in vitro* 57
Colocalization of TECPR1 with phosphoinositides *in vivo* 58
Mistargeting of TECPR1 to PtdIns(3)P-rich membranes 59

3.5 Recruitment of LC3C to TECPR1$^{\Delta PH\text{-}2xFYVE}$ structures 64

3.6 TECPR1 and hATG8 proteins in selective autophagy 69
Recruitment of TECPR1 and hATG8s to protein aggregates 70
Impact of TECPR1 and hATG8s on the clearance of protein aggregates 73
Interaction of TECPR1 with WDR81 75

4 DISCUSSION 77

4.1 The role of TECPR1 in the hATG8 conjugation system 78
Knockout of TECPR1 leads to an accumulation of LC3C and GABARAPL2 puncta 78
TECPR1 promotes conjugation of LC3C and GABARAP family members to artificial membranes 79
Deletion of the ATG5 interaction site in TECPR1 does not alter its subcellular distribution 79

4.2 Interaction of TECPR1 with hATG8 proteins 80
TECPR1 interacts with lipidated LC3C and dynamically interacts with LC3C-positive compartments 80
TECPR1 possesses a LIR motif 80

4.3 Subcellular localization of TECPR1 and LC3C 81
TECPR1 localizes to (auto-)lysosomes 81
The PH domain binds to PtdIns(4)P and targets TECPR1 to lysosomal membranes 81
Replacing the PH domain of TECPR1 by a tandem FYVE domain mistargets TECPR1 to MVBs 82
LC3C localizes to a large number of electron-dense structures and colocalizes with STX17 and ubiquitin 83

4.4 The role of TECPR1 and LC3C in selective autophagy 84
TECPR1 is involved in the clearance of protein aggregates 84

5 OUTLOOK 86

6 APPENDIX 89

7 REFERENCES 95

8 ACKNOWLEDGEMENTS 103

LIST OF ABBREVIATIONS

ATG	Autophagy-related
ALR	Autophagic lysosome reformation
CLEM	Correlative light and electron microscopy
CMA	Chaperone-mediated autophagy
Co-IP	Co-immunoprecipitation
DR	Disordered region
EE	Early endosome
EGFR	Epidermal growth factor receptor
EM	Electron microscopy
ER	Endoplasmic reticulum
GUV	Giant unilamellar vesicle
IF	Immunofluorescence
IM	Isolation membrane
KO	Knockout
LE	Late endosome
LIR	LC3-interacting region
LUV	Large unilamellar vesicle
MVB	Multivesicular body
ORF	Open reading frame
PCR	Polymerase chain reaction
PE	Phosphatidylethanolamine
PH	Pleckstrin homology
PtdIns(3)P	Phosphatidylinositol 3-phosphate
PtdIns(4)P	Phosphatidylinositol 4-phosphate
RE	Recycling endosome
SEC	Size exclusion chromatography
SIM	Structured illumination microscopy
SUV	Small unilamellar vesicle
TGN	Trans-Golgi network
Ub	Ubiquitin
UBL	Ubiquitin-like
wt	wildtype

SUMMARY

Autophagy is a highly conserved eukaryotic recycling pathway that protects from various diseases, including cancer, infections, and neurodegenerative disorders. It involves the formation of the double-membraned autophagosome, which sequesters cytoplasmic material, such as aggregated proteins, damaged organelles, or pathogens, and delivers it to the lysosome for degradation. During this process, a ubiquitin-like conjugation system plays a crucial role. In humans, six ubiquitin-like hATG8 proteins are conjugated to autophagosomal membranes. The hATG8 family can be divided into the two subfamilies, LC3 and GABARAP, which have been suggested to have non-redundant functions in autophagosome formation. A central component of the ubiquitin-like conjugation system is the E3-like ATG12−ATG5 conjugate, which forms mutually exclusive complexes with either ATG16L1 or TECPR1. While ATG16L1 is known to function during hATG8 conjugation, little is known about the role of TECPR1 in this system. TECPR1 has been implicated in the fusion of autophagosomes with lysosomes as well as in selective types of autophagy. However, the molecular details of these processes remain unknown. Here, it was found that knockout of TECPR1 in HeLa cells leads to a selective accumulation of the two hATG8 proteins, LC3C and GABARAPL2, in puncta-like structures. Moreover, TECPR1 selectively recruits LC3C-positive autophagosomes to lysosomes by interacting with lipidated LC3C through an N-terminal LC3-interacting region. *In vitro*, TECPR1 selectively promotes the conjugation of LC3C to artificial membranes, confirming that TECPR1 selectively recognizes LC3C. Strikingly, TECPR1 and LC3C colocalize at ubiquitinated protein aggregates and depletion of TECPR1 impairs the removal of protein aggregates in presence of the proteasome inhibitor MG132. Furthermore, it was found that TECPR1 possesses a PH domain that specifically binds to PtdIns(4)P and targets TECPR1 to PtdIns(4)P-rich lysosomal membranes. Replacing this PH domain by a PtdIns(3)P-binding domain mistargets TECPR1 to endosomes, which appear as multivesicular bodies in electron micrographs. Importantly, LC3C-positive electron-dense structures that contain ubiquitin and the late autophagosomal marker STX17 are selectively recruited to these endosomal structures. Collectively, the data presented in this thesis suggest that TECPR1 recruits LC3C-positive autophagosomes to lysosomes, thereby facilitating the selective degradation of protein aggregates through autophagy.

1 INTRODUCTION

Cells need to constantly adapt to different environmental conditions and respond to endogenous as well as exogenous stress. Thus, regulated biogenesis and degradation of proteins is essential for the survival and health of cells. In eukaryotic cells, proteins are degraded by the two following major pathways: (1) the ubiquitin-proteasome pathway that involves the selective degradation of ubiquitinated proteins by the proteasome; (2) the lysosomal pathway that does not only lead to degradation of proteins but also of lipids or carbohydrates by lysosomal enzymes. Lysosomes are central recycling compartments that can receive extracellular or intracellular material. While extracellular material is transported to lysosomes through the endocytic pathway, intracellular material is delivered to the lysosomal lumen through autophagy.

Autophagy was first discovered in the 1960s by Christian De Duve who also invented the term autophagy (from ancient Greek, meaning ‘self-eating’; Klionsky, 2008). Afterwards, genetic screens in yeast identified the core autophagy-related (ATG) proteins involved in this pathway (Tsukada and Ohsumi, 1993; Thumm et al., 1994; Harding et al., 1995). Yoshinori Ohsumi’s major contribution to the discovery and understanding of the underlying mechanism was awarded with the Nobel Prize of Physiology or Medicine in 2016. Autophagy is important for cell survival since it regulates cellular homeostasis and promotes clearance of toxic protein aggregates and pathogens. Therefore, dysfunctions in autophagic processes are associated with cancer, neurodegenerative diseases, microbial infection, and ageing (Mizushima et al., 2008). There are three main types of autophagy: macroautophagy, microautophagy, and chaperone-mediated autophagy (CMA).

Macroautophagy is the best characterized form of autophagy and involves the de novo formation of a double-membraned organelle - the autophagosome (**Figure 1**). The biogenesis of the autophagosome starts with an initial cup-shaped membrane, called isolation membrane (IM), which captures cytoplasmic material and expands by fusing with small vesicles (Moreau et al., 2011). The membrane surrounding the cargo matures and closes before the outer membrane finally fuses with the lysosome to form the autolysosome. The sequestration of substrates into the autophagosome can be non-selective or selective. In non-selective macroautophagy, a portion of the cytoplasm is enclosed by the autophagosome and recycled to maintain homeostasis and provide nutrients. This process can be induced by starvation of cells and other cytotoxic stress. In contrast, selective macroautophagy is mediated by autophagy receptors that select cargo and tether it to the inner membrane of the autophagosome (Rogov et al., 2014). Examples for selective cargo are protein aggregates (aggrephagy), mitochondria (mitophagy), peroxisomes (pexophagy), part of the endoplasmic reticulum (ER-phagy), ribosomes (ribophagy), lipid droplets (lipophagy), or intracellular pathogens (xenophagy; Mancias and Kimmelman, 2016).

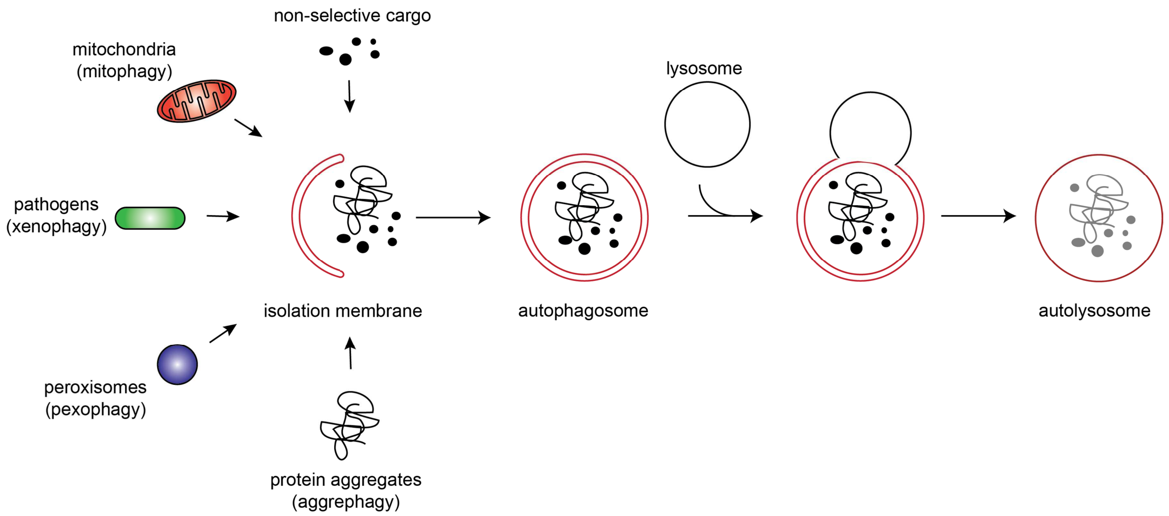

Figure 1: Autophagosome formation in macroautophagy. The double-membraned autophagosome engulfs either non-selective or selective cargo. After maturation, the completed autophagosome fuses with lysosomes resulting in the autolysosome, which degrades the inner autophagosome membrane as well as its content.

The second autophagy pathway is microautophagy, which involves the direct uptake of cytoplasmic material by lysosomes via membrane invagination. Microautophagy does not only include the uptake of non-selective cytosol but also of selective substrates, such as peroxisomes ('micropexophagy'; Farre and Subramani, 2004).

Chaperone-mediated autophagy degrades proteins bearing a KFERQ-like motif, which is recognized by the chaperone Hsc70 (Dice, 1990). The complex of chaperone and substrate binds to the receptor LAMP2A, a channel within lysosomal membranes, resulting in translocation of the cytosolic protein into the lysosomal lumen (Bandyopadhyay et al., 2008). Both microautophagy and CMA are independent of de novo membrane formation and only macroautophagy (in the following referred to as 'autophagy') involves the biogenesis of a new compartment - the autophagosome.

1.1 Regulation and initiation of autophagy

Under normal growth conditions, there is a constant low level of basal autophagy, whereas under stress conditions, like starvation, autophagy is induced to ensure cell survival. Both, the level of basal and starvation-induced autophagy, are highly tissue specific (Mizushima et al., 2004). The induction of non-selective autophagy by stress such as nutrient deprivation is tightly regulated through inhibition of the mammalian target of rapamycin complex 1 (mTORC1) or activation of AMP activated protein kinase (AMPK), which promotes autophagy under glucose starvation (Kim et al., 2011). Under normal growth conditions, mTORC1 is active and inhibits autophagosome formation. Thus, initiation of autophagy can be achieved by inactivation of mTORC1 through various upstream signals, including amino acid levels, growth factors, or the mTOR specific inhibitor rapamycin (Sengupta et al., 2010).

Initiation of autophagy in mammalian cells has been suggested to occur at special subdomains of the endoplasmic reticulum (ER), which are phosphatidylinositol 3-phosphate (PtdIns(3)P)-enriched omega-shaped structures, also known as the omegasome (Itakura and Mizushima, 2010; Nishimura et al., 2017; Axe et al., 2008). Furthermore, the de novo formation and growth of the autophagosome involves the incorporation of membranes originating from various sources, such as the ER, the ER-Golgi intermediate compartment (ERGIC), or the plasma membrane (Juhasz and Neufeld, 2006; Ge et al., 2013; Ravikumar et al., 2010). Moreover, small vesicles containing the transmembrane protein ATG9 were suggested to serve as membrane donors in early steps of autophagosome formation (Yamamoto et al., 2012; Orsi et al., 2012; Young et al., 2006).

More than 40 autophagy-related proteins have been identified in yeast. The 'core' machinery, which is conserved from yeast to humans, comprises about 20 proteins organized in several complexes. These complexes are sequentially recruited to preautophagosomal membranes and cooperate to form mature autophagosomes (**Figure 2**). Autophagosome initiation starts with the formation and activation of the ULK1/2 (Atg1 in yeast) kinase complex consisting of ATG13, ATG101, RB1CC1 (FIP200), and the kinase ULK1 or ULK2. The complex is activated by dephosphorylation of ATG13 and ULK1/2, two substrates of the kinase mTORC1 (Jung et al., 2009; Hosokawa et al., 2009). Subsequently, a class III phosphatidylinositol 3-kinase (PI3K) complex is recruited, which contains Beclin-1 (BECN1), phosphatidylinositol 3-kinase catalytic subunit type 3 (PIK3C3/VPS34), phosphoinositide 3-kinase regulatory subunit 4 (PIK3R4/VPS15), and ATG14 (Kihara et al., 2001; Itakura et al., 2008). Phosphorylation of Beclin-1 by ULK1 activates the PI3K complex (Russell et al., 2013), which generates PtdIns(3)P at the ER. Various PtdIns(3)P-binding proteins are then recruited, including the double FYVE domain-containing protein 1 (DFCP1; Axe et al., 2008) and members of the WD-repeat protein interacting with phosphoinositide (WIPI) family. WIPI1, a mammalian WIPI family member, was proposed to interact with ATG2A at early autophagosomal membranes (Pfisterer et al., 2014). Furthermore, WIPI2b was shown to recruit the ATG12−ATG5-ATG16L1 complex to the IM, a crucial step for autophagosome biogenesis (Dooley et al., 2014).

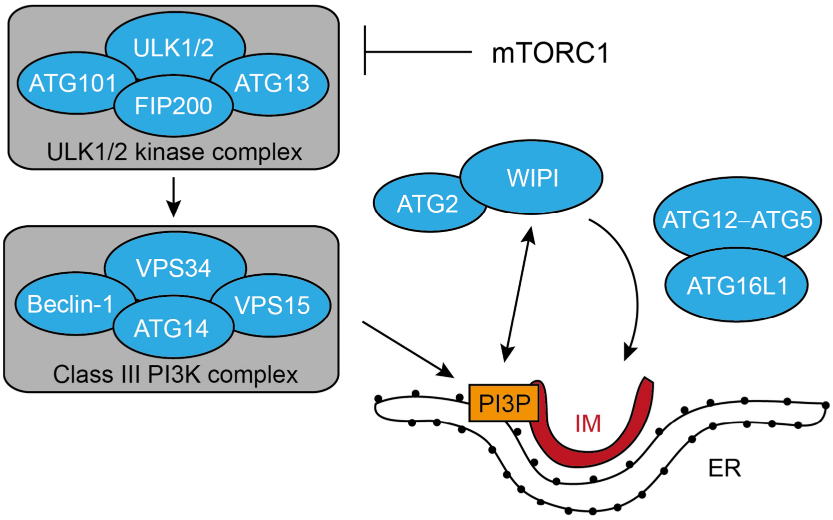

Figure 2: Initiation of autophagy. When mTORC1 is inactive the ULK1/2 kinase complex activates the class III PI3K complex, which produces PtdIns(3)P (PI3P) at the ER. Subsequently, WIPI proteins bind to PtdIns(3)P and recruit the ATG12–ATG5-ATG16L1 complex to the IM.

1.2 The role of ubiquitin-like conjugation systems in autophagy

Autophagosomal membranes need to expand to capture and engulf cytoplasmic material. They seal to generate the autophagosome and finally fuse with lysosomes for their degradation. In this maturation process, two ubiquitin-like (UBL) conjugation systems play an important role (Suzuki et al., 2007). Canonical ubiquitination cascades require three types of enzymes: E1, E2, and E3 enzymes. First, ubiquitin is activated by an E1 enzyme, which catalyzes the adenylation of the C-terminal glycine of ubiquitin and transfers it to an inherent reactive cysteine within its catalytic center. This first step is ATP-dependent and results in a thioester linkage between ubiquitin and E1. Second, ubiquitin is transferred to a cysteine in an E2 enzyme and forms another thioester intermediate with the E2 enzyme. Finally, an E3 enzyme mediates conjugation of the C-terminal glycine of ubiquitin to a lysine in the target protein, generating an isopeptide bond (Pickart, 2001).

The following two UBL conjugation systems are involved in autophagosome biogenesis: (1) the conjugation of ATG12 to ATG5, and (2) the conjugation of ATG8 proteins to the lipid phosphatidylethanolamine (PE) (**Figure 3**). For the conjugation of ATG12 to ATG5, ATG12 is first activated by ATG7 (an E1-like enzyme), next transferred to ATG10 (an E2-like enzyme), and finally covalently linked to ATG5. This UBL conjugation results in the ATG12–ATG5 conjugate, which forms complexes with ATG16L1 and TECPR1 (Mizushima et al., 1998; Kim et al., 2015). Human ATG8 family proteins (hATG8s; Atg8 in yeast) are expressed as pro-proteins with C-terminal amino acid extensions, which mask a glycine residue. As a consequence, they first have to be processed by the cysteine protease ATG4 to expose the C-terminal glycine (Kabeya et al., 2004). Similar to the conjugation of ATG12 to ATG5, hATG8s are activated by ATG7, but subsequently transferred to ATG3. Finally, hATG8s are linked to PE in autophagosomal membranes, resulting in a stable amide bond between hATG8 proteins and PE (Ichimura et al., 2000). Therefore, the conjugation of hATG8s to PE is also referred to as the hATG8 lipidation. This final step is catalyzed by the ATG12−ATG5 conjugate, which serves as an E3-like enzyme and links the two UBL conjugation systems (Hanada et al., 2007). ATG16L1 forms a complex with ATG12−ATG5 by binding to ATG5 and has been reported to specify the hATG8 lipidation site (Fujita et al., 2008; Mizushima et al., 2003).

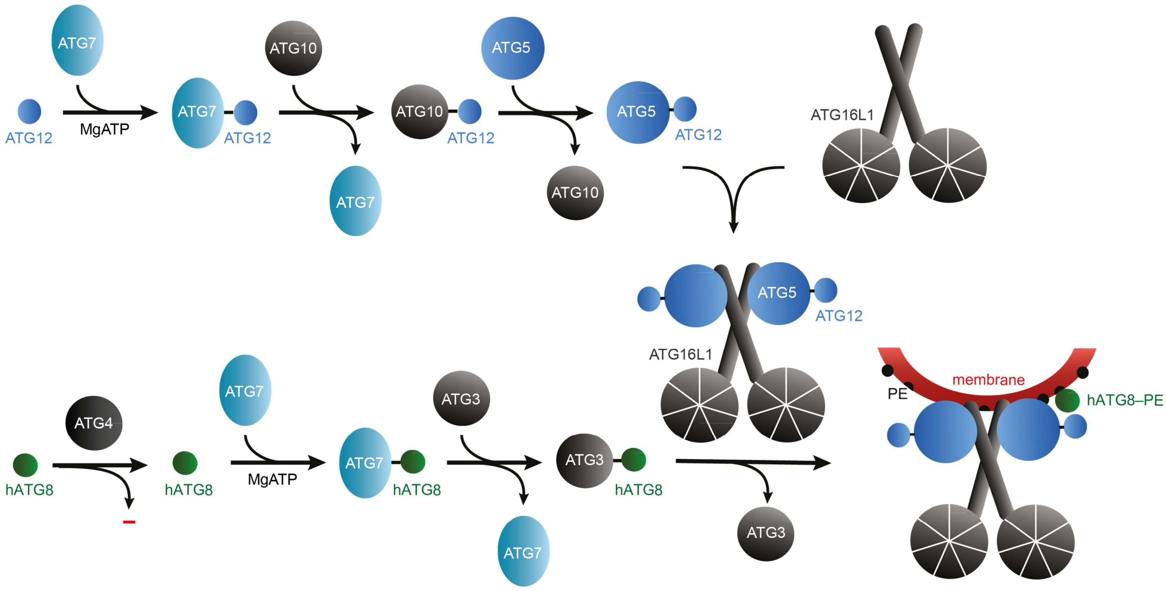

Figure 3: Ubiquitin-like conjugation systems in autophagy. The two UBL systems are interconnected through the ATG12−ATG5 conjugate that forms a complex with ATG16L1 and catalyzes the last step of the hATG8 conjugation to the lipid PE in autophagosomal membranes.

1.3 The role of ATG8 proteins in autophagy

The mammalian ATG8 homologs are conjugated to the inner and outer membrane of autophagosomes (Kabeya et al., 2000; Kabeya et al., 2004). At the inner membrane, they tether selective cargo to the IM by binding autophagy receptors. Their role at the outer autophagosomal membrane, however, is poorly understood. *In vitro* studies have proposed that ATG8 proteins are involved in tethering and fusion of membranes, which suggests a role for ATG8 proteins in closure of the autophagosome or in autophagosome-lysosome fusion (Nakatogawa et al., 2007; Weidberg et al., 2011; Landajuela et al., 2016). Yet, this hypothesis has not been validated *in vivo* and alternative functions of ATG8 proteins on the outer autophagosomal membrane have been proposed. In yeast, it has been shown that Atg8 is able to form a scaffold together with Atg12−Atg5-Atg16 on membranes, which can be disassembled by the protease Atg4 and is critical for autophagosome biogenesis (Kaufmann et al., 2014). Therefore, scaffold formation on the outer autophagosomal membrane has been suggested to regulate the size and shape of autophagosomes.

Similar to yeast, mammalian ATG8 proteins are substrates of the protease family ATG4, which consists of the four homologs ATG4A, ATG4B, ATG4C, and ATG4D. ATG4 family members process PE-conjugated ATG8 proteins with different specificities, while ATG4B seems to be the most active ATG4 homolog in human cells (Li et al., 2011; Kabeya et al., 2004). The activity of ATG4 is tightly regulated by phosphorylation (Sanchez-Wandelmer et al., 2017). ATG4B, for example, can be phosphorylated by ULK1, resulting in inactivation of the protease. On the other hand, ATG4B can be dephosphorylated by the phosphatase PP2A-PP2R3B, which leads to its activation (Pengo et al., 2017). ATG4 is not only priming ATG8 proteins by C-terminal processing of the pro-protein but also recycling ATG8 family members by cleaving them of the membrane (Kabeya et al., 2004; Kirisako et al., 2000). The release of yeast Atg8 from the autophagosomal membrane has been proposed to trigger the fusion of autophagosomes with lysosomes (Nair et al., 2012).

The importance of mammalian ATG8 proteins in autophagosome biogenesis was demonstrated by various studies, which inhibited lipidation of ATG8 proteins by knockout of proteins of the UBL conjugation cascade, like ATG7, ATG3, or ATG5 in mice (Komatsu et al., 2005; Sou et al., 2008; Kuma et al., 2004). These knockout mice were neonatal lethal and showed impaired autophagosome formation, including defective elongation and closure of the isolation membrane. Therefore, ATG8 proteins were suggested to play a role in stabilizing and shaping autophagosomal membranes.

Mammalian ATG8 homologs

Mammalian ATG8 proteins were first described to be involved in other cellular processes than in autophagy. For example, LC3A and LC3B were found to be associated with microtubules (Kuznetsov and Gelfand, 1987; Mann and Hammarback, 1994), where they got their name microtubule-associated proteins 1A/1B light chain 3 (MAP1LC3) from. In contrast, gamma-aminobutyric acid receptor-associated protein (GABARAP) was found to interact with GABA(A) receptors (Wang et al., 1999) and GABARAPL2 has been identified as an essential factor for intra-Golgi protein transport (Legesse-Miller et al., 1998). Besides these functions in various cellular pathways, all ATG8 proteins have been found to play an important role in autophagy.

Mammalian ATG8 proteins can be divided into two subfamilies: the LC3 and the GABARAP subfamily. The presence of the subfamilies and the number of homologs vary in metazoans. Humans have at least seven different genes coding for hATG8 homologs: four members of the LC3 subfamily (MAP1LC3A, MAP1LC3B, MAP1LC3B2, and MAP1LC3C; short names LC3A, LC3B, LC3B2, and LC3C) and three members of the GABARAP subfamily (GABARAP, GABARAPL1/GEC1, and GABARAPL2/GATE-16/GEF2; Shpilka, 2011). A significance of LC3B2 in autophagy or other pathways has not been reported. Although most hATG8s are ubiquitously expressed, some hATG8 homologs exhibit tissue specific expression levels. LC3C, for example, was reported to be predominantly expressed in the lung and only at low levels in other tissues (He et al., 2003). GABARAPL1 was shown to be highly expressed in the central nervous system, whereas GABARAP is more expressed in endocrine glands (Nemos et al., 2003). The variations in expression levels suggest that hATG8 homologs can have distinct functions in different cell types and partially compensate for each other.

To date, many crystal structures of ATG8 family members have been solved and show that all ATG8 proteins share a ubiquitin-like fold with two additional N-terminal α-helices. Those additional α-helices vary among the ATG8 proteins and could explain why some proteins specifically interact with only one or several ATG8 homologs. It was suggested that, depending on the association with membranes, the variable α-helices in ATG8 proteins have two distinct conformations, which might modify the binding capacity of ATG8 interaction partners (Coyle et al., 2002; Ichimura et al., 2004; Nakatogawa et al., 2007). Despite the differences in their amino acid sequence, there is little known about the individual functions of the different mammalian ATG8 homologs in autophagosome biogenesis.

Specific functions of the different mammalian ATG8 homologs

The first report of different functions of hATG8 homologs in autophagy utilized an siRNA-mediated knockdown of either the LC3 or the GABARAP subfamily in HeLa cells. This approach confirmed that both subfamilies are important for autophagosome biogenesis and further indicated that they act at different time points in autophagosome formation (Weidberg et al., 2010). In particular, this study suggested that the LC3 subfamily is involved in elongation of the isolation membrane, whereas the GABARAP subfamily plays a role at a later stage. However, in LNCaP prostate cancer cells, autophagic sequestration of the cytosolic cargo LDH was not impaired when the LC3 subfamily was depleted, but was strongly decreased when expression of the GABARAP subfamily was inhibited (Szalai et al., 2015). Similar results were obtained for CRISPR/Cas9-mediated knockouts of either the three LC3s, the three GABARAPs, or all six hATG8 homologs in HeLa cells (Nguyen et al., 2016). Surprisingly, neither the LC3s nor the GABARAPs were necessary for the formation and sealing of autophagosomes, although the loss of all six hATG8s resulted in a smaller size of autophagosomes. However, the GABARAPs were essential for PINK1/Parkin-mediated mitophagy as well as for autophagosome-lysosome fusion, whereas the LC3 subfamily seems to play a minor role in these processes. These observations were suggested to result from the stronger *in vivo* affinity of the GABARAPs over the LC3s to PLEKHM1, a protein that recruits the HOPS complex and drives the autophagosome-lysosome fusion process (McEwan et al., 2015).

Most studies that investigated the different functions of mammalian ATG8 homologs focused on the differences between the LC3 and the GABARAP subfamily and only few analyzed the role of a specific hATG8 protein. The most widely studied member of the hATG8 family is LC3B, which is commonly used as an autophagic marker, although there is no evidence that it is always associated with autophagosomes (Klionsky et al., 2016). Other hATG8 family members seem to have very specific functions in autophagy, including LC3C and GABARAP. LC3C has been mainly implicated in selective types of autophagy, like xenophagy, mitophagy, and aggrephagy. For example, LC3C has been shown to be essential in the clearance of intracellular *Salmonella*, being selectively recognized by the autophagy receptor NDP52 (von Muhlinen et al., 2012; Verlhac et al., 2015). Furthermore, LC3C has been reported to be involved in HIV-1 release (Madjo et al., 2016), in PINK1/Parkin-independent basal mitophagy (Le Guerroué et al., 2017), and in aggrephagy, being recruited to protein aggregates by WDR81 (Liu et al., 2017). In addition, LC3C is bound by TECPR2, thereby regulating ER exit sites, which contributes to autophagosome formation (Stadel et al., 2015). GABARAP has been demonstrated to be transported from the centrosome to autophagosomes during starvation-induced autophagy and contributes to autophagosome formation by activation of ULK1 (Joachim et al., 2015; Joachim et al., 2017). Moreover, GABARAP has been suggested to be essential for autophagosome-lysosome fusion by recruiting the PtdIns(4)P-generating kinase PI4KIIα to autophagosomes (Wang et al., 2015). Collectively, these recent studies indicate that the mammalian ATG8 homologs have distinct functions in autophagosome biogenesis and can partially compensate for each other.

ATG8-interacting proteins

Many mammalian ATG8-interacting proteins contain a short hydrophobic LC3-interacting region (LIR), which in yeast is referred to as Atg8-interacting motif (AIM; Wild et al., 2014). The LIR motif is a W-X-X-L sequence that is commonly preceded by acidic residues. The tryptophan (W) in the LIR motif can also be replaced by other bulky aromatic residues, including tyrosine (Y) or phenylalanine (F). Moreover, the leucine (L) can be replaced by isoleucine (I) or valine (V). The two hydrophobic residues bind into two corresponding pockets of the LIR docking site in ATG8 proteins (Noda et al., 2008). The interaction via a LIR motif can be regulated by phosphorylation. For example, phosphorylation of the autophagy receptor optineurin (OPTN) at serine 177, which is adjacent to its LIR motif, enhances its interaction with LC3B (Wild et al., 2011). Interactions with ATG8-interacting proteins can also be regulated by phosphorylation of ATG8 proteins. LC3A and LC3B, for example, are phosphorylated by protein kinase A (PKA), which has an inhibitory effect on their activity (Cherra et al., 2010). Moreover, mouse LC3B gets phosphorylated by STK3 and STK4 at threonine 50, resulting in a block of autophagy and clearance of intracellular bacteria (Wilkinson et al., 2015).

The LIR motif was first discovered in the autophagy receptor p62/SQSTM1 (sequestosome-1, hereafter referred to as p62), which was also the first autophagy receptor described (Pankiv et al., 2007; Bjørkøy et al., 2005). Like many autophagy receptors, p62 can bind to ATG8 proteins and to ubiquitin at the same time, thereby mediating the contact between autophagosomal membranes and polyubiquitinated cargo. The cargo of p62 can be ubiquitinated protein aggregates, damaged mitochondria, peroxisomes, or intracellular bacteria. A number of additional autophagy receptors have been identified that recognize different types of polyubiquitin chains, such as NBR1, NDP52, or OPTN, which have all been implicated in aggrephagy, mitophagy, and xenophagy (Rogov et al., 2014).

The binding preferences of ATG8-interacting proteins are very diverse. Some proteins possess a canonical LIR motif that interacts with all ATG8 homologs, others are specific for one subfamily or even for a single ATG8 homolog. A proteomic study revealed that insight of autophagosomal membranes the interactome of LC3 and GABARAP subfamilies only minimally overlaps, which suggests that they mediate capturing of different cargo (Le Guerroué et al., 2017). From comparison of LIR motifs that are specific for one subfamily, a GABARAP interaction motif (GIM; [W/F]-[V/I]-X-V) was defined. This GIM motif is for example present in the adaptor protein PLEKHM1 that preferably binds to GABARAPs over LC3s. On the other hand, there is a number of ATG8-interacting proteins that do not contain a canonical LIR motif (Behrends et al., 2010). The autophagy receptor NDP52, for example, binds exclusively to LC3C via an L-V-V (also referred to as CLIR) motif (von Muhlinen et al., 2012). Furthermore, some ATG8 interaction partners have a preference towards the lipidated form of ATG8 proteins, while other proteins show stronger interaction with the unlipidated form (Behrends et al., 2010). For example, p62 binds to both LC3B and GABARAPL2 in their unlipidated form, but only lipidated LC3B is able to recruit p62 to autophagosomes (Shvets et al., 2011). When the N-terminus of LC3B is removed or mutated it fails to bind p62, indicating that the specific interaction with lipidated LC3B is mediated by its N-terminal domain.

Taken together, ATG8 proteins play a crucial role in autophagosome biogenesis. Many ATG8-interacting proteins have been identified that regulate the activity or selectivity of autophagy. However, the precise function of the mammalian ATG8 homologs and their interaction with specific binding partners remain elusive.

1.4 The role of the endocytic pathway in autophagy

The endocytic pathway

The endocytic pathway consists of several membrane compartments that are specialized for the uptake, sorting, recycling, and degradation of molecules originating from the plasma membrane. The main components of the endocytic pathway are early endosomes (EEs), late endosomes (LEs), and lysosomes. Initially, vesicles that contain extracellular material or proteins of the plasma membrane, like transmembrane receptors, form at the plasma membrane. These vesicles fuse with Rab5- and EEA1-positive early endosomes to deliver their membrane and content. During maturation of early endosomes to late endosomes, specific proteins and lipids are exchanged or converted. For example, the small GTPase Rab5 is replaced by Rab7 and the lipid PtdIns(3)P that is predominantly found on early endosomes is converted into other phosphoinositides, like PtdIns(3,5)P_2 or PtdIns(4)P. The regulation of phosphoinositides is important for the maturation and fusion of various endocytic compartments (Jeschke et al., 2015).

Endocytic cargo is sorted in early endosomes and can be targeted to at least three different destinations: (1) the plasma membrane through Rab11-positive recycling endosomes (REs), (2) the trans-Golgi network (TGN) mediated by retromer, or (3) intraluminal vesicles of multivesicular bodies (MVBs) using the endosomal sorting complexes required for transport (ESCRT) machinery. For degradation of their content, MVBs and LEs fuse with lysosomes, which results in a decrease of the luminal pH (Elkin et al., 2016). The integrity of lysosomes depends on hydrolases that degrade specific substrates as well as on integral membrane proteins, such as the vacuolar H^+-ATPase, LAMP1, and LAMP2. Lysosomal membrane proteins can have diverse functions, including acidification of the lysosomal lumen, protein import from the cytoplasm, and transport of degradation products to the cytoplasm (Saftig and Klumperman, 2009).

Endocytic membrane compartments undergo dynamic fusion and fission events. Generally, the fusion of two membrane compartments requires tethering factors and *s*oluble N-ethylmaleimide-sensitive-factor attachment receptor (SNARE) proteins. In the endocytic pathway, at least two tethering complexes are important: (1) the CORVET complex that functions in endosome-endosome fusion by binding to Rab5, and (2) the HOPS complex that is important for endosome-lysosome fusion and is a Rab7 effector (Balderhaar and Ungermann, 2013). SNARE proteins are located on two opposing membranes and drive membrane fusion by a zipper-like mechanism. This process involves the formation of a four-helix bundle of a Qa-, Qb, Qc, and R-SNARE. After fusion has occurred, the stable SNARE complexes must be disassembled by the ATPase NSF and α-SNAP (Chen and Scheller, 2001).

Autophagy and the endocytic pathway

Autophagy and the endocytic pathway are interconnected at different stages in autophagosome biogenesis. Most important, complete autophagosomes fuse either directly with lysosomes or first with early or late endosomes, such as MVBs. The fusion with endosomes results in amphisomes, which then fuse with lysosomes to form autolysosomes. However, the contribution of the endocytic pathway to autophagosome biogenesis is diverse and still poorly described.

Rab11-positive REs, for example, are involved in starvation-induced autophagy by delivering ULK1 and ATG9 to forming autophagosomes (Longatti et al., 2012). A factor that was suggested to regulate ATG9 trafficking between recycling endosomes and Golgi membranes is the TRAPPIII tethering complex (Lamb et al., 2016). The human TRAPPIII complex was first identified in a proteomic study as part of the autophagy interaction network (Behrends et al., 2010). It consists of the core TRAPP subunits and an autophagy-specific subunit (TRAPPC8 in mammals) and was suggested to positively regulate autophagosome formation.

The formation of the isolation membrane involves ATG16L1-positive autophagosome precursors that form at the plasma membrane and undergo homotypic fusion. This process depends on the SNARE VAMP7 together with its partner SNAREs (Moreau et al., 2011; Ravikumar et al., 2010). Similar to endosome-lysosome fusion, Rab7 is present on mature autophagosomes and required for autophagosome maturation and autophagosome-lysosome fusion (Jager et al., 2004; Ganley et al., 2011). The Rab7 effector and tethering complex HOPS plays an essential role in the fusion of autophagosomes with lysosomes. Knockdown of components of the HOPS complex leads to an accumulation of LC3- and Syntaxin17 (STX17)-positive puncta (Jiang et al., 2014). STX17 is a late autophagosome marker that has been identified as the autophagosomal SNARE, which localizes to the outer membrane of completed autophagosomes (Itakura et al., 2012). The complex of STX17 and its partner SNAREs SNAP-29 and the lysosomal SNARE VAMP8 is stabilized by ATG14 to promote autophagosome-lysosome fusion (Diao et al., 2015). Furthermore, autophagosome-lysosome fusion has been shown to require the lipid kinase PI4KIIα that generates PtdIns(4)P and is recruited by GABARAP (Wang et al., 2015). This suggests an important role of both PtdIns(4)P and the GABARAP protein family in the fusion of autophagosomes with lysosomes.

After fusion with LEs or autophagosomes, lysosomes need to be recycled to maintain their function. In case of autolysosomes this process is called autophagic lysosome reformation (ALR) and is regulated by reactivation of mTORC1, which causes the formation of protolysosomal tubules emerging from the autolysosome (Yu et al., 2010). ALR depends on clathrin and on the conversion of PtdIns(4) to PtdIns(4,5)P_2 by phosphatidylinositol-4-phosphate 5-kinases like PIP5K1B (Rong et al., 2012). Although there is evidence that autophagy and the endocytic pathway closely cooperate, the mechanism of how autophagosomes interact with the endosomal system is still poorly understood.

1.5 The role of TECPR1 in autophagy

The fusion of autophagosomes with endosomes or lysosomes must be tightly regulated to ensure correct degradation of autophagic cargo. One factor that was suggested to promote autophagosome-lysosome fusion is tectonin beta-propeller repeat containing protein 1 (TECPR1). In a proteomic analysis, TECPR1 was identified for the first time and found to be associated with ATG5, ATG12, and ATG3, all components of the hATG8 lipidation machinery (Behrends et al., 2010). Moreover, the same study showed that TECPR1 is associated with the TRAPPIII complex. However, a direct interaction has only been confirmed between TECPR1 and ATG5 and is mediated through an ATG5-interacting region (AIR; Chen et al., 2012; Ogawa et al., 2011; Kim et al., 2015). ATG16L1 also binds to ATG5 via its N-terminal AIR motif. Consequently, complex formation of ATG16L1 or TECPR1 with ATG12−ATG5 is mutually exclusive (Chen et al., 2012; Kim et al., 2015).

TECPR1 is a multidomain protein of 130 kDa, containing two WD-repeat domains composed of four or five β-propeller repeats, two dysferlin motifs, a pleckstrin homology (PH) domain, and a disordered region (DR) adjacent to the PH domain (**Figure 4**). The lipid-binding PH domain has been reported to interact with PtdIns(3)P and this interaction was suggested to depend on the binding of ATG12−ATG5 to TECPR1 (Chen et al., 2012). TECPR1 was further shown to colocalize with the autophagosomal and lysosomal proteins LC3 and LAMP2, respectively, suggesting that it is predominantly present on autolysosomes (Chen et al., 2012). Contradictory data exist about the function of TECPR1 in canonical autophagy. On the one hand, knockdown of TECPR1 in U_2OS cells resulted in an increase of the autophagosome markers LC3-II (lipidated LC3) and p62, suggesting that TECPR1 depletion leads to an accumulation of autophagosomes (Chen et al., 2012). Furthermore, the same study reported that in TECPR1 depleted cells lysosomal degradation of the RFP-GFP-LC3 reporter is reduced, indicating that autophagosome maturation and fusion with lysosomes is affected. On the other hand, knockdown of TECPR1 in HeLa or HEK293T cells resulted in a slight decrease of LC3-II (Ogawa et al., 2011). These data suggest that TECPR1 does not play an essential role in canonical autophagy. Instead, TECPR1 has been implicated in selective types of autophagy, including xenophagy, mitophagy, and aggrephagy. For example, it was demonstrated that TECPR1 localizes together with LC3, ATG5, and WIPI-2 to intracellular *Shigella* and is important for their autophagic clearance (Ogawa et al., 2011).

In conclusion, TECPR1 plays an important role in selective autophagy, likely by acting in a late step in autophagosome maturation. However, how TECPR1 is targeted to autolysosomal membranes and how it coordinates the fusion of selective autophagosomes with lysosomes remains to be elucidated.

1.6 Aims of this study

Autophagy is crucial for many cellular processes by maintaining cellular homeostasis and recycling damaged organelles. As a consequence, perturbation of the pathway has been implemented in the onset of various diseases, like cancer and neurodegeneration. Unraveling the underlying mechanism is thus of eminent importance to identify potential drug targets to treat these diseases. To date, the molecular mechanism of autophagosome formation in yeast is well described; however, the mechanism in higher eukaryotes is not well understood. For example, there are at least six different mammalian ATG8 homologs, while yeast has only one Atg8 gene. In addition, there is no TECPR1 ortholog in yeast despite its important function in animals.

TECPR1 has been shown to play a role in selective types of autophagy as well as in autophagosome-lysosome fusion. Moreover, it interacts with ATG12−ATG5, the E3-like ligase of the UBL conjugation cascade, which is known to also form a complex with ATG16L1. However, the function of TECPR1 in the human UBL conjugation system has not been investigated. Additionally, there is contradictory data about the effect of TECPR1 depletion on autophagy, and therefore the precise function of TECPR1 in autophagosome biogenesis needs to be clarified.

Previously, our lab has successfully reconstituted the human UBL system *in vitro* using recombinant proteins and giant unilamellar vesicles (GUVs) as model membranes (Dempfle, 2014; Kaufmann, 2015). I have further succeeded in expressing and purifying human TECPR1 from insect cells and demonstrated that TECPR1, in addition to ATG16L1, is able to promote hATG8 lipidation (Dempfle, 2014). Based on these data, four specific aims of this study were defined: First, the catalytic activity of TECPR1 with respect to the different hATG8 homologs was to be further characterized, both *in vitro* and *in vivo*. Therefore, CRISPR/Cas9-mediated knockouts of ATG16L1 and TECPR1 were required. Second, the interaction of TECPR1 with components of the UBL conjugation system, such as the different hATG8s, should be analyzed. Third, the cellular localization of TECPR1 and interacting proteins was to be investigated. For this purpose, the proteins should be fluorescently tagged and visualized by immunofluorescence or electron microscopy. In addition, expressing single domains of TECPR1 or deleting them should provide information on their function. Especially the deletion of the lipid-binding PH domain in combination with *in vitro* lipid binding assays should reveal how TECPR1 is targeted to its cellular destinations. Finally, the role of TECPR1 and hATG8 proteins in selective and non-selective autophagy had to be clarified. Therefore, degradation of selective and non-selective autophagic cargo should be analyzed under depletion of the respective proteins.

2 MATERIALS AND METHODS

2.1 Reagents

Used buffers and media are listed in **Table 1**, **Table 8**, and **Table 10**. Antibodies are specified in **Table 15** and **Table 16**.

Table 1: Buffers for agarose gels, SDS-PAGE, and western blotting

Buffer	Components
TAE buffer	40 mM Tris-HCl (Sigma-Aldrich) 20 mM acetic acid (Sigma-Aldrich) 1 mM EDTA, pH 8.0 (Carl Roth)
5x SDS loading buffer	225 mM Tris-HCl, pH 6.8 50% glycerol (Carl Roth) 5% (w/v) SDS (Carl Roth) 0.05% bromphenol blue (Merck) 250 mM DTT (PanReac AppliChem)
SDS running buffer	25 mM Tris-HCl 19.21 mM glycine (Sigma-Aldrich) 0.1% (w/v) SDS
MES SDS running buffer	50 mM MES (PanReac AppliChem) 50 mM Tris-HCl, pH 7.3 0.1% (w/v) SDS 1 mM EDTA
Coomassie staining solution	0.25% (w/v) Coomassie R-250 (PanReac AppliChem) 30% (v/v) ethanol (Sigma-Aldrich) 10% (v/v) acetic acid
Coomassie destaining solution	40% (v/v) ethanol 10% (v/v) acetic acid
Shrinking solution	50% (v/v) methanol (Sigma-Aldrich) 3% (v/v) glycerol
Blotting (transfer) buffer	25 mM Tris 192 mM glycine 0.1% (w/v) SDS 20% (v/v) methanol
Tris-buffered saline with Tween 20 (TBS-T) buffer	25 mM Tris-HCl, pH 7.6 150 mM NaCl 0.05% (v/v) Tween-20 (Fisher Scientific)

2.2 Cloning

In general, cDNA was amplified from an open reading frame (ORF) template (**Table 2**) by polymerase chain reaction (PCR) using gene specific primers and Phusion High-Fidelity DNA Polymerase (NEB) according to the manufacturer’s instructions. The quality of PCR products was controlled by agarose gel electrophoresis using self-casted 1% agarose (Biomol) gels containing one drop of Ethidium Bromide solution 0.07% (PanReac AppliChem) per gel in TAE buffer (**Table 1**). PCR products were either purified using the QIAquick PCR Purification Kit (Qiagen) or isolated from a 1% agarose gel using the QIAquick Gel Extraction Kit (Qiagen). Vectors (**Table 3**) were either linearized by PCR as described above or by restriction enzyme digest. For the latter, 2 µg of vector was mixed with 1 µl of each enzyme (all NEB) in the provided buffer and incubated for at least 1 hour at 37 °C. The digested vector was then extracted from a 1% agarose gel. If the PCR product of the insert contained the corresponding restriction sites (which were added to the 5'-end of the primers) the PCR product was also digested with the same restriction enzymes as the vector. 100 ng of digested vector was mixed with the digested insert in a ratio of 1:2 to 1:7 and incubated with T4 DNA ligase (NEB) in the provided 1X T4 DNA Ligase Reaction Buffer for 1 hour at room temperature or 16 °C overnight. If the PCR product of the insert contained extensions at the 5'-end that were complementary to the ends of the linearized vector, insert and vector were combined via homologous recombination. For linearized pCoofy vectors the recombinase RecAf (NEB) was used according to Scholz et al., 2013. For the recombination of other linearized vectors with inserts the In-Fusion HD Cloning Kit (Clontech Laboratories) was used according to the manufacturer's instructions. 1-5 µl of ligated or recombined plasmids were then transformed into 50 µl XL1 Blue or omniMAX competent cells by heat shock at 42 °C for 45 sec. Transformed cells were plated on LB-Agar plates containing the appropriate antibiotics and incubated at 37 °C overnight. Single colonies were picked, grown in 5 ml LB with the respective antibiotics, and plasmid DNA was isolated using the QIAprep Spin Miniprep Kit (Qiagen). The correct insertion of cDNAs into the vectors was validated by sanger sequencing (Eurofins Genomics).

Table 2: Used open reading frames (ORFs) for cloning

ORF	gene name	accession number	origin	cDNA clone name/ID
TECPR1	TECPR1	NM_015395.2	ImaGenes cDNA library	IRATp970H0679D
LC3A	MAP1LC3A	NM_032514.3	ImaGenes cDNA library	IRATp970E0811D
LC3B	MAP1LC3B	NM_022818.4	ImaGenes cDNA library	IRAUp969H0456D
LC3C	MAP1LC3C	NM_001004343.2	LC3C in pmCherry-C1, provided by Prof. Ivan Dikic	
GABARAP	GABARAP	NM_007278.1	ImaGenes cDNA library	IRCMp5012H094D
GABARAPL1	GABARAPL1	NM_031412.2	GABARAPL1 in pmCherry-C1, provided by Prof. Ivan Dikic	
GABARAPL2	GABARAPL2	NM_007285.6	ImaGenes cDNA library	IRAUp969E1044D
WDR81	WDR81	NM_001163809.1	HeLa mRNA extract + ImaGenes cDNA library	BC114568
HGS	HGS	NM_004712.4	ImaGenes cDNA library	BC003565

Table 3: Used vectors

Vector name	Tag/insert	origin
pEGFP-C1	eGFP (N-terminal)	Dr. Zuzana Storchova
pMRFP-C1	mRFP (N-terminal)	cloned from pEGFP-C1 and ptfLC3
pLPCX	-	Dr. Julia von Blume
pSpCas9(BB)-2A-Puro (PX459)	hSpCas9-2A-Puro	Feng Zhang (Addgene plasmid # 48139)
ptfLC3	mRFP-eGFP-LC3b (rat)	Tamotsu Yoshimori (Addgene plasmid # 21074)
pCoofy1	His6 (N-terminal)	MPIB core facility
pCoofy4	His6-MBP (N-terminal)	MPIB core facility
pCoofy29	His6-MBP (N-terminal)	MPIB core facility
mCherry-P4M-SidM	mCherry-P4M-SidM(546-647)	Tamas Balla (Addgene plasmid # 51471)
pYM-N8	3xHA	Prof. Roland Wedlich-Söldner

pMRFP-C1

The vector pMRFP-C1 was cloned by replacing the ORF of eGFP by mRFP in the vector pEGFP-C1. Therefore, the vector pEGFP-C1 was digested with NheI and BspEI and the vector pTfLC3 was digested with NheI and AgeI. pEGFP-C1 backbone and pTfLC3 insert (mRFP) were extracted from an agarose gel and ligated with T4 DNA ligase.

PtdInsP-sensors

The PtdIns(4)P-sensor mCherry-P4M-SidM (**Table 3**; Hammond et al., 2014) and the PtdIns(3)P-sensor RFP-2xFYVE were used. For cloning of RFP-2xFYVE, two repeats of the FYVE domain of HGS (AA 147-222; **Table 2**) were amplified using the primers listed in **Table 4** and recombined with a BamHI and XhoI digested pMRFP-C1 vector in one step using the In-Fusion HD Cloning Kit. This resulted in a vector with N-terminal mRFP-tag and the two FYVE domains separated by the linker QGQGS.

Table 4: Primers used for cloning of RFP-2xFYVE. Gene specific sequences are black, homolog sequences to either the linearized vector or the preceding ORF sequence are marked in green, and additionally added base pairs are marked in red.

DNA Construct	Name of Primer	Sequence (5'→3')
RFP-2xFYVE	FYVE-F1-FW	ggactcagatctcgaggagagcgatgccatgtttg
	FYVE-F1-REV	ggatccttgtccttgtttcctgttcagctgctcg
	FYVE-F2-FW	caaggacaaggatccgagagcgatgccatgtttg
	FYVE-F2-REV	tagatccggtggatcctatttcctgttcagctgctcg

hATG8s and other ATG proteins

Cloning of LC3A, LC3B, GABARAP, GABARAPL2, ATG3, ATG7, ATG16L1, and TECPR1 in pCoofy vectors was performed by Anna Kaufmann as described in her doctoral thesis (Kaufmann, 2015). LC3C and GABARAPL1 were cloned into pCoofy1 and pEGFP-C1 by Sumit Kumar.

Primers used for cloning of hATG8s are listed in **Table 5**. hATG8s were inserted into pEGFP-C1 and pTfLC3 between BglII and KpnI restriction sites, resulting in GFP-hATG8s and RFP-GFP-hATG8s, respectively. Therefore, hATG8 cDNAs were amplified and vectors and inserts digested with BglII and KpnI, followed by ligation with T4 DNA ligase. LC3C was cloned into pTfLC3 by linearizing the vector using PCR, amplifying the cDNA, and recombining linearized vector and cDNA with RecAf.

For cloning of hATG8s with N-terminal HA-tag, LC3A, LC3B, GABARAP, and GABARAPL2 were first amplified with primers containing the HA-sequence and ligated with HindIII and NotI digested pLPCX vector. LC3C and GABARAPL1 were first cloned into pLPCX without HA-tag using PCR linearized vector and insert, followed by recombination with the In-Fusion HD Cloning Kit. Since the antibody signal for 1xHA-tagged proteins was not strong enough, three repeats of HA instead of one were added to the N-terminus of hATG8s in pLPCX. Therefore, the 3xHA tag was amplified from pYM-N8 (**Table 3**), pLPCX vectors containing hATG8 inserts were linearized, and both were recombined using the In-Fusion HD Cloning Kit. In the following, 3xHA-tagged hATG8 proteins are referred to as HA-hATG8s.

Table 5: Primers used for cloning of hATG8s. Gene specific sequences are black, restriction sites are marked in blue, homolog sequences to the linearized vector are marked in green, and additionally added base pairs are indicated in red.

DNA Construct	**Name of Primer**	**Sequence (5'→3')**
GFP-LC3A	LC3a_BglII_fw	tatagatctatgccctcagaccggcct
	LC3a_KpnI_rev_2	taaggtacctcagaagccgaaggtttcc
GFP-LC3B	LC3b_BglII_fw	tatagatctatgccgtcggagaagacc
	LC3b_KpnI_rev	ggcggtaccttacactgacaatttcatcccg
GFP-GABARAP	GABARAP_BglII_fw	ggcagatctatgaagttcgtgtacaaagaagagc
	GABARAP_KpnI_rev_2	gacggtacctcacagaccgtagacactttcg
GFP-GABARAPL2	GATE-16_BglII_fw	ggcagatctatgaagtggatgttcaaggagg
	GATE-16_KpnI_rev_2	gacggtacctcagaagccaaaagtgttctca
RFP-GFP-LC3C	pTf_lin_fw	cagacatacagccacttccaactaa
	pTf_lin_rev	tctagatctgagtccggacttgtac
	LC3C-SLIC-fw	agtccggactcagatctagaatgccgcctccacaga
	LC3C-SLIC-rev	tggaagtggctgtatgtctgctagagaggattgcagggtctg
1xHA-LC3A	LC3a_HindIII_HA_fw	cagaagcttatgtacccatacgacgtcccagactacgctatgccctcagaccggc
	LC3a_NotI_rev	tatgcggccgctcagaagccgaaggtttcc
1xHA-LC3B	LC3b_HindIII_HA_fw	cagaagcttatgtacccatacgacgtcccagactacgctatgccgtcggagaagacc
	LC3b_NotI_rev	caggcggccgcttacactgacaatttcatcccg
1xHA-GABARAP	GABARAP_HindIII_HA_fw	cggaagcttatgtacccatacgacgtcccagactacgctatgaagttcgtgtacaaagaagagc
	GABARAP_NotI_rev	caagcggccgctcacagaccgtagacactttcg
1xHA-GABARAPL2	GATE-16_HindIII_HA_fw	cagaagcttatgtacccatacgacgtcccagactacgctatgaagtggatgttcaaggagg
	GATE-16_NotI_rev	caagcggccgctcagaagccaaaagtgttctctc
pLPCX linearization	LP1_pLPCX_RV	aagcttgagctcgagatctg
	LP2_pLPCX_FW	cgttaggccattaaggcc
LC3C in pLPCX	FW_LC3C_for_pLPCX	ctcgagctcaagcttatgccgcctccacag
	RV_LC3C_for_pLPCX	cttaatggcctaacgctagagaggattgcagggtc
GABARAPL1 in pLPCX	FW_GABL1_for_pLPCX	ctcgagctcaagcttatgaagttccagtacaaggagg
	RV_GABL1_for_pLPCX	cttaatggcctaacgtcatttcccatagacactctcatc
3xHA insert	FW_HA_for_pLPCX	ctcgagctcaagcttccccggaatgggttacc
	RV_HA_link+LC3A	ccggtctgagggcatcgatgaattctctgtcggac
	RV_HA_link+LC3B	gtcttctccgacggcatcgatgaattctctgtcggac
	RV_HA_link+LC3C	ctgtggaggcggcatcgatgaattctctgtcggac
	RV_HA_link+GAB	gtacacgaacttcatcgatgaattctctgtcggac
	RV_HA_link+GABL1	gtactggaacttcatcgatgaattctctgtcggac
	RV_HA_link+GATE16	gaacatccacttcatcgatgaattctctgtcggac
linearization of hATG8s in pLPCX	LP1_pLPCX_RV	aagcttgagctcgagatctg
	LP2_pLPCX_LC3A_FW	atgccctcagaccgg
	LP2_pLPCX_LC3B_FW	atgccgtcggagaagac
	LP2_pLPCX_LC3C_FW	atgccgcctccacag
	LP2_pLPCX_GAB_FW	atgaagttcgtgtacaaagaagag
	LP2_pLPCX_GABL1_FW	atgaagttccagtacaaggagg
	LP2_pLPCX_GATE-16_FW	atgaagtggatgttcaaggag

TECPR1 and TECPR1 constructs

TECPR1 domains and constructs used in this thesis are depicted in **Figure 4**.

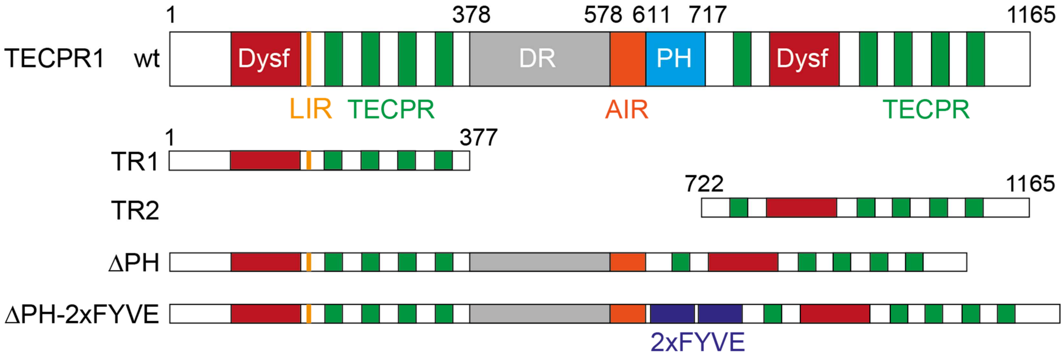

Figure 4: TECPR1 domains. TECPR1 contains a pleckstrin homology (PH, AA 611-717) domain, a disordered region (DR, AA 378-606), an ATG5-interacting region (AIR, AA 578-605), a potential LC3-interacting region (LIR, AA 175-178), nine β-propeller repeats (TECPR, AA 209–240, 254–285, 301–332, 344–376, 729–756, 953–984, 1044–1075, 1087–1127), and two dysferlin domains (Dysf, AA 64-170, 816-922). The TECPR1 constructs TR1 (AA 1-377), TR2 (AA 722-1165), TECPR1$^{\Delta PH}$ (ΔAA 611-717), and TECPR1$^{\Delta PH\text{-}2xFYVE}$ are illustrated beneath.

Cloning of the TECPR1 domains TR1 and TR2 into pCoofy4 is described in my master thesis (Dempfle, 2014). Primers used in this thesis for cloning of TECPR1 and TECPR1 constructs are listed in **Table 6**.

TECPR1 full-length and TECPR1 constructs (TR1, AA 1-377; DR, AA 378-606; TR2, AA 722-1165) were inserted into pEGFP-C1 between XhoI and HindIII or EcoRI restriction sites. TECPR1 cDNA was amplified and both vector and inserts were digested with the respective restriction enzymes before ligation with T4 DNA ligase.

TECPR1 was further cloned into pMRFP-C1 between XhoI and HindIII restriction sites. Therefore, TECPR1 cDNA was amplified and restriction enzyme digest was performed on both insert and vector followed by ligation with T4 DNA ligase.

The deletion of the PH domain (AA 611-717) in TECPR1 was introduced by amplification of GFP-TECPR1 and RFP-TECPR1 using PCR followed by recombination with RecAf. In the following the PH deletion constructs are referred to as GFP-TECPR1$^{\Delta PH}$ and RFP-TECPR1$^{\Delta PH}$.

The TECPR1$^{\Delta PH\text{-}2xFYVE}$ constructs were cloned by linearizing GFP-TECPR1 and RFP-TECPR1 and amplifying the FYVE domain from HGS (AA 147-222), followed by recombination of vector and two repeats of the FYVE domain using the In-Fusion HD Cloning Kit.

The TECPR1 constructs TECPR1^{wt}, TECPR1$^{\Delta PH}$, and TECPR1$^{\Delta PH\text{-}2xFYVE}$ were additionally inserted into pLPCX without tag. Therefore, the pLPCX vector was linearized by PCR and TECPR1 constructs were amplified from GFP-TECPR1, GFP-TECPR1$^{\Delta PH}$, and GFP-TECPR1$^{\Delta PH\text{-}2xFYVE}$, followed by recombination with RecAf.

GFP-TECPR1$^{\Delta AIR}$ (ΔAA 578-605) and GFP-TECPR1$^{\Delta PH\text{-}2xFYVE\text{-}\Delta AIR}$ were cloned using the QuikChange Lightning Site-directed Mutagenesis Kit (Agilent) according to the manufacturer's instructions with GFP-TECPR1 or GFP-TECPR1$^{\Delta PH\text{-}2xFYVE}$ as template.

TECPR1 peptides (TECPR1$^{74\text{-}103}$ and TECPR1$^{158\text{-}187}$) containing potential LIR motifs were cloned into pCoofy4 by homologous recombination as described (Scholz et al., 2013).

TECPR1 LIR mutations W175A/I178A and LLL(87-89)SSS were introduced into GFP-TECPR1, GFP-TR1, GFP-TECPR1$^{\Delta PH\text{-}2xFYVE}$, MBP-TR1 (pCoofy4), TECPR1$^{74\text{-}103}$ (pCoofy4), and TECPR1$^{158\text{-}187}$ (pCoofy4) using the QuikChange Lightning Site-Directed Mutagenesis Kit according to the manufacturer's instructions.

Table 6: Primers used for cloning of TECPR1 and TECPR1 constructs. Gene specific sequences are black, restriction sites are marked in blue, homolog sequences to either the linearized vector or the preceding ORF sequence are marked in green, and additionally added or altered base pairs are marked in red.

DNA Construct	Name of Primer	Sequence (5'→3')
GFP-TECPR1	TECPR_XhoI_fw TECPR_HindIII_rev_2	taactcgaggcatgcccaactcagtgctgtg tataagctttcagcagcagacggggc
GFP-TR1	TR1_XhoI_fw TR1_HindIII_rev	= TECPR_XhoI_fw gacaagctttcacgcgatgatggctttcca
GFP-DR	DR_XhoI_fw DR_HindIII_rev	taactcgagcggcccgagagtgtgaccg tataagctttcactgctccacggcctgct
GFP-TR2	TR2_XhoI_fw_new TR2_EcoRI_rev	tatactcgagaggtgcagggccgcc tatagaattctcagcagcagacggggc
RFP-TECPR1	TECPR-XhoI-fw-2 TECPR_HindIII_rev_2	gtaactcgagatgcccaactcagtgctgtg tataagctttcagcagcagacggggc
GFP-TECPR1$^{\Delta PH}$/ RFP-TECPR1$^{\Delta PH}$	TECPR1dPH-FW TECPR1dPH-REV	ggtgtgggtggagagccggaaggtgcag tccggctctccacccacaccgactgctc
GFP-TECPR1$^{\Delta PH\text{-}2xFYVE}$ and RFP-TECPR1$^{\Delta PH\text{-}2xFYVE}$	TECPR1dPH-FW_b TECPR1dPH-REV_b FYVE-F1-FW_b FYVE-F1-REV FYVE-F2-FW FYVE-F2-REV_b	gagagccggaaggtgcag cacccacaccgactgctc cagtcggtgtgggtggagagcgatgccatgtttg ggatccttgtccttgtttcctgttcagctgctcg caaggacaaggatccgagagcgatgccatgtttg caccttccggctctctttcctgttcagctgctcg
TECPR1, TECPR1$^{\Delta PH}$, and TECPR1$^{\Delta PH\text{-}2xFYVE}$ in pLPCX	pLPCX-lin-fw pLPCX-lin-rev TECPR1-pLPCX-SLIC-fw TEPR1-pLPCX-SLIC-rev	cattaaggcctgtcgacaagcg gaattcgaagcttgagctcgagatc cgagctcaagcttcgaattcatgcccaactcagtgctgtg cttgtcgacaggccttaatgtcagcagcagacgggg
GFP-TECPR1$^{\Delta AIR}$	TECPR1dAIR-fw-QCL TECPR1dAIR-rev-QCL	cccacaccgactgggcagcggtctgg ccagaccgctgcccagtcggtgtggg
TECPR1$^{74\text{-}103}$ and TECPR1$^{158\text{-}187}$ in pCoofy4	TECPR1_74-103_fw TECPR1_74-103_rev TECPR1_158-187_fw TECPR1_158-187_rev	aagttctgttccaggggcccaatcagcgctggaatcccatg ccccagaacatcaggttaatggcgtcagtgctggagcccactcac aagttctgttccaggggcccgtgcggcgccggaag ccccagaacatcaggttaatggcgttacagctccttggggtcatcc
TECPR1 LIR mutants: TECPR1$^{W175A/I178A}$ and TECPR1$^{LLL(87\text{-}89)SSS}$	TECPR1-W175A-I178A-fw TECPR1-W175A-I178A-rev TECPR1-3L(87-89)3S-fw TECPR1-3L(87-89)3S-rev TECPR1-W175A-fw TECPR1-W175A-rev TECPR1-I178A-fw TECPR1-I178A-rev	catccttcgaggggccttggccgcgatgtcccgggact agtcccgggacatcgcggccaaggcccctcgaaggatg ctccacccccagcggtcactcgacgaggacttctcacagaagccgcccat atgggcggcttctgtgagaagtcctcgtcgagtgaccgctgggggtggag ggggatcttggccgcgatgtcccgggac gtcccgggacatcgcggccaagatcccc gtcatccttcgaggggccttggcccagatgtcc ggacatctgggccaaggcccctcgaaggatgac

WDR81

WDR81 was cloned with N-terminal 3xHA-tag into pLPCX and into pEGFP-C1 using the primers listed in **Table 7**. Only cDNA of the C-terminal part of WDR81 was available in the ImaGenes cDNA library provided by the MPIB core facility (clone BC114568, see **Table 2**). Thus, WDR81 cDNA was obtained by reverse transcription of RNA, which was extracted from HeLa cells using TRIzol Reagent (Invitrogen) according to the manufacturer's protocol. Subsequently, the cDNA was synthesized with RevertAid H Minus Reverse Transcriptase (Thermo Scientific) using 1 µg of RNA extract as template and Random Hexamer Primer (Thermo Scientific). Next, WDR81 cDNA was amplified in 3 fragments of which each one was about 2 kb using Phusion High-Fidelity DNA Polymerase. The PCR products of fragment 1 and 2 were used as template for a second PCR with primers containing sequences homolog to either the vector or the preceding WDR81 fragment. Fragment 3 was amplified directly from the ImaGenes cDNA library clone BC114568.

To obtain 3xHA-WDR81 (in the following referred to as HA-WDR81), 3xHA-LC3B in pLPCX was digested with EcoRI and NotI and fused with the three WDR81 fragments containing homolog overlaps using the In-Fusion HD Cloning Kit. The insert of GFP-WDR81 was then amplified from 3xHA-WDR81 and recombined with pEGFP-C1 that was digested with SacI and BamHI before.

Table 7: Primers used for cloning of WDR81. Gene specific sequences are black, homolog sequences to the linearized vector are marked in green, and additionally added base pairs are marked in red.

DNA Construct	Name of Primer	Sequence (5'→3')
WDR81 fragment 1	cDNA_WDR81_1_fw_new	gcggcctggaggagatg
	cDNA_WDR81_1_rev_new	gctgaggccactgagaaaga
WDR81 fragment 2	cDNA_WDR81_2_fw_new	gacgacttggaacaggccac
	cDNA_WDR81_2_rev_new	tgatcttctgagtcagcgtcac
3xHA-WDR81 in pLPCX	3xHA-WDR81_1_fw	gtccgacagagaattcatcgatggcccagggcagc
	WDR81_1_rev	gaggagcccagctggtc
	WDR81_2_fw	gaccagctgggctcctc
	WDR81_2_rev	cctccttacggctgttcagtc
	WDR81_3_fw	gactgaacagccgtaaggagg
	3xHA-WDR81_3_rev	gtttggccgaggcggccctatgccaggaggcggataac
GFP-WDR81	GFP-WDR81_1_fw	cggactcagatctcgagctatggcccagggcagc
	GFP-WDR81_3_rev	ctagatccggtggatcctatgccaggaggcggataac

2.3 Recombinant expression and purification of proteins

Buffers and media used for expression and purification of proteins are listed in **Table 8**. Constructs, strains, and medium used for protein expression are summarized in **Table 9**.

Table 8: Buffers for protein expression, purification, and lipidation assays

Buffer	**Components**
LB (lysogeny broth) medium	0.5% (w/v) yeast extract (Bacto) 1% (w/v) tryptone (Bacto) 7.5% (w/v) NaCl (AnalaR Normapur)
Lysis buffer	100 mM Tris-HCl, pH 8.0 300 mM NaCl 20 mM imidazole, pH 8.0 (Merck) 10% (v/v) glycerol 5 mM β-mercaptoethanol (Merck) 1% (v/v) protease inhibitor cocktail (Sigma)
Washing buffer (Ni-NTA)	50 mM Tris-HCl, pH 8.0 300 mM NaCl 5 mM imidazole, pH 8.0 10% (v/v) glycerol 5 mM β-mercaptoethanol
Elution buffer (Ni-NTA)	50 mM Tris-HCl, pH 7.4 300 mM NaCl (400mM for TECPR1) 500 mM imidazole 10% (v/v) glycerol
SEC running buffer = 2x lipidation buffer (SEC, size exclusion chromatography)	25 mM Tris-HCl, pH 7.4 275 mM NaCl
Lipidation buffer (1x)	12.5 mM Tris-HCl, pH 7.4 137.5 mM NaCl
Floatation buffer	25 mM HEPES (Biomol), pH 7.0 100 mM NaCl

Table 9: Constructs, strains, and medium used for protein expression.

Insert	**Vector**	**Expression strain**	**Medium**
Cys-LC3A	pCoofy1	*E. coli*, Rosetta	LB
Cys-LC3B	pCoofy1	*E. coli*, Rosetta	LB
Cys-LC3C	pCoofy1	*E. coli*, Rosetta	LB
Cys-GABARAP	pCoofy1	*E. coli*, Rosetta	LB
Cys-GABARAPL1	pCoofy1	*E. coli*, Rosetta	LB
Cys-GABARAPL2	pCoofy1	*E. coli*, Rosetta	LB
ATG3	pCoofy1	*E. coli*, Rosetta	LB
ATG7-ATG10-His$_{10}$-Cys-ATG12–ATG5	pST39	*E. coli*, Rosetta	LB
ATG7	pCoofy27	Insect cells SF9	EX-CELL 420 + 5% FCS
ATG16L1	pCoofy29	Insect cells High Five	EX-CELL 420
ATG16NT (11-43)	pCoofy4	*E. coli*, Rosetta	LB
TECPR1	pCoofy29	Insect cells High Five	EX-CELL 420
TECPR1 TR1 (AA 1-384)	pCoofy4	*E. coli*, Rosetta	LB
TECPR1 TR2 (AA 722-1165)	pCoofy4	*E. coli*, Rosetta	LB
TECPR1$^{74\text{-}103}$	pCoofy4	*E. coli*, Rosetta	LB
TECPR1$^{158\text{-}187}$	pCoofy4	*E. coli*, Rosetta	LB

TECPR1 and TECPR1 constructs

The expression and purification of TECPR1 is described in detail in my master thesis (Dempfle, 2014). In brief, TECPR1 was expressed with N-terminal His_6-MBP tag in High Five insect cells from the vector pCoofy29, while shaking the culture for 72 hours at 25 °C in EX-CELL 420 medium (**Table 10**). The cell lysate was incubated with Ni-NTA agarose (Qiagen) for 1 hour at 4 °C and His_6-MBP-TECPR1 was eluted with elution buffer (**Table 8**) containing 400 mM instead of 300 mM NaCl. The His_6-MBP tag was then cleaved using PreScission protease (His-tagged, provided by MPIB core facility) in presence of 10 mM DTT. Finally, the protein was purified by size-exclusion chromatography using a HiLoad 16/60 Superdex 200 column (GE Healthcare).

TECPR1 domains TR1 (AA 1-384) and TR2 (AA 722-1165) as well as the TR1 LIR mutants W175A and LLL(87-89)SSS were expressed in *E. coli* Rosetta cells from the vector pCoofy4 according to the protocol in my master thesis (Dempfle, 2014).

TECPR1 peptides containing a potential LIR motif (TECPR1$^{74\text{-}103}$ and TECPR1$^{158\text{-}187}$) and the corresponding LIR mutants (W175A, I178A, and W175A/I178A) were expressed as N-terminal His_6-MBP fusion constructs from pCoofy4 in *E. coli* Rosetta cells. Cultures were grown in LB-medium containing kanamycin (Sigma-Aldrich, 30 µg/ml) and chloramphenicol (SERVA, 34 µg/ml) at 37 °C and 180 rpm. When OD_{600nm} reached 0.6, cultures were induced with 0.3 mM IPTG (Carl Roth) and grown for 3 hours before cells were harvested by centrifugation at 4500 g for 10 min. Cell pellets were resuspended in lysis buffer supplemented with Sm DNAse (1:1000, provided by MPIB core facility) and lyzed by sonication (2x 5 min). The suspension was centrifuged at 45000 g for 1 hour and the supernatant was incubated with 1 mL Ni-NTA agarose for 1 hour at 4 °C, followed by washing with 500 mL washing buffer and elution with 5 mL elution buffer. Eluted proteins were directly (without cleavage of the His_6-MBP tag) subjected to a HiLoad 16/60 Superdex 200 column and eluted with SEC running buffer.

hATG8s and other ATG proteins

Cys-LC3C and Cys-GABARAPL1 were expressed from pCoofy1 in *E. coli* Rosetta overnight at 18 °C. Purification was performed using buffers without β-mercaptoethanol (**Table 8**) as described in Anna Kaufmann's doctoral thesis for the other hATG8 proteins (Kaufmann, 2015). The expression and purification of all other ATG proteins used in this thesis, including ATG3, ATG7, ATG12–ATG5, ATG16L1, and ATG16NT are also described in the same thesis.

Protein methods and storage

All purified proteins were concentrated using Vivaspin cellulose centrifugation filters (Sartorius) according to the size of the protein. They were subsequently flash frozen in liquid nitrogen and stored at -80 °C. Protein concentrations were determined using the Pierce BCA Protein Assay Kit (Thermo Scientific) according to the manufacturer's instructions. Protein identity and integrity was confirmed by liquid chromatographymass spectrometry (LC-MS), using a Bruker Daltonik ESI-MS microTOF (operated by the MPIB core facility).

Purity and quality of proteins was further monitored by SDS-PAGE using self-casted gels as previously described (Dempfle, 2014; Kaufmann, 2015). 6 M urea SDS-PAGE was performed as described elsewhere (Nakatogawa and Ohsumi, 2012).

Proteins and lipids were labeled with Atto dyes (ATTO-TEC), Alexa dyes (Molecular Probes), or CF405M (Biotium) as previously described (Kaufmann, 2015; Dempfle, 2014).

In vitro pull-down experiments were performed as described in my master thesis (Dempfle, 2014).

2.4 Preparation of liposomes

Lipid mixes

All lipids were purchased from Avanti Polar Lipids. Normal lipid mixtures contained 39.9 mol% 1-palmitoyl-2-oleoyl-*sn*-glycero-3-phosphocholine (POPC), 10 mol% 1-palmitoyl-2-oleoyl-*sn*-glycero-3-phosphoserine (POPS), 30 mol% 1,2-dioleoyl-*sn*-glycero-3-phosphoethanolamine (DOPE), 20 mol% cholesterol, and 0.1 mol% lissamine-rhodamine-PE. The 'Otomo' mix contained 39.9 mol% DOPC, 40 mol% DOPE, 20 mol% liver L-α-phosphatidylinositol (PI), and 0.1 mol% lissamine-rhodamine-PE (Otomo et al., 2013). Lipid mixes for floatation assays with TECPR1 peptides contained 59.9 mol% DOPC, 40 mol% DOPE, and 0.1 mol% lissamine-rhodamine-PE.

Lipid compositions for PtdInsP-binding assays were similar to the normal lipid mixtures, but contained additionally 3 mol% 1,2-dioleoyl-*sn*-glycero-3-phosphoinositol-3'-phosphate (PtdIns(3)P), 1,2-dioleoyl-*sn*-glycero-3-phosphoinositol-3',5'-bisphosphate (PtdIns(3,5)P_2), or 1,2-dioleoyl-*sn*-glycero-3-phosphoinositol-4'-phosphate (PtdIns(4)P) and instead 3 mol% less POPC. Before incorporation into liposomes, PtdInsPs were protonated. Therefore, 100 µg of PtdInsP powder was resuspended in 1 mL chloroform, dried under nitrogen gas stream and dessicated for 1 hour in vacuum. The powder was resuspended in $CHCl_3$:MeOH:1N HCl in a ratio of 2:1:0.01, incubated for 15 min at room temperature, dried under nitrogen gas stream and dessicated for 1 hour in vacuum. PtdInsPs were then washed with $CHCl_3$:MeOH (3:1) and subsequently with $CHCl_3$. Finally, the powder was dissolved in 100 µl chloroform to obtain a concentration of 0.5 mg/ml.

Small unilamellar vesicles

To form small unilamellar vesicles (SUVs), lipids were dried under nitrogen flow in a small glass vial (Duran) and further in vacuum overnight. Dried lipids were resuspended in 1x lipidation buffer (**Table 8**) to a total lipid concentration of 2 mM by vortexing until the mixture was opaque. The solution was subjected to three freeze-thaw cycles, followed by sonication (3x 5 min, 30% power) and centrifugation at full speed for 5 min.

Large unilamellar vesicles

For large unilamellar vesicles (LUVs), 1 mg total lipid was dried under nitrogen flow in a small glass vial (Duran) and further in vacuum overnight. Dried lipids were resuspended in 1 ml 1x lipidation buffer by vortexing. LUVs were then formed by extruding the mixture using a Mini-Extruder (Avanti) and a 100 nm pore size membrane (Whatman # 800309).

Giant unilamellar vesicles

Giant unilamellar vesicles (GUVs) were prepared by electroformation. Therefore, 7 µl of the lipid mixture (1 mg/ml in chloroform) was spread on two platinum wires of a custom-made teflon chamber and dried under vacuum for at least 30 min. The chamber was filled with 600 mM sucrose solution (Sigma-Aldrich) and assembled. Electroformation was performed by applying alternating electric current (2 V, 10 Hz) for 1.5 hours. Subsequently, the frequency was decreased to 2 Hz for 30 min in order to detach the vesicles from the electrodes. The solution was mixed in a 1:1 ratio with 600 mM sucrose solution. 100 µl of the solution was transferred to one well in a 8-well chamber (Lab-Tek). The chamber was previously coated with bovine serum albumin (BSA, AMRESCO) by incubation with 5 mg/ml BSA in 25 mM Tris, pH 7.4 for 10 min at room temperature. For PtdInsP-binding assays, proteins were incubated with GUVs containing 3 mol% PtdInsP for 30 min at 37 °C and subsequently analyzed using confocal microscopy.

2.5 *In vitro* lipidation reaction

If not stated differently, concentrations in the samples were: 0.1 mM DTT, 1 mM ATP/Mg^{2+}, 1 µM ATG7, 1.5 µM ATG3, 6 µM hATG8, 0.5 µM ATG12–ATG5, and 0.5 µM ATG16L1 or TECPR1.

GUV experiments

For GUV experiments ATG7, ATG3, and hATG8s were first incubated with ATP/Mg^{2+} and DTT in 2x lipidation buffer (**Table 8**) for 30 min at 37 °C, followed by the addition of ATG12–ATG5 and ATG16L1 or TECPR1, respectively. hATG8s were used in a 2:1 ratio of unlabeled to labeled protein. The protein mix (V = 100 µl) was added to 100 µl of GUV suspension (see above) in an 8-well imaging chamber and mixed carefully. The reaction was then incubated for 1 hour at 37 °C before imaging. To measure intensities of labeled proteins on GUVs, 2 µl of fluorescent beads with 1% intensity from the InSpeck Green (505/515) Microscope Image Intensity Calibration Kit, 6 µm (Invitrogen) were added to each sample.

Floatation assay

For floatation assays with SUVs or LUVs, reactions were performed as described above in 150 µl 1x lipidation buffer and added to 150 µl liposome suspension, followed by incubation for 1 hour at 37 °C. The protein/liposome mix was then mixed 1:1 with 80% (w/v) Histodenz (Sigma-Aldrich) in floatation buffer (**Table 8**) in a centrifugation tube. The mix was overlaid with 300 µl of 30% Histodenz in floatation buffer and on top with 100 µl of floatation buffer to generate a Histodenz step gradient (40%/30%/0%). Samples were immediately centrifuged at 165000 g for 1 hour using a S55-S Swinging-Bucket Rotor. 80 µl of proteoliposomes was collected from the 0/30% Histodenz interface (sample 'L') and 80 µl from the bottom fraction containing unbound proteins (sample 'P'). Samples were mixed with 20 µl 5x SDS loading buffer (**Table 1**) and 15 µl of each sample was run on a 4-20% Mini-PROTEAN TGX gel (Bio-Rad).

2.6 Cell culture

Reagents and buffers used for cell culture are listed in **Table 10**.

Table 10: Reagents and buffers used for cell culture

Reagent/Buffer	Components
DMEM (Gibco #31966-021)	
FCS (Sigma-Aldrich #F4135)	
Penicillin-Streptomycin (Gibco #15140-122)	
EBSS (Sigma #E2888)	
DPBS (Gibco #14190-094)	
Trypsin-EDTA (Gibco #2530054)	
Opti-MEM I Reduced Serum Medium (Gibco #31985-062)	
EX-CELL 420 Serum-Free Medium for Insect Cells (Sigma #24420C)	
PBS	137 mM NaCl 2.7 mM KCl (Carl Roth) 10 mM Na_2HPO_4 (Merck) 2 mM KH_2PO_4 (Carl Roth)
Permeabilization solution	0.2% (v/v) Triton X-100 (Carl Roth) 0.5% (w/v) SDS 4% (w/v) BSA (Fisher Scientific) in PBS
Mammalian lysis buffer	20 mM Tris, pH 7.5 150 mM NaCl 1 mM EDTA 1 mM EGTA (PanReac AppliChem) 1% (v/v) Triton X-100 1% (v/v) Protease inhibitor (Sigma #P8340)
Co-IP buffer	50 mM Tris, pH 7.5 150 mM NaCl 1 mM EDTA 1 mM EGTA 0.1% (v/v) NP-40 1% (v/v) Protease inhibitor

HeLa and HEK293 cells (both provided by Dr. Julia von Blume) were cultured in DMEM supplemented with 10% FCS and 1% Penicillin-Streptomycin in 75 cm^2 flasks (Corning #353136) at 37°C in a 5% CO_2 incubator. Cells were tested for mycoplasma contamination once a month using the Mycoplasma Detection Kit-QuickTest (Biotool). Cultured cells were discarded in case of a contamination or latest after 30 passages. To starve cells, they were washed 3 times with DPBS and then incubated in Earle's Balanced Salt Solution (EBSS) for 2 hours. In selected experiments, 100 nM Bafilomycin A1 (BafA) was added and cells were incubated for 2 hours. When treating cells with lysotracker, 100 nM LysoTracker Deep Red (Thermo Fisher Scientific) was added 30 min prior to imaging. To induce PINK1/Parkin-mediated autophagy, HEK293 cells were treated with 10 µM CCCP (Sigma # C2759) for 4 hours before cell lysis.

Transfection of cells

To transfect cells, they were seeded in TC-treated 6- or 24-well plates (Corning) or in µ-Slide 8 Well chambers (ibidi #80826) for live cell imaging. Cells were seeded such that the confluency was 60-80% on the day of fixation, lysis, or imaging (dilution usually 1:10). Plasmid transfection in HeLa cells was performed with *Trans*IT-HeLaMONSTER Transfection Kit and HEK293 cells were transfected with *Trans*IT-293 Transfection Reagent (both Mirus) according to the manufacturer’s instructions. Cells were usually analyzed 24 hours after transfection.

Transfection of siRNAs was performed with HighPerfect Transfection Reagent (Qiagen). Therefore, siRNAs were diluted in Opti-Mem medium and mixed with 3 µl or 12 µl of transfection reagent per transfection in a 24- or 6-well plate, respectively. After 5-10 min incubation at room temperature, the mix was added to the cells and incubated for in total 72 hours. Used siRNAs had a final concentration of 10 nM each and are listed in **Table 11**. When cells were transfected with both, siRNAs and plasmids, plasmids were transfected 48 hours after siRNA transfection as described above.

Table 11: Used siRNAs from Invitrogen.

siRNA	order number	sequence (5’-3’)
siControl	Stealth RNAi	CAACUUGAUCCGUCUGACGUGGAAU
siLC3A	s39156	
siLC3B	s37748	
siLC3C	Stealth RNAi	GCUUGGCAAUCAGACAAGAGGAAGU
siGABARAP	s22361	
siGABARAPL1	s24332	
siGABARAPL2	s223228	
siTECPR1	Stealth RNAi	CCAGUUGGAUUGAGAUGGUUGGUGA

Generation of KO lines using CRISPR/Cas9 gene editing

Knockouts (KO) of TECPR1 and ATG16L1 were performed in HeLa cells using the CRISPR/Cas9 system according to Ran et al., 2013. Generation of ATG16L1 KO cells was performed by Sumit Kumar. 3-5 different guide RNAs (sgRNAs) were tested and are listed in **Table 12**. The sgRNAs were inserted into pSpCas9(BB)-2A-Puro (**Table 3**). Cloning was performed as previously described (Ran et al., 2013) with the exception that the ligation was conducted with T4 DNA ligase instead of T7 DNA ligase. In brief, HeLa cells were transfected with sgRNAs cloned into pSpCas9(BB)-2A-Puro in 24-well plates and transfected cells were selected with 2 µg/ml puromycin for 1-2 days. Clonal cell lines were then isolated by diluting them in 96-well plates. The wells containing one single colony after 1 week were expanded and screened for genomic mutations. Therefore, the DNA was extracted using 50 µl QuickExtract solution (Epicentre) per well of a 24-well plate according to the manufacturer's instructions. Using the extracted DNA as template together with gene specific primers, a sequence of 400-600 bp containing the editing site was amplified by PCR with the Q5 High-Fidelity DNA polymerase (NEB) according to the manufacturer's instructions. The primers used for the genomic PCR are listed in **Table 13**. The mutations of the KO cell lines are depicted in **Table 14**. PCR products were purified using the QIAquick PCR Purification Kit (Qiagen) and sequenced with one of the two primers used for amplification. To detect heterogeneous mutations, the PCR product of clone TECPR1 sgRNA4 A3 was additionally cloned into the vector pCoofy1 according to Scholz et al., 2013 using the primers listed in **Table 13**.

Table 12: Guide RNAs used for CRISPR/Cas9-mediated gene knockout of TECPR1 and ATG16L1. Added BbsI restriction sites are indicated in blue and additionally added G-C pairs are indicated in red.

Name	**Guide RNA**	**Target**	**Primers (5'→3')**
TECPR1 sgRNA 1	CTAGACGATTCCAAGAATGC	Exon 9	top: CACCGCATTCTTGGAATCGTCTAG bottom: AAACCTAGACGATTCCAAGAATGC
TECPR1 sgRNA 2	CGGCTGCTTCTTCGGTGATG	Exon 9	top: CACCGCGGCTGCTTCTTCGGTGATG bottom: AAACCATCACCGAAGAAGCAGCCGC
TECPR1 sgRNA 3	ATCCGCCGCCGAGAGGAGGC	Exon 1	top: CACCGCCTCCTCTCGGCGGCGGAT bottom: AAACATCCGCCGCCGAGAGGAGGC
TECPR1 sgRNA 4	CTTCGGGAGAGTGTACACGC	Exon 1	top: CACCGCGTGTACACTCTCCCGAAG bottom: AAACCTTCGGGAGAGTGTACACGC
TECPR1 sgRNA 5	GCTGGAGTTCAAGCGCGTCA	Exon 1	top: CACCGTGACGCGCTTGAACTCCAGC bottom: AAACGCTGGAGTTCAAGCGCGTCAC
ATG16L1 sgRNA 3	GCTGCAGAGACAGGCGTTCG	Exon 1	top: CACCGCTGCAGAGACAGGCGTTCG bottom: AAACCGAACGCCTGTCTCTGCAGC
ATG16L1 sgRNA 4	GCAGCAAGTGACATGTCGTC	Exon 1	top: CACCGCAGCAAGTGACATGTCGTC bottom: AAACGACGACATGTCACTTGCTGC
ATG16L1 sgRNA 5	CCGCTGGAAGCGCCACATCT	Exon 1	top: CACCGAGATGTGGCGCTTCCAGCGG bottom: AAACCCGCTGGAAGCGCCACATCTC

Table 13: Primers used for genomic PCR and cloning of PCR products into pCoofy1. Sequences marked in green are homolog to pCoofy1.

Primer name	**Sequence (5'→3')**	**sgRNA contained in PCR product**
TECPR_KO_fw_new	GTGATGGGTCTGCCCTGATT	TECPR1 sgRNA 1 and 2
TECPR_KO_rev_new	GCAGGCATCTTCCACGGTAT	
S_TECPR1-KO-FW	CTGGGCTGGGAGCCTGAAC	TECPR1 sgRNA 3 - 5
S_TECPR1-KO-REV	CTGGGGCCTCTATTTCCCTTCT	
ATG16-KO-For	CCTCTCGAAAATCATTTCCGG	ATG16L1 sgRNA 3 - 6
ATG16-KO-Rev	CTCCAAAGATAAAACGCAGGTTA	
TEC-KO-fw-pC1	AAGTTCTGTTCCAGGGGCCCCTGGGCTGGGAGCCTGAAC	TECPR1 sgRNA 3 - 5
TEC-KO-rev-pC1	CCCCAGAACATCAGGTTAATGGCGCTGGGGCCTCTATTTCCCTTCT	

Table 14: Mutations in HeLa KO cell lines. Underlined sequences correspond to the guide RNAs, deletions are indicated in red, insertions in blue, and stop codons in bold. The resulting changes in the amino acid sequences are highlighted in red.

Clone Name	**Genomic sequence (5'→3')**	**Amino acid sequence**
TECPR1 KO sgRNA2 A11	…TTCCCCTGCAAGGGAGTGATGGGTCTGCCCTGATTTGTCCCCAGTGCCGGCTGCTTCTTCGGTGATGAGGTGAGGGGTAGTGGCGAGTCTGCCCCCAGCGACACCGATGCCTCCTCGGAAGTCGAGAGACCAGGGCCTGGCCAGATTCTCCCTGCAGAACCTC**TAG**	MPNSVLWAVDLFGRVYTLSTAGQYWEMCKDSQLEFKRVSATTQCCWGIACDNQVYVYVCASDVPIRRREEAYENQRWNPMGGFCEKLLLSDRWGWSDVSGLQHRPLDRVALPSPHWEWESDWYVDENFGGEPTEKGGWTYAIDFPATYTKDKKWNSCVRRRKWIRYRRYKSRDIWAKIPSKDDPKELPDPFNDLSVGGWEITEEPVGRLSVWAVSLQGKVWYREDVSHSNPEGSSWSLLDTPGEVVQISCGPHDLLWATLWEGQALVREGINRSNPKGSSWSIVEPPGSENGVMHISVGVSVVWAVTKDWKVWFRRGVNSHNPCGTSWIEMVGEMTMVNVGMNDQVWGIGCEDRAVYFRQGVTPSELSGKTWKAIIAARECDRSHSGSSSSLSAGCFFGVVASLPPATPMPPRKSRDQGLARFSLQNL-
TECPR1 KO sgRNA4 A3	Allele 1: ATGCCCAACTCAGTGCTGTGGGCGGTGGACCTCTTCGGGAGAGTGTACACGCTGTCCACAGCAGGCCAGTACTGGGAAATGTGCAAGGACTCCCAGCTGGAGTTCAAGCGCGTCAGCGCCACCACGCAGTGCTGCTGGGGCATTGCCTGTGACAACCAGGTCTACGTGTATGTGTGTGCCAGCGATGTCCCCATCCGCCGCCGAGAGGAGGCCTATGAGAATCAG……CGCTGGAATCCCATGGGCGGCTTCTGTGAGAAGCTCCTGC**TGA** Allele 2: ATGCCCAACTCAGTGCTGTGGGCGGTGGACCTCTTCACTAAAAGGGCTGTTCCAGCCGTCCGTGCTGGCGCCTGGGGATCCAGGCCAGTTCCCGGTACCCGCCCATGCCCAGCCCGGCGGCCTAGGGCGTTACCT**TGA**	MPNSVLWAVDLLRCPQQASTGKCARTPSWSSSASAPPRSAAGALPVTTRSTCMCVPAMSPSAAERRPMRISAGIPWAASVRSSC- MPNSVLWAVDLFTKRAVPAVRAGAWGSRPVPGTRPCPARRPRALP-
ATG16L1 KO sgRNA3 B3	ATGTCGTCGGGCCTCCGCGCCGCTGACTTCCCCCGCTGGAAGCGCCACATCTCGGAGCAACTGAGGCGCCGGGACCGGCTGCAGAGACAGGCGTTCGAGGAGATCATCCTGCAGT…A**TAA**	MSSGLRAADFPRWKRHISEQLRRRDRLQRQARGDHPAV-

Generation of stable cell lines

HeLa cells stably expressing GFP-hATG8s were generated by transfection of cells with GFP-hATG8 plasmids. 48-72 hours after transfection, cells were selected with 600 µg/ml G418 until all cells in the non-transfected control were dead. Stable cell lines were expanded and cultured in presence of 300 µg/ml G418 and analyzed by confocal microscopy or western blotting.

Immunofluorescence

To perform immunofluorescence (IF), cells were grown on coverslips in 6-well plates. They were first washed with PBS (**Table 10**) and fixed in 4% formaldehyde (Carl Roth) in PBS for 10 min at room temperature. After washing the cells 3 times with PBS they were permeabilized in permeabilization solution (**Table 10**) for 5 min. Cells were washed again 3 times with PBS before treating them with blocking buffer (4% BSA in PBS) for 1 hour at room temperature. Following blocking, cells were incubated with primary antibodies in 4% BSA in PBS (dilutions see **Table 15**) for 1 hour at room temperature. Cells were washed at least 5 times with PBS before incubation with Alexa Fluor-conjugated secondary antibodies in 4% BSA in PBS (dilution 1:500, **Table 16**) for 1 hour at room temperature. Cells were washed again at least 5 times with PBS and finally mounted on a microscope slide with one droplet of ProLong Gold antifade reagent (Invitrogen).

For the antibodies anti-PtdIns(4)P, anti-LC3 (M152-3), and anti-Rab11 the ‘Golgi staining protocol’ was used according to Hammond et al., 2009. The immunofluorescence staining with anti-PtdIns(3)P was performed according to the protocol provided by the manufacturer (Echelon).

For DAPI staining, fixed cells were permeabilized with 0.2% Triton X-100 in PBS for 5 min followed by washing 3 times with PBS. Cells were then incubated in 2 µg/ml DAPI (PanReac AppliChem) in PBS for 3 min at room temperature, washed 3 times with PBS, and mounted as described above.

Table 15: Used primary antibodies

Antibody name	**Host**	**Supplier**	**Article number**	**Dilution for WB**	**Dilution for IF**
anti-GFP (clones 7.1 and 13.1)	mouse	Roche	11814460001	1:1000 in 3% BSA (TBS-T)	
HA-probe (F-7)	mouse	Santa Cruz	sc-7392	1:200 in 5% milk (TBS-T)	1:100
β-actin antibody (C4)	mouse	Santa Cruz	sc-47778	1:200 in 5% milk (TBS-T)	
beta Actin Monoclonal Antibody (15G5A11/E2)	mouse	Invitrogen	MA1-140	1:10000	
LAMP-2 Antibody (H4B4)	mouse	Santa Cruz	sc-18822		1:100
anti-LAMP1 (H4A3)	mouse	BD Biosciences	555798		1:100
LC3B antibody	rabbit	Novus Biologicals	NB100-2220	1:2000 in 5% milk + 1% BSA (TBS-T)	
LC3A/B (D3U4C)	rabbit	Cell Signaling	12741	1:1000 in 5% milk (TBS-T)	
Anti-LC3 (Human) mAb	mouse	MBL	M152-3		1:100 (Golgi staining protocol)
GABARAP Polyclonal Antibody	rabbit	Invitrogen	OSG00009W	1:1000 in 5% milk (TBS-T)	
GABARAPL2 antibody	rabbit	GeneTex	GTX102006	1:2000 in 1% BSA (TBS-T)	
Anti-p62 lck lig-and Clone 3/P62	mouse	BD Biosciences	610833		1:100
STX17 antibody	rabbit	GeneTex	GTX130212		1:100
Anti-mAtg9	rabbit	S.A. Tooze (Young et al., 2006)	-		1:100
EEA1 (C45B10)	rabbit	Cell Signaling	3288		1:100
Rab5 (C8B1)	rabbit	Cell Signaling	3547		1:100
Rab7 (D95F2)	rabbit	Cell Signaling	9367		1:100
RAB11 Antibody (3H18L5)	rabbit	Invitrogen	700184		1:100 (Golgi staining protocol)
Anti-TGN46 antibody	rabbit	Sigma-Aldrich	T7576		1:100
Anti-Sec31A	mouse	BD Biosciences	612350		1:500
Mono- and polyubiquitinylated conjugates monoclonal antibody (FK2)	mouse	Enzo lifesciences	BML-PW8810		1:100
Anti-Ubiquitin Antibody, Lys48-Specific, clone Apu2	rabbit	Merck	05-1307		1:100
HSP60 (D6F1)	rabbit	Cell Signaling	12165	1:1000 in 5% milk (TBS-T)	1:100
Anti-PMP70 antibody	mouse	Sigma-Aldrich	SAB4200181		1:100
EGFR (1005)-G	goat	Santa Cruz	sc-03-G	1:200 in 5% milk (TBS-T)	
Anti-PtdIns(4)P IgM	mouse	Echelon	Z-P004		1:100 (Golgi staining protocol)
Anti-PtdIns(3)P IgG	mouse	Echelon	Z-P003		1:200

Table 16: Used secondary antibodies

Antibody name	Host	Supplier	Article number	Dilution for WB	Dilution for IF
Goat anti-Mouse IgG Antibody, (H+L) HRP conjugate	goat	Merck	AP308P	1:5000 in TBS-T	
RABBIT IgG (H&L) Secondary Antibody Peroxidase Conjugated	goat	Rockland	611-1302	1:5000 in TBS-T	
donkey anti-goat IgG-HRP	donkey	Santa Cruz	sc-2020	1:5000 in TBS-T	
Alexa Fluor 488/594/647-conjugated secondary antibodies	goat	Molecular Probes			1:500

Western blot

Cells grown in wells were washed 3 times with PBS, followed by incubation with mammalian lysis buffer (**Table 10**; 200 µl or 50 µl per well for 6-well or 24-well plate, respectively) for 20 min on ice. Subsequently, cells were scraped off the well and centrifuged for 15 min at full speed. Samples were normalized using the Pierce BCA Protein assay kit (Thermo Scientific) according to the manufacturer’s instructions. Normalized samples were mixed with 5x SDS loading buffer and heated for 5 min at 95 °C.

For gel electrophoresis, either self-made SDS-PAGE gels, NuPAGE 4-12% Bis-Tris gels (Novex), or 4-20% Mini-PROTEAN TGX Precast Gels (Bio-Rad) were used. For subsequent western blotting, Sharp Pre-Stained Protein Standard was used as protein marker. SDS-PAGE and Mini-PROTEAN TGX Precast Gels were run in SDS running buffer and NuPAGE 4-12% Bis-Tris gels were run in MES SDS running buffer (**Table 1**). Electrophoresis was performed at 40 mA for self-made gels and at 200 V for precast gels.

Gels were equilibrated in blotting buffer (**Table 1**) for 10 min and the PVDF membrane (Bio-Rad) was activated for 1 min in methanol. Blotting was performed in a semi dry blotting chamber at 15 V for 20-60 min, depending on the protein size. The membrane was blocked in blocking buffer (5% milk in TBS-T or 3% milk, 25 mg/mL BSA in TBS-T) for 1 hour at room temperature, followed by incubation with primary antibody (dilutions and buffers see **Table 15**) overnight at 4 °C. The membrane was then washed 3 times with TBS-T (**Table 1**) for 5 min each and incubated with secondary antibody (1:5000 in TBS-T, **Table 16**) for 1 hour at room temperature. The membrane was washed again 3 times with TBS-T for 5 min each and developed using Western BLoT Hyper HRP Substrate (TaKaRa). Chemiluminescence was detected with the luminescent Image Analyzer LAS-3000 (Fuji).

Co-Immunoprecipitation

To perform co-immunoprecipitation (Co-IP), transfected HeLa cells grown in 6-well plates were lyzed with Co-IP buffer (Table 10) for 20 min on ice. Cells were then scraped off the well, centrifuged for 15 min at full speed, and normalized using the Pierce BCA Protein assay kit. For immunoprecipitation of one sample, 20 µl of anti-HA Affinity Matrix (Roche) or 50 µl of GFP-Trap (anti-GFP V_HH coupled to agarose beads, provided by MPIB core facility) was used. The beads were first washed twice with 500 µl Co-IP buffer before cell lysates were added in 1 ml Co-IP buffer and incubated for 2 hours at 4 °C while rotating. Subsequently, beads were pelleted, washed 3 times with 1 ml Co-IP buffer, and bound protein was eluted with 30 µl 2x SDS loading buffer, followed by heating for 5 min at 95 °C. Samples were analyzed on a Western Blot using NuPAGE 4-12% Bis-Tris gels as described above.

Formation of aggregates and aggregate clearance assay

Formation of aggregates was induced by treatment of cells with 5 µg/ml puromycin for 2 hours or with 10 µM (S)-MG132 (Cayman Chemical, in the following referred to MG132) for 8 hours. For the aggregate clearance assay, cells were treated with 5 µg/ml puromycin for 4 hours. Cells were then washed 3 times with DPBS (‘0h’ sample) and incubated for another 4 hours in full medium without puromycin (‘4h’ sample). Subsequently, cells were fixed and stained for ubiquitin (FK2, **Table 15**).

EGFR degradation assay

To perform EGFR degradation assays, cells were treated with 50 ng/ml EGF (Tebu-bio # AF-100-15) for 0, 30, 60, and 120 min. Cells were lyzed with mammalian lysis buffer, normalized using the Pierce BCA Protein assay kit, and subjected to SDS-PAGE using NuPAGE 4-12% Bis-Tris gels. Samples were then immunoblotted using anti-EGFR and anti-β-actin antibodies as described above (**Table 15**).

2.7 Confocal microscopy and image analysis

Microscopy experiments were conducted on a TCS SP8 AOBS Confocal Laser Scanning Microscope (Leica) with a 63x/1.4NA objective for fixed cells and GUVs and a 63x/1.2NA objective for live cell imaging. 405 nm, 488 nm, 514 nm, 561 nm, 594 nm, and 633 nm laser lines were used for excitation of fluorophores. Confocal images were acquired using Leica LAS AF SP8 Software and analyzed using Fiji (Schindelin et al., 2012). Structured Illumination Microscopy (SIM) samples were imaged and processed on a Zeiss Elyra PS.1 microscope (63x/1.4NA objective) using the Zeiss ZEN 2 software with SR-SIM module.

For analysis of GFP-hATG8 puncta per cell and aggregate clearance assays, Z-stacks of images were acquired and merged into a projection with max intensity. GFP-hATG8 puncta per cell were counted using the tool ‘Analyze Particles’ and cells containing large protein aggregates as well as GUVs were counted manually using the ‘Cell Counter’ plugin. Intensities of GUVs were measured by drawing a segmented line on the GUV membrane. The mean intensity of each GUV was then corrected with the background intensity of the sample and normalized to the intensity of InSpeck Fluorescent beads. Colocalization parameters were analyzed using a script provided by Giovanni Cardone from the imaging facility of the MPI of Biochemistry and is based on the Fiji plugin

Coloc2. Images of western blots were quantified using the software Image Studio Lite (LI-COR, Ver. 5.2). Intensities were normalized to the respective β-actin band intensities.

Statistical analysis

Data are expressed as mean ± standard deviation (SD) of at least three independent experiments or 20 cells, unless otherwise stated. Box plots were generated using the OriginPro 9.1G software. Bottom and top of the box represent the first (25%) and third (75%) quartiles, respectively. The band insight the box represents the median, whereas the white circle represents the mean value. Moreover, the whiskers mark the standard deviation (SD). For statistical comparison of two groups of samples, the two-tailed unpaired t-test was used. P-values of <0.05 were considered statistically significant and are indicated as following: *p<0.05; **p<0.01; ***p<0.001.

2.8 Electron microscopy of cells

Cellular electron microscopy experiments were conducted at the European Molecular Biology Laboratory (EMBL) in Heidelberg using equipment and material from the electron microscopy core facility of the EMBL.

Immunoelectron microscopy

Immunoelectron microscopy (immuno-EM) was performed by cryosectioning and immunolabeling using the Tokuyasu method (Tokuyasu, 1973). Therefore, HeLa cells were seeded in a 10 mm petri dish, transfected with GFP-tagged constructs, starved for 2 hours in EBSS, and fixed in two steps. First they were incubated in 8% paraformaldehyde (PFA) and 0.4% glutaraldehyde (GA) in PHEM Buffer (60 mM Pipes, 25 mM Hepes, 2 mM $MgCl_2$, 10 mM EGTA, pH 6.9) for 5 min at room temperature, followed by incubation in 4% PFA/0.2% GA in PHEM Buffer for 30 min at room temperature. The cells were embedded in 12% gelatin and sliced into small pieces. Samples were then infused with 2.3 M sucrose overnight on a rotary stirrer at 4 °C, mounted onto pins, and plunge-frozen in liquid nitrogen. Ultrathin sections (60 nm) were cut with a diamond knife using a Leica EM FC6 cryo-ultramicrotome. Sections were collected on 100 mesh formvar-coated Cu/Pd grids. They were blocked in 0.8-1.5% BSA + 0.1% fish skin gelatin (FSG) in PBS and stained with anti-GFP (1:50, rabbit, Molecular Probes A6455) and protein A conjugated to 10 nm gold in blocking buffer. Samples were contrasted and embedded in methylcellulose and 0.3% uranyl acetate and viewed on a Philips CM120 BioTWIN Electron Microscope.

Correlative light and electron microscopy

Correlative light and electron microscopy (CLEM) was performed according to Kukulski et al., 2012. Cells were grown on carbon-coated sapphire discs in 35 mm petri dishes, transfected, and some samples were starved for 2 hours in EBSS. For high pressure freezing with a HPM-010 High Pressure Freezing Machine (ABRA Fluid), sapphire discs were clamped between two carriers and a gold spacer. After disassembling the sandwich under liquid nitrogen, samples were embedded in Lowicryl HM20 by freeze substitution using a Leica EM AFS2. Therefore, the following program was used: Freeze substitution was performed at -90 °C for 9 or 11 hours with 0.1% (w/v) uranyl acetate in glass distilled acetone. The temperature was then raised to -45 °C (5 °C/h) and stayed at -45 °C for 5 hours. Samples were washed 3 times with acetone and infiltrated with increasing concentrations (10%, 25%, 50%, 75%, 2 or 4 hours each) of Lowicryl HM20 in acetone while the temperature was further increased to -25 °C. 100% Lowicryl was exchanged 3 times in 10 hours steps and UV polymerized at -25 °C for 48 hours, after which the temperature was raised to 20 °C (5 °C/h). After polymerization, the samples were stored protected from light.

Sections of 70 nm or 300 nm were cut with a diamond knife on a Leica EM UC7 ultramicrotome and picked up on carbon coated 200 mesh finder copper grids. As fluorescent fiducial markers TetraSpeck Microspheres (100 nm, Invitrogen) were diluted 1:200 in PBS, sonicated, and adhered to the sections. For fluorescent imaging, grids were sandwiched between two coverslips each carrying a drop of water and hold together by a ring holder, followed by imaging with a widefield Olympus IX81 microscope equipped with an Olympus PlanApo 100x/1.40NA oil immersion objective. Images were collected with GFP- and Cy3-specific settings to identify fiducial markers. Grids with 70 nm sections were removed and post-stained with 2% uranyl acetate and lead citrate. They were imaged on a Philips CM120 BioTWIN Electron Microscope. Grids carrying 300 nm sections were incubated with 10 nm protein A-coupled gold beads on both sides of the grid as tomographic fiducial markers, followed by post-staining with 2% uranyl acetate and lead citrate. Tomograms were collected on a TECNAI F30 Transmission Electron Microscope (FEI company) as dual-axis tilt series over a -60° to 60° tilt range with 1° increment and a magnification of 9400x or 15500x. Furthermore, a montage of the whole cell was created with lower magnification in order to correlate the EM image with the fluorescent image using the ec-CLEM plugin of ICY (Paul-Gilloteaux et al., 2017). Montages were aligned and tomograms reconstructed using the IMOD software package (Kremer et al., 1996).

3 RESULTS

3.1 Conjugation of hATG8 proteins to membranes

Conjugation of hATG8 proteins to GUVs by ATG12−ATG5-TECPR1

The ATG12−ATG5 conjugate serves as an E3-like enzyme in the UBL conjugation of hATG8 proteins to the lipid PE. Moreover, ATG16L1 binds with an N-terminal region to ATG5 in the ATG12−ATG5 conjugate, thereby promoting LC3 lipidation (Fujita et al., 2008). For yeast Atg8, it has been shown that Atg12−Atg5 is necessary and at the same time sufficient for an efficient conjugation to PE *in vitro* (Hanada et al., 2007). However, our lab demonstrated that ATG12−ATG5 needs to be activated by ATG16L1 to efficiently catalyze the *in vitro* lipidation of hATG8 homologs (Kaufmann, 2015). Furthermore, TECPR1 forms a complex with ATG12−ATG5 that is mutually exclusive from the ATG12−ATG5-ATG16L1 complex (Chen et al., 2012; Kim et al., 2015). It was previously shown that the ATG12−ATG5-TECPR1 complex is, in addition to ATG12−ATG5-ATG16L1, able to promote lipidation of hATG8 proteins (Dempfle, 2014). Therefore, the aim was to further characterize the catalytic activity of TECPR1 in respect to the different hATG8 homologs.

Our lab was successful in expressing and purifying the full-length proteins of the human UBL conjugation machinery, including ATG7, ATG3, ATG12−ATG5, ATG16L1, TECPR1, and the six hATG8 proteins (**Figure 38 in the appendix**). This was an essential requirement to systematically compare the conjugation of the different hATG8 proteins to giant unilamellar vesicles (GUVs). In absence of ATG16L1 or TECPR1, there was no conjugation of LC3A, LC3B, or GABARAPL2, and only limited conjugation of LC3C, GABARAP, and GABARAPL1. Note that although a substantial percentage of GUVs was positive for Alexa Fluor 488-labeled LC3C and GABARAP (**Figure 5A**), the intensity of labeled LC3C and GABARAP on the membrane was very low (**Figure 5B**). However, in the presence of ATG16L1, the hATG8 lipidation efficiency was strongly increased with best lipidation of the LC3s and GABARAP, followed by GABARAPL1 and GABARAPL2. Remarkably, in absence of ATG16L1 but presence of TECPR1 the lipidation of LC3C and GABARAP and to a smaller extend GABARAPL1 and GABARAPL2 was promoted (**Figure 5C**). Although the lipidation efficiency in presence of TECPR1 was reduced compared to ATG16L1, TECPR1 was highly selective for LC3C and the GABARAP family members.

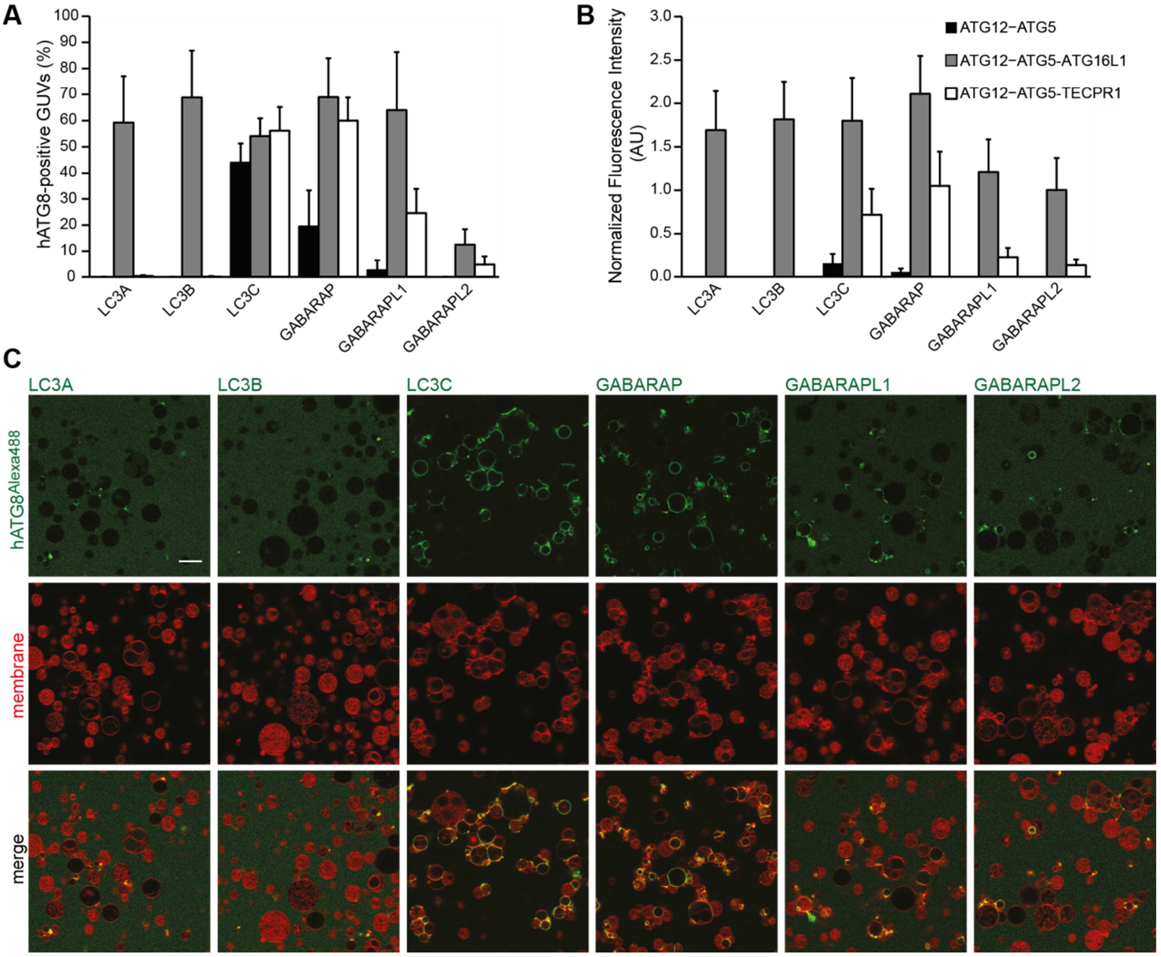

Figure 5: Conjugation of hATG8 homologs to GUVs in absence and presence of ATG16L1 or TECPR1. **(A)** Percent of GUVs that are positive for Alexa Fluor 488-labeled hATG8s (n > 150 GUVs from 3 independent experiments). **(B)** Fluorescence intensity of Alexa Fluor 488-labeled hATG8s on the GUV membrane (n = 30 GUVs from 3 independent experiments). **(C)** Conjugation of Alexa Fluor 488-labeled hATG8 homologs to GUVs in presence of ATG12–ATG5-TECPR1. Scale bar, 10 µm.

In vivo hATG8 conjugation and puncta formation

The ability of both, ATG16L1 and TECPR1, to promote conjugation of hATG8s to PE on GUV membranes gave rise to the question whether both proteins contribute to hATG8 lipidation *in vivo* and whether they can compensate for each other. Therefore, CRISPR/Cas9-mediated HeLa knockout cell lines were generated that are deficient for ATG16L1 (ATG16L1$^{-\backslash-}$) or TECPR1 (TECPR1$^{-\backslash-}$, **Table 14**). To monitor lipidation of the different hATG8 homologs, wildtype (wt) and knockout cells were transfected with HA-tagged hATG8s and analyzed by western blotting. Using SDS-PAGE, the difference in retention time between non-lipidated (form I) and lipidated (form II) members of the LC3 subfamily was clearly visible, whereas only a faint band corresponding to lipidated HA-GABARAPL2 and no band for lipidated GABARAP or GABARAPL1 could be observed (**Figure 6A**). Strikingly, the band corresponding to the lipidated form of hATG8s completely disappeared in ATG16L1$^{-\backslash-}$ cells, while in TECPR1$^{-\backslash-}$ cells the same level of hATG8 lipidation was observed as in wt cells. This observation indicates that ATG16L1 is essential for the lipidation of hATG8 proteins, whereas TECPR1 does not promote hATG8 lipidation *in vivo*.

Consistent with the loss of hATG8 lipidation, almost no GFP-hATG8 puncta were observed in ATG16L1$^{-\backslash-}$ cells with the most drastic effect on LC3 subfamily members (**Figure 6B**). In contrast, knockout of TECPR1 had no effect on the number of GFP-LC3A, GFP-GABARAP, and GFP-GABARAPL1 puncta. However, the number of GFP-LC3B puncta was reduced, while GFP-LC3C and GFP-GABARAPL2 puncta significantly accumulated in TECPR1$^{-\backslash-}$ cells (**Figure 6C**). In accordance, complementing the TECPR1 knockout with transient expression of a wt TECPR1 construct (RFP-TECPR1) reduced the number of GFP-LC3C and GFP-GABARAPL2 puncta to wt levels. In conclusion, the accumulation of LC3C and GABARAPL2 puncta in TECPR1$^{-\backslash-}$ cells suggests that TECPR1 is important for the turnover of LC3C- and GABARAPL2-positive membrane compartments.

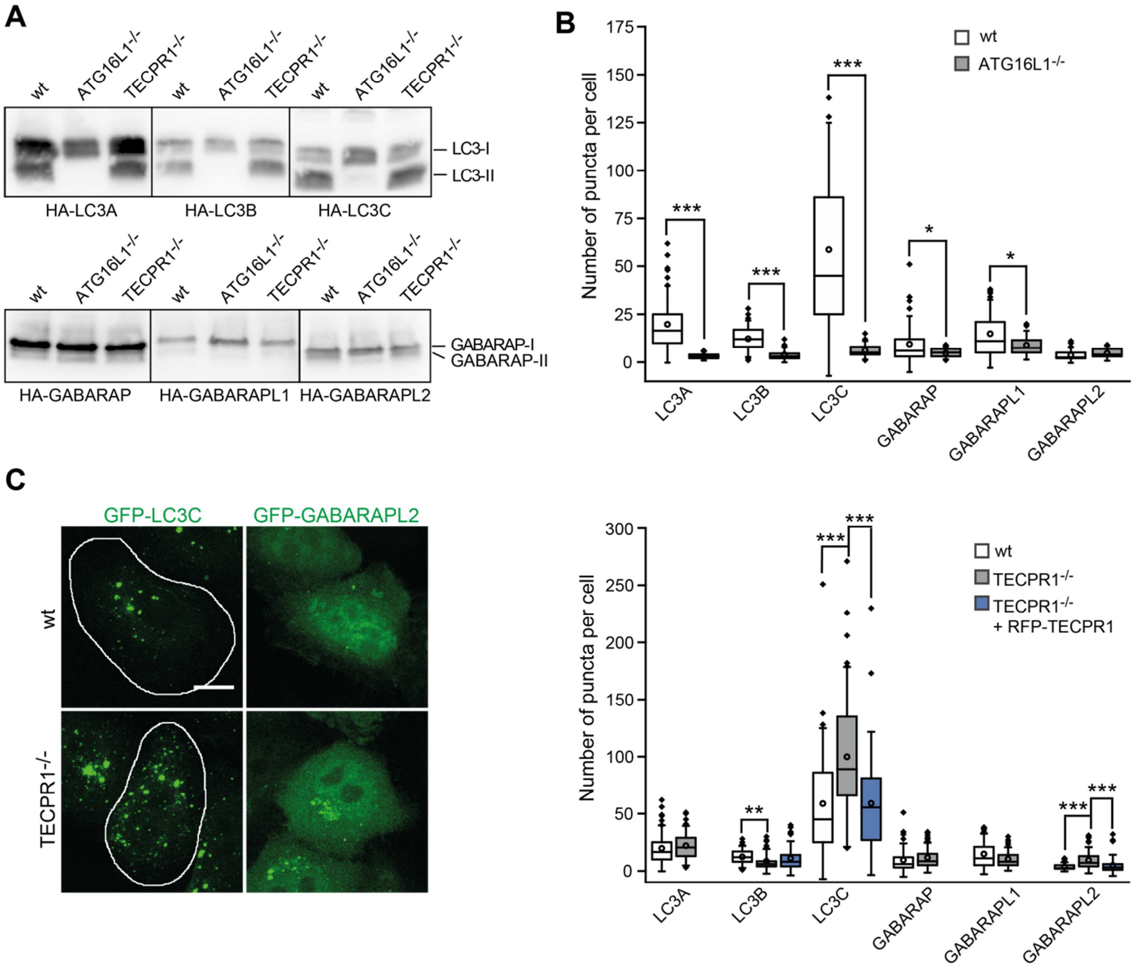

Figure 6: *In vivo* hATG8 conjugation and puncta formation. **(A)** HeLa wt, ATG16L1$^{-\backslash-}$, or TECPR1$^{-\backslash-}$ cells transiently expressing HA-tagged hATG8s were starved for 2 hours. Cell lysates were run on a 6 M urea SDS-PAGE gel (LC3 subfamily) or on a 4-20% Mini-PROTEAN TGX gel (GABARAP subfamily) and subsequently immunoblotted with anti-HA antibody. **(B)** HeLa wt or ATG16L1$^{-\backslash-}$ cells were transfected with GFP-tagged hATG8s and starved for 2 hours before fixation. The number of GFP-hATG8 puncta was counted in at least 30 cells per sample. **(C)** Confocal images of HeLa wt or TECPR1$^{-\backslash-}$ cells that were transfected with GFP-tagged hATG8s or cotransfected with GFP-hATG8s and RFP-TECPR1 and starved for 2 hours before fixation. The number of GFP-hATG8 puncta was counted in at least 50 cells per sample. Scale bar, 10 µm.

Turnover of endogenous LC3B in wt and TECPR1$^{-\backslash-}$ cells

There is contradictory data on the influence of TECPR1 on canonical autophagy, which involves LC3B conjugation to autophagosomal membranes. It has been reported that levels of lipidated LC3B can be increased or decreased upon TECPR1 depletion, which seems to depend on the cell type (Ogawa et al., 2011; Chen et al., 2012). To clarify the effect of TECPR1 knockout on the flux of endogenous LC3B in the here used HeLa cells, LC3B-II levels were monitored in absence or presence of the lysosome inhibitor Bafilomycin A1 (BafA). Due to reduced lysosomal activity by inhibition of the vacuolar H$^+$-ATPase, BafA causes an accumulation of LC3B-II that has been transported into the lysosomal lumen. Importantly, LC3B-II levels were slightly but not significantly reduced compared to wt cells in both, absence and presence, of BafA (**Figure 7**). This observation is in agreement with the data of Ogawa et al., 2011, suggesting that TECPR1 plays a minor role in canonical autophagy.

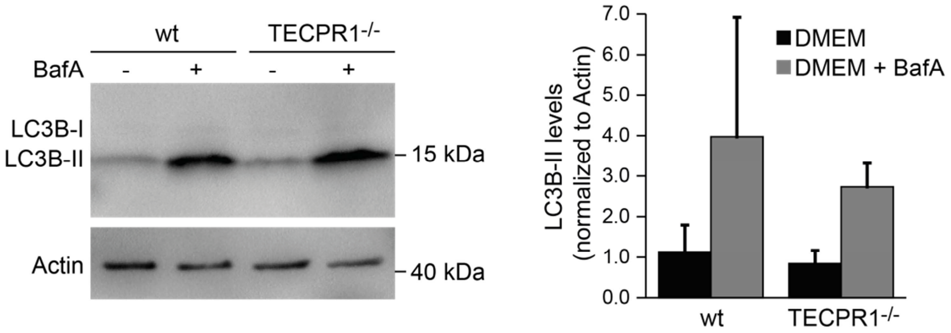

Figure 7: Turnover of endogenous LC3B in wt and TECPR1$^{-\backslash-}$ cells. HeLa wt or TECPR1$^{-\backslash-}$ cells were incubated for 2 hours in either full growth medium (DMEM), or DMEM including BafA. Cell lysates were run on a 4-20% Mini-PROTEAN TGX gel and immunoblotted using antibodies against LC3B and β-actin. LC3B-II levels were normalized to β-actin (n=3 independent experiments).

3.2 Subcellular localization of TECPR1

Previously, it was reported that TECPR1 localizes to early autophagosomal structures to target bacteria to autophagosomal membranes (Ogawa et al., 2011), whereas another study observed that TECPR1 localizes to autolysosomes (Chen et al., 2012). To clarify the subcellular localization of TECPR1, two different electron microscopy (EM) techniques were performed using HeLa cells transiently expressing GFP-tagged TECPR1: correlative light and electron microscopy (CLEM) and immunogold-labeling of ultrathin cryo-sections (immuno-EM). CLEM revealed that bright GFP-TECPR1 structures correspond to electron-dense compartments containing intraluminal membranes (**Figure 8A**). These TECPR1-positive structures likely represent lysosomes or autolysosomes. Immuno-EM, however, showed that a subpopulation of GFP-TECPR1 also localizes to membranes of small vesicles with a size of 100 to 200 nm in diameter that form large clusters (**Figure 8B**). These data indicate that GFP-TECPR1 is recruited to diverse membrane compartments.

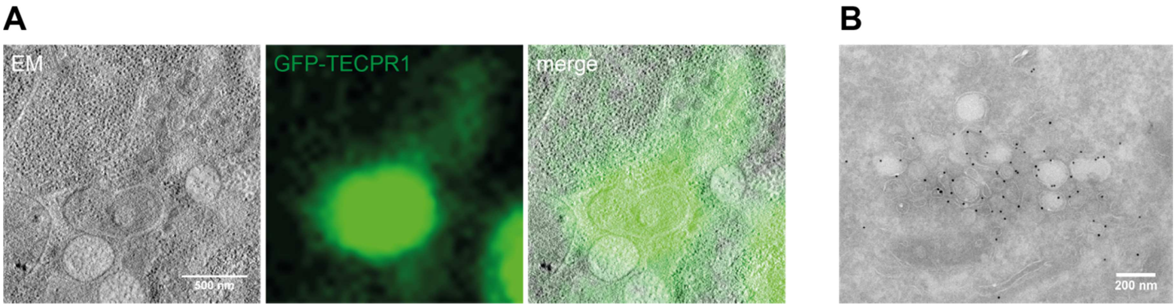

Figure 8: Subcellular localization of GFP-TECPR1 revealed by EM. **(A)** CLEM of HeLa cells transiently expressing GFP-TECPR1 and starved for 2 hours. Tomograms of 300 nm sections were acquired and one representative slice of the tomogram and the correlated fluorescent image are depicted here. **(B)** Immuno-EM of HeLa cells expressing GFP-TECPR1 and starved for 2 hours using anti-GFP antibody (10 nm gold).

To identify the nature of the different membrane compartments to which TECPR1 gets recruited, immunofluorescent staining of HeLa cells expressing GFP-TECPR1 was performed (**Figure 9**). Staining for endosomal markers showed that TECPR1 is not colocalizing with the early endosomal marker EEA1. However, large TECPR1 structures strongly colocalized with the late endosomal marker Rab7 as well as with the lysosomal marker LAMP2. This result is consistent with the CLEM data that showed that TECPR1 localizes to late endosomal or lysosomal compartments. Interestingly, there was partial colocalization of GFP-TECPR1 with the recycling endosomal marker Rab11A. Notably, small GFP-TECPR1 puncta were negative for the tested endosomal markers.

The vesicle clusters observed in immuno-EM resemble ATG9 vesicles or vesicles belonging to the trans-Golgi network. Therefore, antibody staining for appropriate markers was performed and revealed that GFP-TECPR1 significantly colocalizes with ATG9, whereas there was only weak colocalization between GFP-TECPR1 and TGN46.

This suggests that the vesicle clusters observed in immuno-EM correspond to ATG9 vesicles.

Since TECPR1 has been implicated in selective autophagy (Ogawa et al., 2011), colocalization with the autophagy receptor p62 was analyzed. Most GFP-TECPR1 structures were p62-positive, indicating that TECPR1 does indeed play a role in selective autophagy. Furthermore, it has been shown that TECPR2, a homolog of TECPR1, is involved in formation of ER exit sites. To test if TECPR1 could have a similar function, the colocalization of TECPR1 with the COPII-coat protein SEC31A was analyzed. However, TECPR1 did not colocalize with SEC31A, suggesting that it does not play a role in ER exit site formation. Taken together, TECPR1 localizes to late endosomes and (auto-)lysosomes as well as to small vesicle clusters that might correspond to ATG9 vesicles.

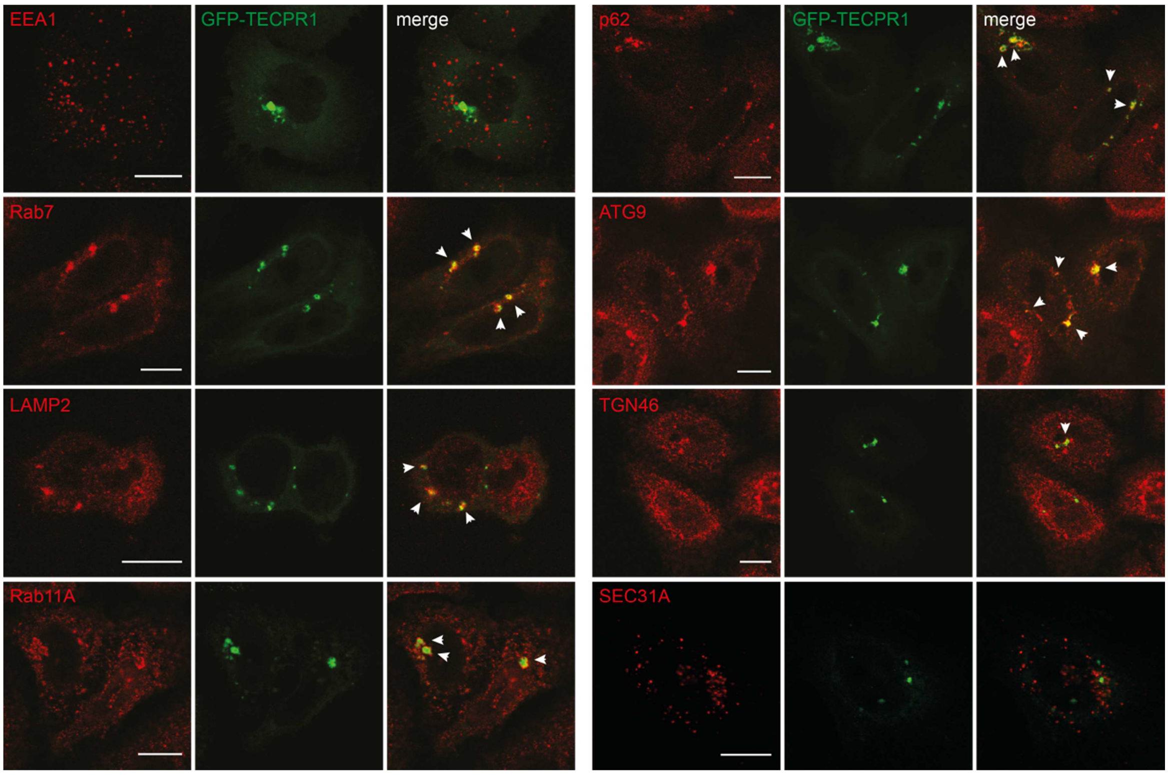

Figure 9: Subcellular localization of GFP-TECPR1 revealed by immunofluorescence. Confocal images of HeLa cells that are transiently expressing GFP-TECPR1 and were stained for indicated cellular marker proteins by immunofluorescence. Cells stained for EEA1, Rab7, LAMP2, Rab11A, and p62 were starved for 2 hours. Arrows indicate colocalizing structures. Scale bars, 10 µm.

3.3 Interaction of TECPR1 with hATG8 proteins

Colocalization of TECPR1 with hATG8 proteins

The specific accumulation of LC3C and GABARAPL2 in TECPR1$^{\backslash-}$ cells as well as the selective lipidation of LC3C and the GABARAPs in presence of TECPR1 *in vitro* raised the question whether TECPR1 interacts with specific hATG8 proteins. Assuming that a selective interaction correlates with a defined colocalization pattern of TECPR1 with hATG8s, the colocalization of RFP-TECPR1 with GFP-tagged hATG8s was analyzed. Interestingly, all hATG8 homologs partly colocalized with RFP-TECPR1, while GFP-LC3C exhibited the strongest colocalization with RFP-TECPR1 (**Figure 10**).

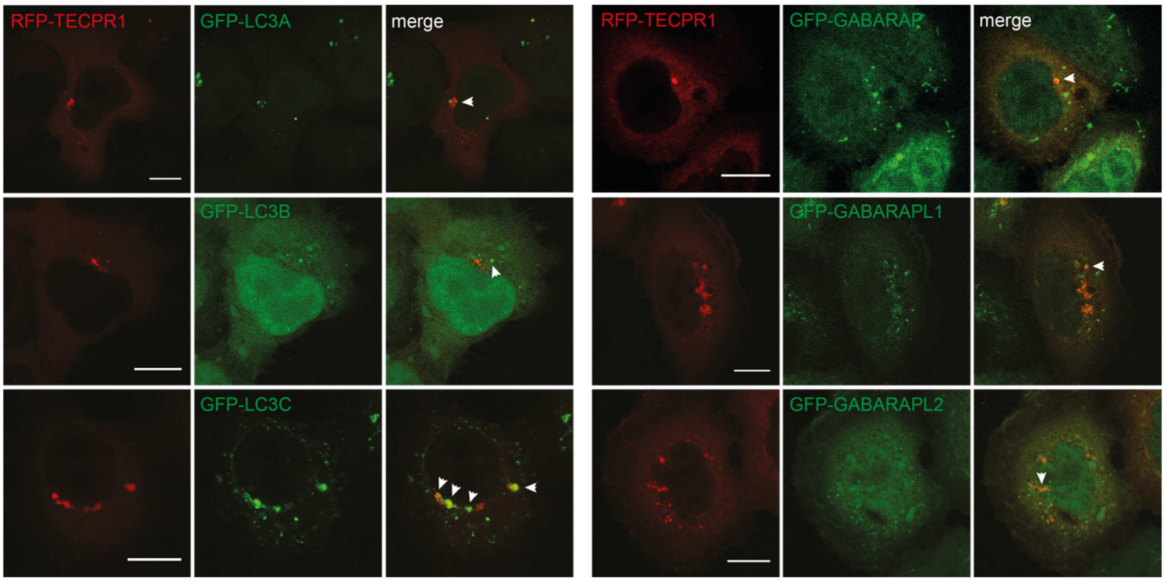

Figure 10: Colocalization of TECPR1 with hATG8 proteins. HeLa cells were cotransfected with RFP-TECPR1 and GFP-tagged hATG8s and analyzed by live cell confocal microscopy. Arrows indicate structures that are colocalizing or in close vicinity. Scale bars, 10 µm.

Since TECPR1 interacts with ATG12–ATG5 through an AIR motif (Kim et al., 2015), this interaction could be important for targeting of TECPR1 to hATG8-positive organelles and lysosomes. For this reason, it was tested if the correct subcellular localization as well as its colocalization with LC3C depend on the interaction with ATG12–ATG5. Therefore, the AIR motif in TECPR1 was deleted to abolish its interaction with ATG5 and the corresponding construct TECPR1$^{\Delta AIR}$ was expressed in TECPR1$^{\backslash-}$ cells. Surprisingly, GFP-tagged TECPR1$^{\Delta AIR}$ still colocalized with both LAMP2 and RFP-LC3C, indicating that targeting of TECPR1 to lysosomes and LC3C-positive structures does not depend on its interaction with ATG12–ATG5 (**Figure 11**).

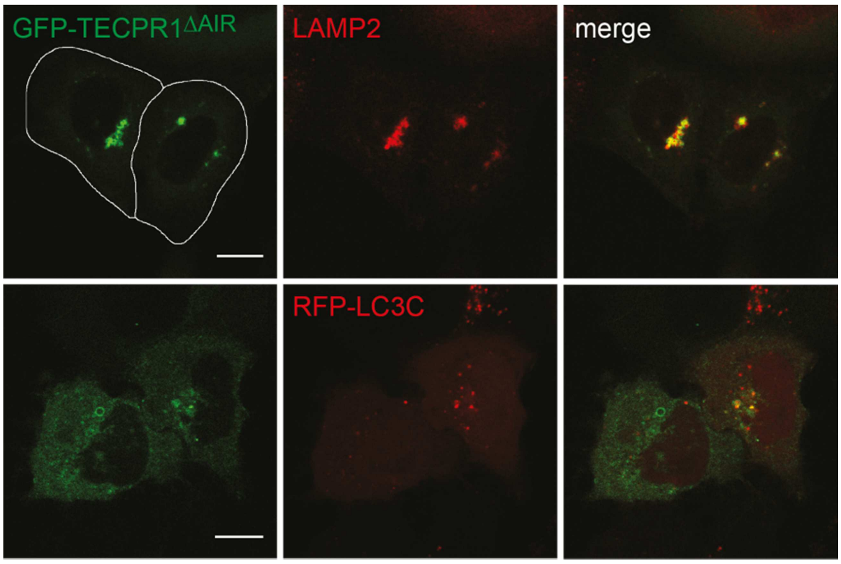

Figure 11: Colocalization of TECPR1$^{\Delta AIR}$ with LAMP2 and LC3C. HeLa TECPR1$^{-/-}$ cells transiently expressing GFP-TECPR1$^{\Delta AIR}$ were stained for LAMP2 and confocal images were acquired. HeLa TECPR1$^{-/-}$ cells cotransfected with GFP-TECPR1$^{\Delta AIR}$ and RFP-LC3C were analyzed using live cell confocal microscopy. Scale bars, 10 µm.

It was demonstrated in this thesis that TECPR1 strongly colocalizes with LC3C. To characterize this colocalization further, cells expressing GFP-LC3C or GFP-TECPR1 were stained for the lysosomal marker LAMP2 and the autophagosomal SNARE protein STX17 (**Figure 12A**). STX17 is a late autophagosomal marker since it is recruited to the outer membrane of completed autophagosomes (Itakura et al., 2012). While GFP-LC3C colocalized strongly with STX17, only few GFP-LC3C puncta were positive for LAMP2. In contrast, GFP-TECPR1 strongly colocalized with LAMP2 and to a lesser extent with STX17. Only occasionally colocalization of TECPR1 or LC3C with both, LAMP2 and STX17, has been observed. The distinct localization of LC3C and TECPR1 to LAMP2- and STX17-positive structures suggests that they are present on different membrane compartments that are often in close proximity. Superresolution structured-illumination microscopy (SIM) showed that indeed TECPR1 localizes to LAMP2-positive structures and LC3C to STX17-positive small puncta that are in juxtaposition to TECPR1 structures (**Figure 12B**). In addition, staining of GFP-TECPR1 expressing cells for endogenous LC3 (antibody recognizes LC3A, LC3B, and LC3C) and visualizing them using SIM confirmed that many small LC3 puncta are in close proximity to larger GFP-TECPR1 structures (**Figure 12C**).

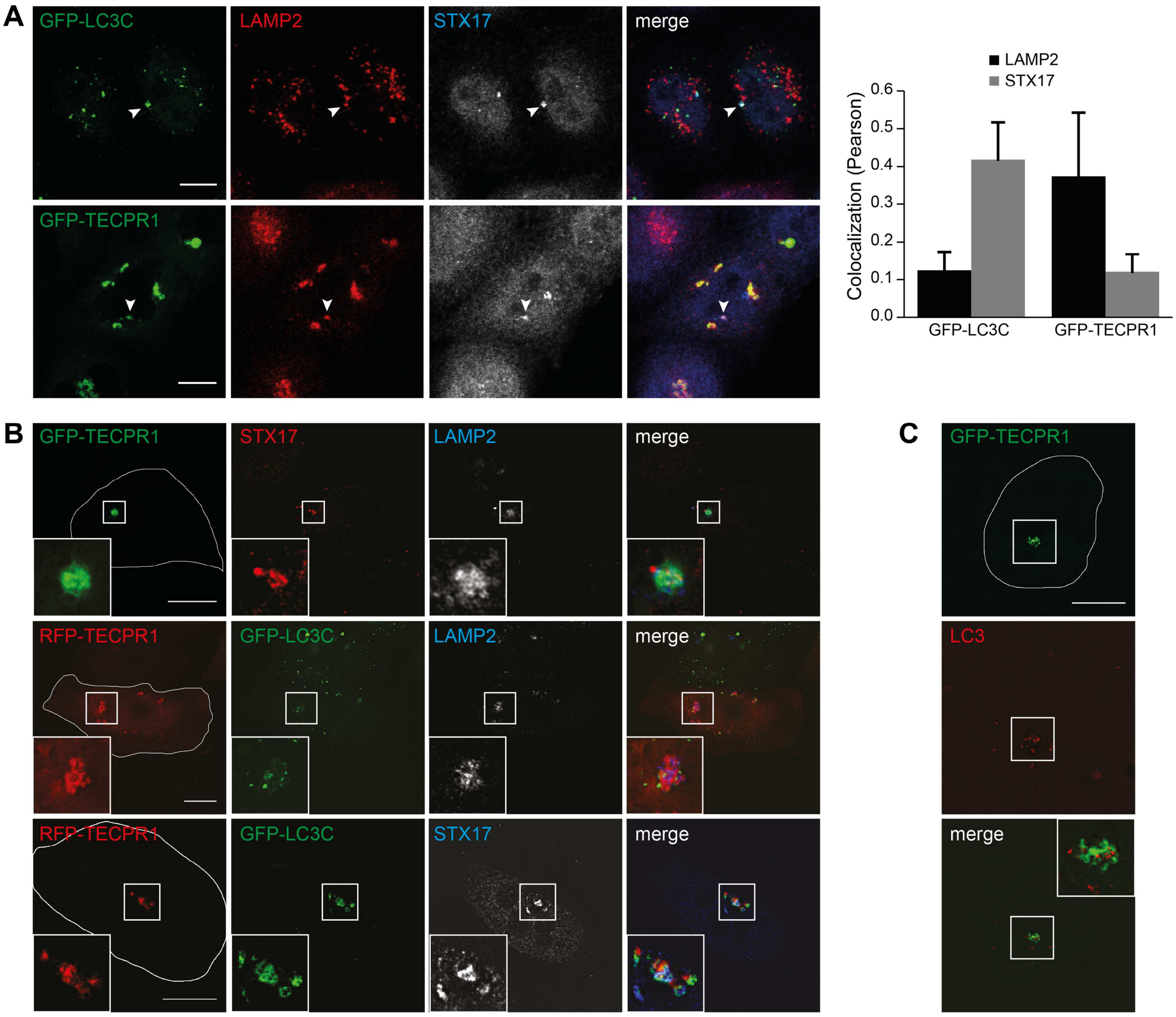
A
GFP-LC3C
LAMP2
STX17
merge
GFP-TECPR1
■ LAMP2
■ STX17
Colocalization (Pearson)
0.6
0.5
0.4
0.3
0.2
0.1
0.0
GFP-LC3C
GFP-TECPR1
B
GFP-TECPR1
STX17
LAMP2
merge
RFP-TECPR1
GFP-LC3C
LAMP2
merge
RFP-TECPR1
GFP-LC3C
STX17
merge
C
GFP-TECPR1
LC3
merge

Figure 12: Characterization of TECPR1 and LC3C colocalization. **(A)** Confocal images of HeLa cells transiently expressing GFP-LC3C or GFP-TECPR1 that were starved for 2 hours and stained for LAMP2 and STX17. Arrows indicate colocalization with both LAMP2 and STX17. Colocalization was quantified using the Pearson coefficient (n > 20 cells). **(B)** Structured-illumination microscopy of HeLa cells transiently expressing GFP-TECPR1 or coexpressing RFP-TECPR1 and GFP-LC3C that were starved for 2 hours and stained for LAMP2 or STX17. **(C)** Structured-illumination microscopy of HeLa cells transiently expressing GFP-TECPR1 that were starved for 2 hours and stained with anti-LC3 antibody (M152-3). Selected regions are cropped and enlarged. Scale bars, 10 µm.

To visualize the ultrastructure of LC3C puncta, CLEM was performed with HeLa cells transiently expressing RFP-LC3C. Interestingly, LC3C localized to structures with different morphologies (**Figure 13**). However, all of these structures shared their dark staining, corresponding to compact electron-dense cytoplasmic material, which is an indication for aggregated proteins. Furthermore, many of the darkly stained LC3C-positive structures resembled either autophagosomes that were surrounded by a double membrane or autolysosomes that contained intraluminal heterogeneous material. Therefore, the observed LC3C-positive structures could be classified into the following four categories: (1) autophagosome-like, (2) autolysosome-like, (3) MVB-like, and (4) others.

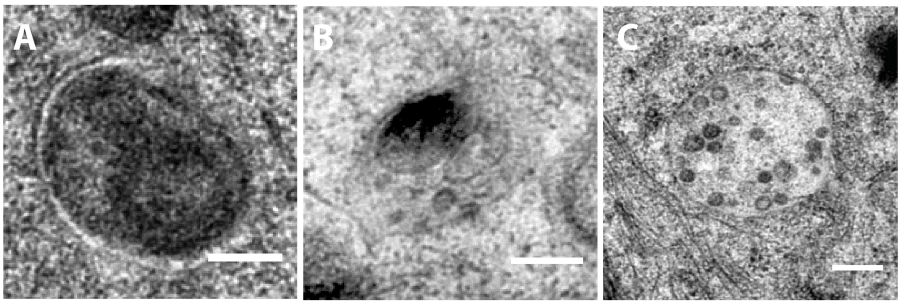

Figure 13: CLEM of HeLa cells transiently expressing RFP-LC3C. Fluorescent signals of 70 nm sections were correlated with EM images. RFP-LC3C localized to predominantly darkly stained structures with different morphologies of the following categories: autophagosome-like **(A)**, autolysosome-like **(B)**, and MVB-like **(C)**. Scale bars, 200 nm.

Video microscopy of LC3C- and TECPR1-positive structures

This study has shown that TECPR1 and LC3C reside on two different membrane compartments, corresponding to lysosomes and mature autophagosomes, respectively. To analyze dynamics of these structures, time-lapse video microscopy was performed. While a number of LC3C puncta was stably associated with TECPR1 structures, another population moved independently of TECPR1 but transiently interacted with TECPR1 structures (**Figure 14A**). Video microscopy of HeLa cells expressing GFP-LC3C or GFP-TECPR1 that were treated with lysotracker revealed that TECPR1 is stably associated with lysosomes, sometimes forming ring-like structures around lysotracker staining (**Figure 14B**). Furthermore, there were again two populations of GFP-LC3C puncta, one that was stably in close proximity to lysotracker-positive structures and one that transiently contacted them (**Figure 14C**). Taken together, these results confirm that TECPR1 resides on lysosomes, while LC3C is present on different compartments that can transiently and stably interact with TECPR1-positive lysosomes.

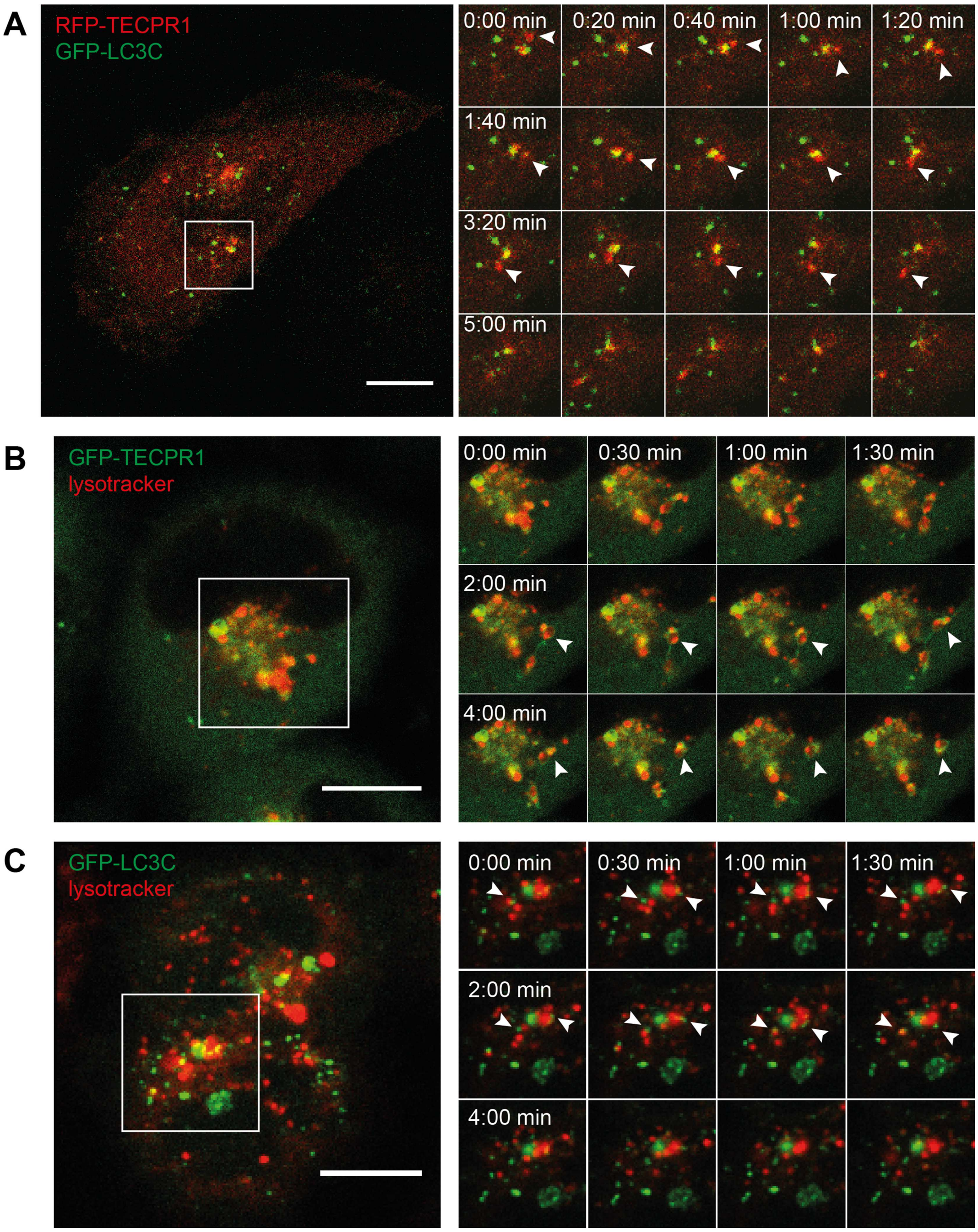
A
RFP-TECPR1
GFP-LC3C
0:00 min
0:20 min
0:40 min
1:00 min
1:20 min
1:40 min
3:20 min
5:00 min
B
GFP-TECPR1
lysotracker
0:00 min
0:30 min
1:00 min
1:30 min
2:00 min
4:00 min
C
GFP-LC3C
lysotracker
0:00 min
0:30 min
1:00 min
1:30 min
2:00 min
4:00 min

Figure 14: Time-lapse video microscopy of LC3C and TECPR1 structures. **(A)** Time-lapse experiment of HeLa TECPR1$^{-\backslash-}$ cells cotransfected with GFP-LC3C and RFP-TECPR1. Confocal images were captured every 10 sec and every other frame is shown. Arrows indicate moving structures that transiently interact. **(B)** and **(C)** Time-lapse experiment of HeLa wt cells that were transfected with GFP-TECPR1 or GFP-LC3C and treated with lysotracker. Arrows indicate moving ring-like TECPR1 structures that are stably associated with lysotracker or moving LC3C puncta that transiently contact lysotracker structures. Images were acquired 30 min after addition of lysotracker deep red. Enlarged sections of confocal frames are displayed at indicated time points. Scale bars, 10 µm.

Interaction of TECPR1 with LC3C and other hATG8 proteins

The colocalization of TECPR1 with LC3C as well as the specific *in vitro* lipidation of LC3C and the GABARAPs in presence of TECPR1 suggests that TECPR1 can directly interact with LC3C. To test this hypothesis, co-immunoprecipitation (Co-IP) and *in vitro* pull-down assays were performed (**Figure 39 in the appendix**). However, GFP-TECPR1 did not co-immunoprecipitate with HA-tagged hATG8s and recombinant LC3C did not specifically bind to His$_6$-MBP-TECPR1 that was immobilized on Ni-NTA beads. In addition, TECPR1 bound to PtdIns(4)P-containing GUVs was not able to recruit soluble LC3C to the membrane (**Figure 15A**). To the contrary, lipidated LC3C that was conjugated to small unilamellar vesicles (SUVs) was recruited to TECPR1-positive GUV membranes and not to membranes that were lacking TECPR1, suggesting that TECPR1 can selectively interact with lipidated LC3C (**Figure 15B**).

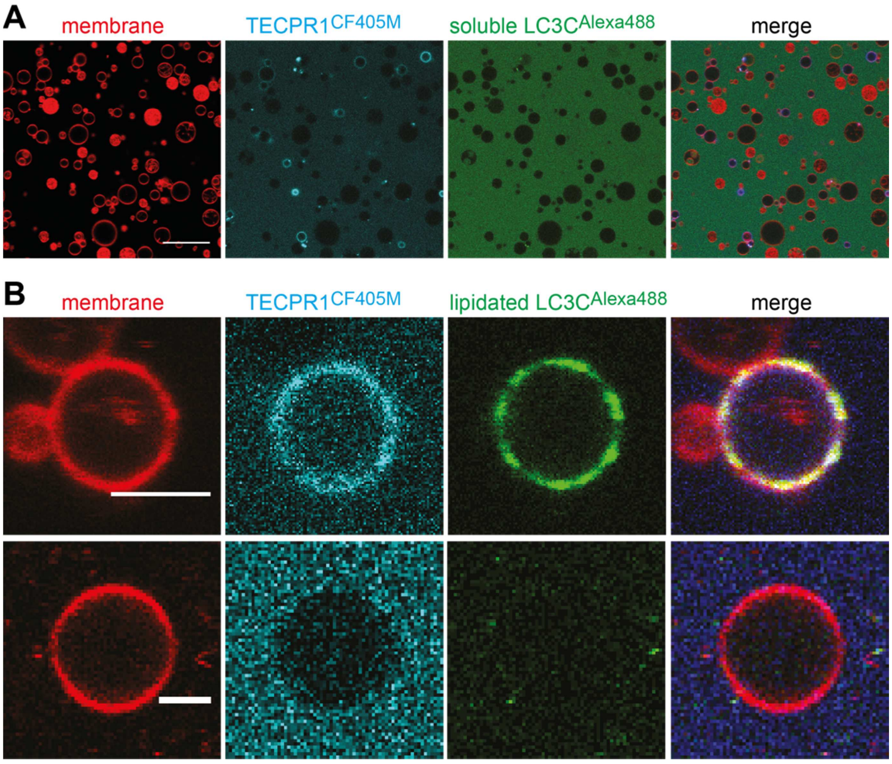

Figure 15: Binding of LC3C to TECPR1 on GUVs. Confocal images of GUVs containing PtdIns(4)P that were incubated with TECPR1 and soluble LC3C **(A)** or LC3C that was conjugated to SUVs in presence of the ATG12–ATG5-ATG16NT complex **(B)**. TECPR1 and LC3C were fluorescently labeled with CF405M and Alexa Fluor 488, respectively. Scale bars, 20 µm (A) or 3 µm (B).

TECPR1 is a multidomain protein and comprises two β-propeller repeat containing domains (TR1 and TR2), which are known protein-protein interaction platforms. To reveal whether a specific TECPR1 domain is responsible for LC3C recognition or the subcellular localization of TECPR1, the domains TR1, TR2, and DR were expressed in TECPR1 deficient HeLa cells (**Figure 4**). Strikingly, GFP-tagged TR1, the N-terminal domain of TECPR1, showed a very similar subcellular localization like full-length TECPR1 (**Figure 16**). TR1 strongly colocalized with Rab7, LAMP2, and LC3C in contrast to DR and

TR2 that were mostly distributed in the cytosol and nucleus and did not colocalize with LAMP2 or LC3C. The subcellular localization of the TR1 domain indicates that it is sufficient for targeting TECPR1 to lysosomal membranes and to interact with LC3C.

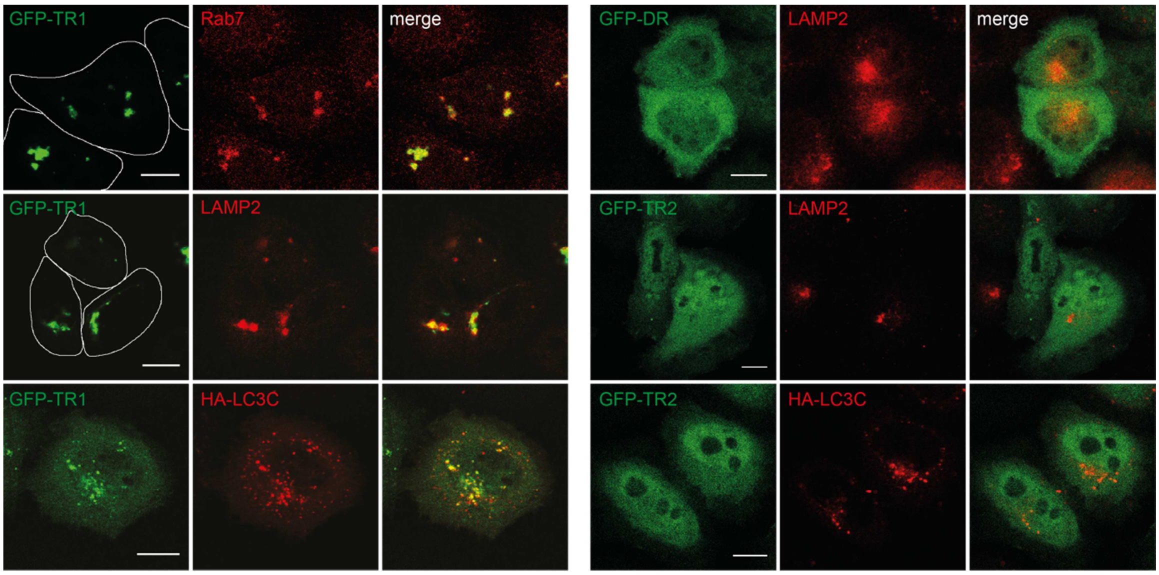

Figure 16: Subcellular localization of TECPR1 domains. Confocal images of HeLa TECPR1$^{-\backslash-}$ cells that were transfected with GFP-TR1, GFP-DR, or GFP-TR2, or cotransfected with HA-LC3C, starved for 2 hours and stained for Rab7, LAMP2, or HA by immunofluorescence. Scale bars, 10 µm.

Many hATG8-binding proteins interact with hATG8 family members through a conserved LC3-interacting region (LIR), which is a short WxxL/I motif. The strong colocalization of the TR1 domain with LC3C suggests that this domain contains a LIR motif and was therefore screened for potential LIRs. Most of the predicted LIRs are located in the β-propeller repeats of TECPR1 und thus not accessible. The motif $W^{175}xxI^{178}$, however, is present in a loop region and can therefore potentially bind to hATG8s. To test if the isolated LIR motif is able to bind lipidated hATG8 proteins, floatation assays were performed with hATG8s that were conjugated to SUVs. Indeed, a TECPR1 peptide containing the $W^{175}xxI^{178}$ motif was found associated with lipidated hATG8s in the liposome fraction without discriminating between the different homologs (**Figure 17**). Mutating the motif to $A^{175}xxA^{178}$ significantly reduced the amount of peptide binding to hATG8-conjugated SUVs. This suggests that the $W^{175}xxI^{178}$ LIR motif binds to hATG8 proteins *in vitro*.

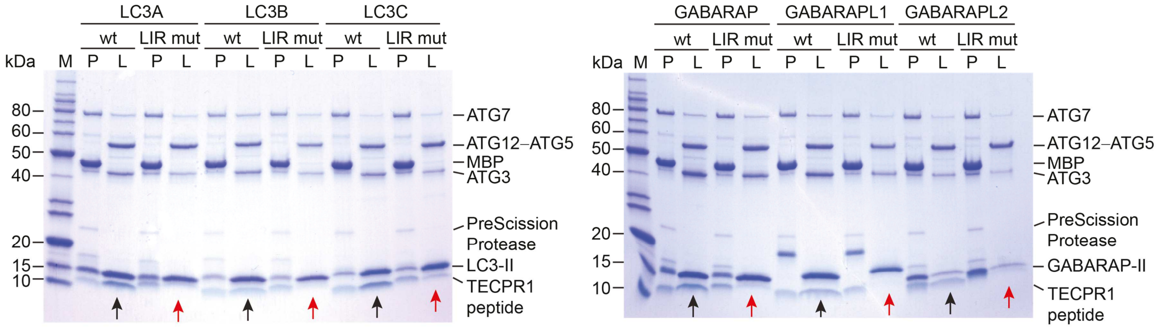

Figure 17: Floatation assay with lipidated hATG8 proteins and a TECPR1 peptide containing the W^{175}xxI^{178} LIR motif. hATG8s (6 µM) were conjugated to SUVs in presence of 1 µM ATG7, 1.5 µM ATG3, 0.5 µM ATG12–ATG5, and 0.1 µM ATG16L1. An MBP-fused TECPR1 peptide (V^{158}RRRKWIRYRRYKSRDI**WAKI**PSKDDPKEL^{187}; 6 µM) containing the W^{175}xxI^{178} motif or the corresponding A^{175}xxA^{178} LIR mutant (LIR mut) was added together with PreScission protease. Floatation assays were performed and protein fractions (P) or liposome fractions (L) were collected and analyzed by coomassie staining of SDS-PAGE gels. Black arrows indicate bands corresponding to the TECPR1 peptide present in liposome fractions and red arrows indicate the corresponding LIR mut.

Since the W^{175}xxI^{178} motif in TECPR1 is able to bind to hATG8 proteins *in vitro*, mutation of the LIR motif in TECPR1 should reduce its colocalization with LC3C in cells. Thus, the LIR motif was mutated to A^{175}xxA^{178} in GFP-tagged TECPR1 (GFP-TECPR1$^{W175A/I178A}$) and cotransfected with RFP-LC3C into TECPR1$^{-/-}$ cells (**Figure 18**). Surprisingly, the introduction of these point mutations completely altered the subcellular localization of TECPR1. GFP-TECPR1$^{W175A/I178A}$ was mainly distributed in the cytoplasm and only few small puncta were occasionally observed that sometimes colocalized with LC3C. Compared to TECPR1 wt, LC3C colocalized considerably less with the TECPR1 LIR mutant, indicating that the W^{175}xxI^{178} LIR motif in TECPR1 is indeed mediating the interaction with LC3C.

Although a direct interaction between TECPR1 and the hATG8 proteins could not be confirmed by Co-IP or pull-down experiments, there is strong evidence that TECPR1 selectively interacts with lipidated LC3C. LC3C strongly colocalized with TECPR1 and LC3C puncta accumulated in TECPR1 depleted cells. Moreover, LC3C lipidation was facilitated by TECPR1 and lipidated LC3C was recruited to TECPR1-positive GUV membranes. Finally, a LIR motif in TECPR1 could be identified that is able to bind to hATG8 proteins *in vitro* and mutation of the LIR motif reduced colocalization between TECPR1 and LC3C *in vivo*. Collectively, these data strongly suggest that TECPR1 specifically interacts with lipidated LC3C through a canonical LIR motif.

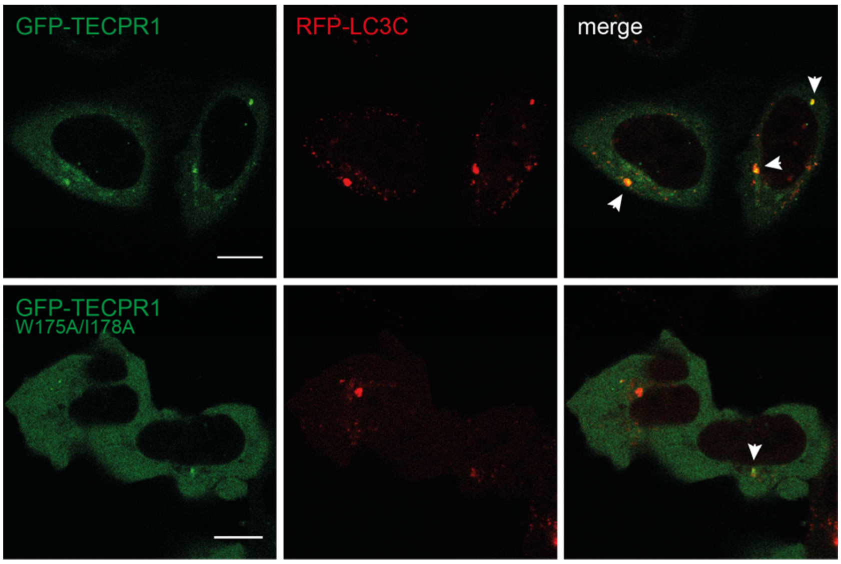

Figure 18: Colocalization of TECPR1 LIR mutant with LC3C. HeLa TECPR1$^{-/-}$ cells were cotransfected with RFP-LC3C and GFP-TECPR1 or GFP-TECPR1$^{W175A/I178A}$, respectively. Cells were analyzed using live cell confocal microscopy. Arrows indicate colocalizing structures. Scale bars, 10 µm.

Tandem RFP-GFP-hATG8 reporter

This study provided evidence that small LC3C-positive structures are recruited by TECPR1 to lysosomes, which implies that LC3C has to be present at the outer membrane of autophagosomes to interact with TECPR1. To confirm this hypothesis, the transport of LC3C and other hATG8s into the lysosomal lumen was analyzed using a pH-sensitive tandem RFP-GFP-hATG8 reporter system.

Wt cells which have been transfected with the commonly used RFP-GFP-LC3 (rat LC3b in ptfLC3) reporter displayed RFP and GFP (yellow) fluorescent puncta as well as puncta that were only RFP-positive (red) due to quenching of GFP fluorescence by the low lysosomal pH (Kimura et al., 2014, **Figure 19A**). Thus, red puncta correspond to autophagosomes that have been fused with lysosomes (autolysosomes). Hence, rat LC3 gets transported to the lysosomal lumen, which is only possible if it is present at the inner autophagosome membrane. Chen et al., 2012 reported that depletion of TECPR1 blocks fusion of autophagosomes with lysosomes, resulting in a reduction of red RFP-GFP-LC3 puncta. Here, however, TECPR1$^{-\backslash-}$ cells exhibited a similar amount of yellow and red puncta compared to wt cells, suggesting that TECPR1 is not essential for fusion of canonical autophagosomes with lysosomes.

Many hATG8 proteins are implicated in selective autophagy since they are binding to autophagy receptors at the inner autophagosome membrane. LC3C, for example, was shown to selectively bind to the receptor NDP52, thereby promoting clearance of intracellular *Salmonella* (von Muhlinen et al., 2012). Thus, the translocation of selected hATG8 proteins to the lysosomal lumen was tested using the pH-sensitive tandem reporter system. In contrast to rat LC3, the other tested human homologs LC3C, GABARAP, and GABARAPL2 almost exclusively displayed GFP- and RFP-positive yellow puncta (**Figure 19B**). This indicates that the majority of these hATG8 proteins is not transported to the lysosomal lumen and therefore present at the outer autophagosome membrane. This further suggests that TECPR1 could potentially recruit autophagosomes through its interaction with LC3C or other hATG8 proteins that are located at the outer membrane of autophagosomes.

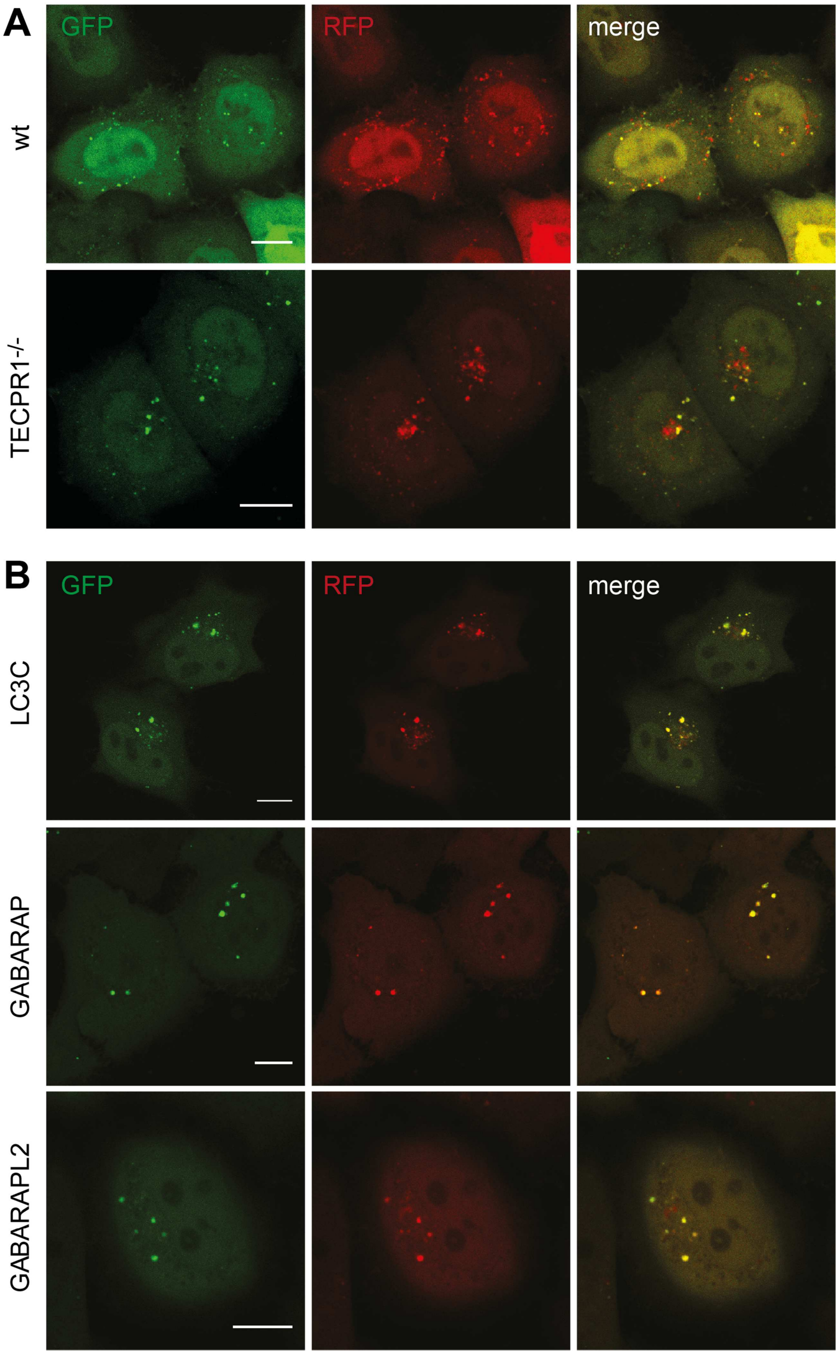

Figure 19: Tandem RFP-GFP-hATG8 reporter. **(A)** HeLa wt or TECPR1$^{-\backslash-}$ cells were transfected with RFP-GFP-LC3 (rat LC3b, ptfLC3), starved for 2 hours, and analyzed using live cell confocal microscopy. **(B)** HeLa cells were transfected with RFP-GFP-LC3C, RFP-GFP-GABARAP, or RFP-GFP-GABARAPL2, starved for 2 hours, and analyzed using live cell confocal microscopy. Scale bars, 10 µm.

3.4 Lipid-binding specificity of TECPR1

Binding of TECPR1 to phosphoinositides *in vitro*

TECPR1 possesses a PH domain, which is a known phosphoinositide-binding domain and has been reported to interact with PtdIns(3)P in a protein-lipid overlay assay (Chen et al., 2012). However, lipids in protein-lipid overlay assays are immobilized on a solid support and binding to these lipids is therefore tested under highly non-physiological conditions. Thus, the interaction of TECPR1 with several phosphoinositides (PtdInsPs) important for autophagosome biogenesis was analyzed using fluorescently labeled recombinant TECPR1 and PtdInsP-positive GUV membranes (**Figure 20**). Besides PtdIns(3)P, which is essential for the formation of the isolation membrane, binding of TECPR1 to PtdIns(3,5)P_2 and PtdIns(4)P was tested. PtdIns(3,5)P_2 has been implicated in maturation and turnover of autophagosomes (Dall'Armi et al., 2013) and substantial amounts of PtdIns(4)P are present on lysosomes and important for autophagosome-lysosome fusion (Wang et al., 2015; Jeschke et al., 2015). As expected, TECPR1 showed low affinity for the GUV membrane without PtdInsPs. Surprisingly, TECPR1 was not found associated with GUVs containing PtdIns(3)P or PtdIns(3,5)P_2. However, TECPR1 was strongly recruited to GUV membranes with PtdIns(4)P, suggesting that it specifically interacts with PtdIns(4)P *in vitro*.

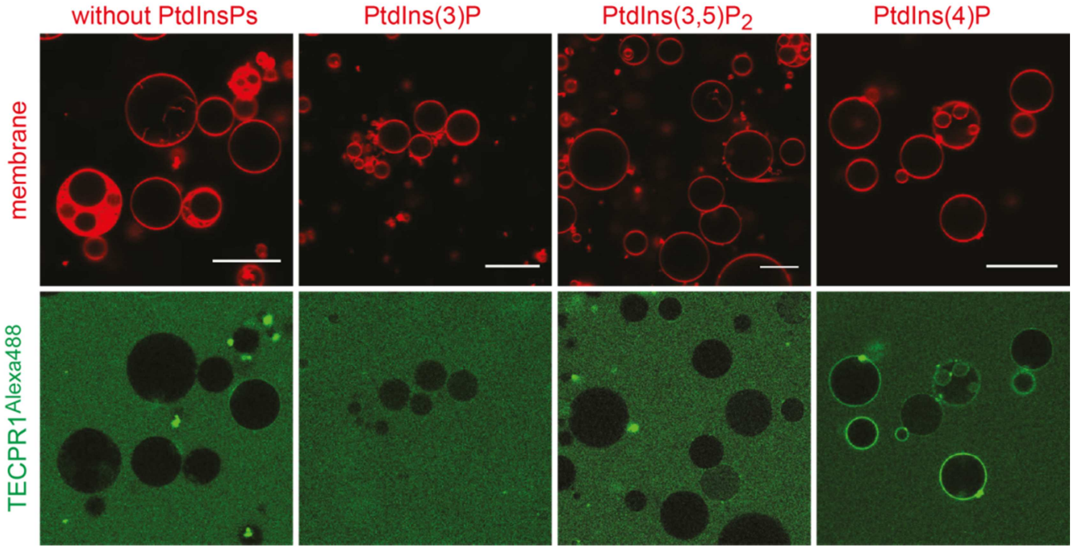

Figure 20: Binding of TECPR1 to GUV membranes containing phosphoinositides. Confocal images of GUVs containing indicated PtdInsPs that were incubated with Alexa Fluor 488-labeled TECPR1. Scale bars, 20 µm.

Colocalization of TECPR1 with phosphoinositides *in vivo*

To test whether TECPR1 localizes to PtdInsP-positive membranes *in vivo*, the colocalization of GFP-tagged TECPR1 with the PtdIns(3)P-sensor RFP-2xFYVE and with PtdIns(4)P was analyzed (**Figure 21**). Importantly, TECPR1 did not colocalize with RFP-2xFYVE, but strongly colocalized with PtdIns(4)P. This finding supports the *in vitro* data, which have demonstrated that TECPR1 selectively binds to PtdIns(4)P.

To identify the influence of the PH domain on the localization of TECPR1 to PtdInsP-rich membranes, two TECPR1 mutants were cloned that modify its lipid-binding specificity: First, the PH domain was deleted (TECPR1$^{\Delta PH}$) and second, the PH domain was replaced by a PtdIns(3)P-binding tandem FYVE zinc finger domain (TECPR1$^{\Delta PH\text{-}2xFYVE}$). The used tandem FYVE domain of HGS has been demonstrated to selectively recognize PtdIns(3)P on early endosomes as well as on internal vesicles of MVBs (David J.Gillooly, 2000; Gillooly et al., 2003; Vicinanza et al., 2015). Similar to TECPR1^{wt}, TECPR1$^{\Delta PH}$ did not colocalize with the PtdIns(3)P-sensor RFP-2xFYVE, but showed reduced colocalization with PtdIns(4)P. This indicates that the PH domain contributes to targeting TECPR1 to PtdIns(4)P-positive membranes. Notably, TECPR1^{wt} and TECPR1$^{\Delta PH}$ colocalized with PtdIns(4)P-positive structures in juxtanuclear regions that could correspond to the Golgi apparatus, which comprises a major pool of PtdIns(4)P (Hammond et al., 2009). TECPR1$^{\Delta PH\text{-}2xFYVE}$ on the other hand did not colocalize with large juxtanuclear PtdIns(4)P structures but often colocalized with smaller PtdIns(4)P-positive puncta, resulting in a Pearson correlation coefficient that was comparable to TECPR1^{wt}. Importantly, the colocalization of TECPR1$^{\Delta PH\text{-}2xFYVE}$ with RFP-2xFYVE was significantly increased, suggesting that TECPR1$^{\Delta PH\text{-}2xFYVE}$ is mistargeted to PtdIns(3)P-positive membranes.

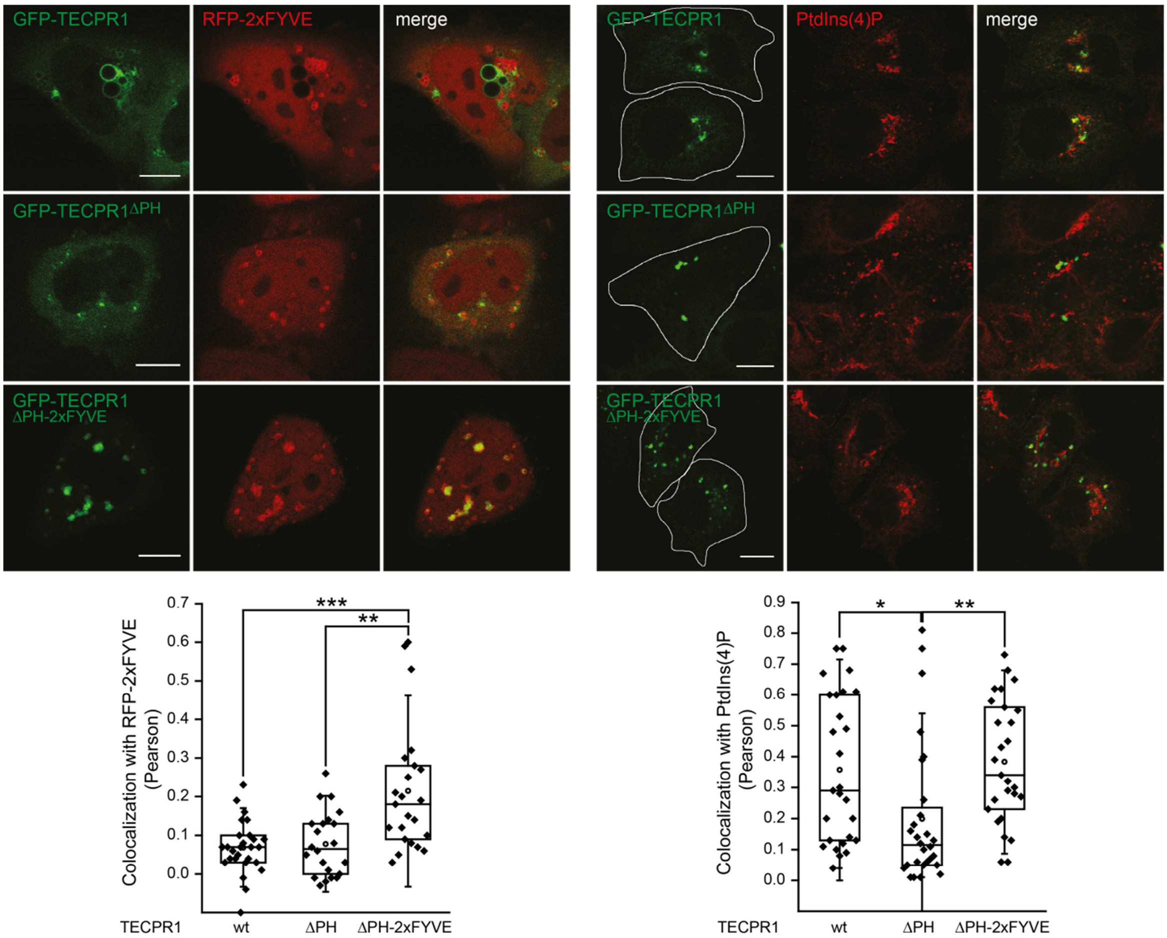
GFP-TECPR1
RFP-2xFYVE
merge
GFP-TECPR1ΔPH
GFP-TECPR1
ΔPH-2xFYVE
GFP-TECPR1
PtdIns(4)P
merge
GFP-TECPR1ΔPH
GFP-TECPR1
ΔPH-2xFYVE
Colocalization with RFP-2xFYVE
(Pearson)
0.7
0.6
0.5
0.4
0.3
0.2
0.1
0.0
***
**
TECPR1
wt
ΔPH
ΔPH-2xFYVE
Colocalization with PtdIns(4)P
(Pearson)
0.9
0.8
0.7
0.6
0.5
0.4
0.3
0.2
0.1
0.0
*
**
TECPR1
wt
ΔPH
ΔPH-2xFYVE

Figure 21: Colocalization of TECPR1 constructs with PtdInsP-positive membranes *in vivo*. HeLa TECPR1$^{-\backslash-}$ cells were cotransfected with GFP-tagged TECPR1 constructs and RFP-2xFYVE (left side) or transfected with GFP-TECPR1 constructs and stained for PtdIns(4)P by immunofluorescence (right side). Samples were analyzed by confocal microscopy and colocalization was quantified using the Pearson coefficient (n > 25 cells). Scale bars, 10 µm.

Mistargeting of TECPR1 to PtdIns(3)P-rich membranes

The distinct localization of TECPR1 constructs to PtdInsP-rich membranes suggests that TECPR1 is present on lysosomes, while TECPR1$^{\Delta PH\text{-}2xFYVE}$ is targeted to PtdIns(3)P-positive compartments. To test this hypothesis, the colocalization of TECPR1 constructs with the lysosomal marker LAMP2 and with the early endosomal marker EEA1 was investigated. As anticipated, a stronger colocalization of TECPR1^{wt} with LAMP2 than with EEA1 was observed (**Figure 22**). Deletion of the PH domain resulted in similar colocalization with EEA1 and reduced colocalization with LAMP2 compared to TECPR1^{wt}, supporting the finding that the PH domain contributes to targeting TECPR1 to PtdIns(4)P-positive membranes.

Colocalization between the mistargeting mutant TECPR1$^{\Delta PH\text{-}2xFYVE}$ and LAMP2 was similar to TECPR1^{wt}. Consistent with the observation that TECPR1$^{\Delta PH\text{-}2xFYVE}$ is recruited to PtdIns(3)P-positive membranes, it colocalized significantly stronger with the early endosomal marker EEA1 compared to TECPR1^{wt} or TECPR1$^{\Delta PH}$. This strongly suggests that replacement of the PH domain by the PtdIns(3)P-binding tandem FYVE domain results in mistargeting of TECPR1 to EEA1-positive compartments that could represent early endosomal compartments. Notably, the distribution of EEA1 structures was dramatically changed in TECPR1$^{\Delta PH\text{-}2xFYVE}$-expressing cells compared to TECPR1^{wt}- or TECPR1$^{\Delta PH}$-expressing cells. Normally, small EEA1 puncta were distributed evenly in the cytoplasm, whereas cells expressing TECPR1$^{\Delta PH\text{-}2xFYVE}$ displayed large EEA1 structures. These large structures colocalized with the lysosomal marker LAMP2, which is unusual for early endosomes. This indicates that TECPR1$^{\Delta PH\text{-}2xFYVE}$ expression induces the formation of aberrant endosomal structures.

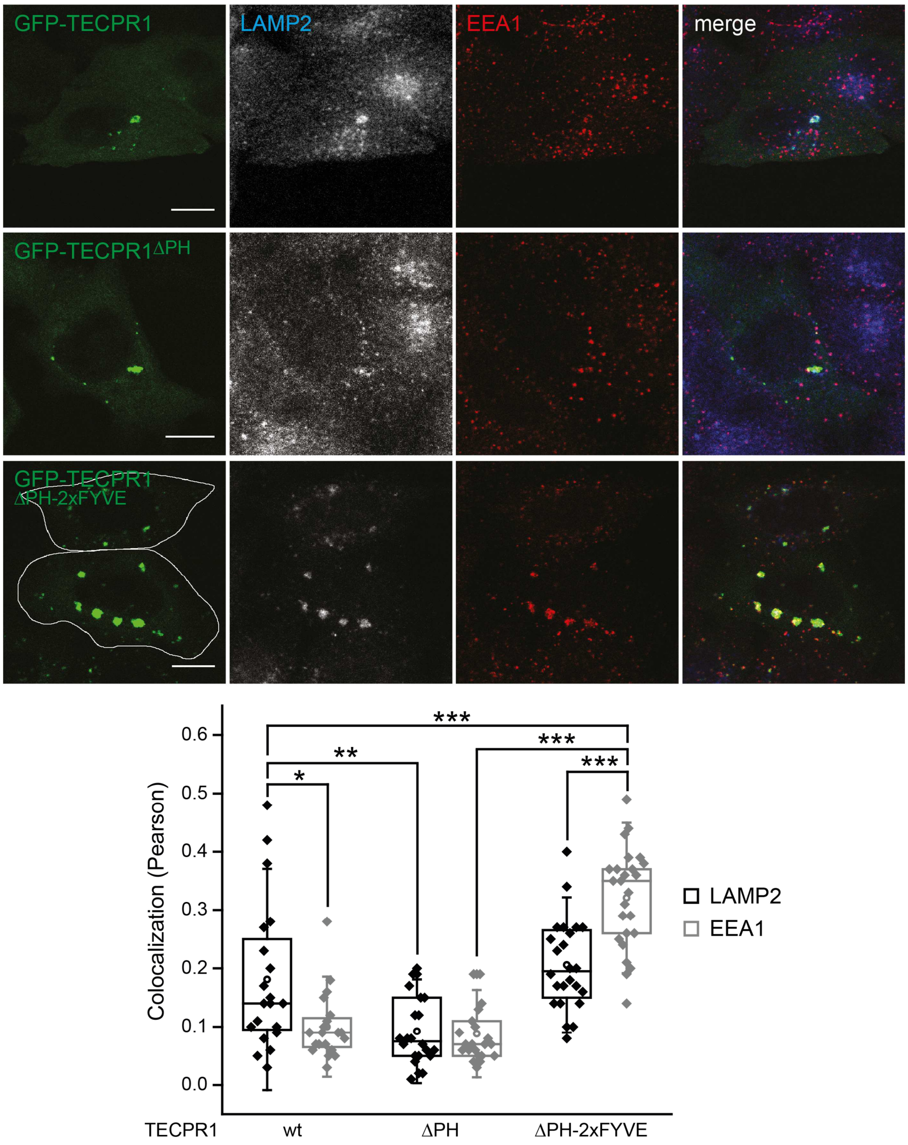

Figure 22: Colocalization of TECPR1 constructs with LAMP2 and EEA1. Confocal images of HeLa TECPR1$^{-\backslash-}$ cells that were transfected with GFP-TECPR1 constructs and stained for LAMP2 and EEA1 by immunofluorescence. Colocalization was quantified using the Pearson coefficient (n > 20 cells). Scale bars, 10 µm.

To characterize these aberrant EEA1- and LAMP2-positive TECPR1$^{\Delta PH\text{-}2xFYVE}$ structures further, their colocalization with endosomal markers and lysotracker was analyzed. Strikingly, GFP-TECPR1$^{\Delta PH\text{-}2xFYVE}$ colocalized strongly with the early endosomal marker

Rab5 and the late endosomal marker Rab7 (**Figure 23A**). Conclusively, TECPR1$^{\Delta PH\text{-}2xFYVE}$ structures are positive for markers from early endosomes to late endosomes and lysosomes, indicating that they cannot be classified into a specific organelle of the endocytic pathway. To test whether TECPR1$^{\Delta PH\text{-}2xFYVE}$ structures are acidified and thus corresponding to late endosomes/MVBs or lysosomes, a lysotracker probe was used that labels compartments with low internal pH. Large TECPR1^{wt} structures colocalized with lysotracker as expected. Frequently, ring-like TECPR1 structures were observed that surrounded lysotracker fluorescence, confirming that TECPR1 localizes to the membrane of late endosomes or lysosomes (**Figure 23B**). Strikingly, large TECPR1$^{\Delta PH\text{-}2xFYVE}$ structures also colocalized with lysotracker, indicating that these structures correspond to acidified compartments, such as late endosomes or lysosomes. Smaller TECPR1$^{\Delta PH\text{-}2xFYVE}$ structures, however, did not colocalize with lysotracker, suggesting that these structures correspond to non-acidified endosomes.

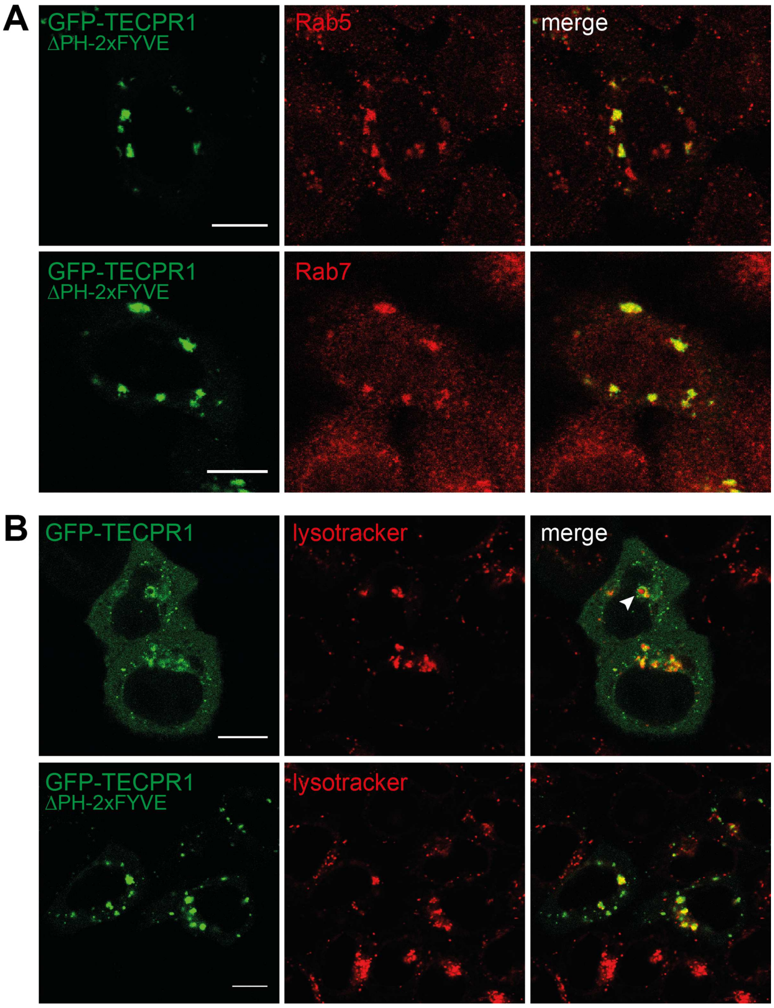

Figure 23: Colocalization of TECPR1$^{\Delta PH\text{-}2xFYVE}$ with Rab5, Rab7, and lysotracker. **(A)** Confocal images of HeLa TECPR1$^{-/-}$ cells that were transfected with GFP-TECPR1$^{\Delta PH\text{-}2xFYVE}$ and stained for Rab5 or Rab7 by immunofluorescence. **(B)** Lysotracker deep red was added to HeLa TECPR1$^{-\backslash-}$ cells transiently expressing GFP-TECPR1 and cells were analyzed by live cell confocal imaging. The arrow marks a GFP-TECPR1 ring-like structure that is surrounding lysotracker staining. Scale bars, 10 µm.

PtdInsP-binding domains are not only important regulators of autophagy but also of the endocytic pathway, for example in MVB biogenesis. Therefore, mistargeting of TECPR1 to EEA1-positive structures could impair autophagy or endocytosis by interfering with the autophagic or endocytic machinery. To test the influence of TECPR1 constructs on autophagic flux, LC3B-II levels were analyzed in TECPR1$^{-\backslash-}$ cells complemented with GFP-TECPR1^{wt}, GFP-TECPR1$^{\Delta PH}$, or GFP-TECPR1$^{\Delta PH\text{-}2xFYVE}$. Expression of all TECPR1 constructs resulted in comparable LC3B-II levels, both in absence and presence of BafA (**Figure 24A**), which suggests that they do not affect canonical autophagy.

To test the influence of TECPR1 on the endocytic pathway, epidermal growth factor receptor (EGFR) degradation assays in wt and TECPR1$^{-\backslash-}$ cells were performed. Lysosomal degradation of EGFR can be induced with the epidermal growth factor (EGF) that leads to EGFR internalization and targeting of EGFR to lysosomes via endocytosis. Importantly, TECPR1 depleted cells showed similar EGFR levels over time compared to wt cells, indicating that TECPR1 is dispensable for the degradation of EGFR (**Figure 24B**). In addition, TECPR1$^{-\backslash-}$ cells that expressed TECPR1$^{\Delta PH}$ or TECPR1$^{\Delta PH\text{-}2xFYVE}$ exhibited similar EGFR degradation kinetics compared to TECPR1$^{-\backslash-}$ cells that expressed TECPR1^{wt}. Although expression of TECPR1$^{\Delta PH\text{-}2xFYVE}$ induced the formation of aberrant endosomal structures, this finding suggests that degradation of EGFR and thus MVB biogenesis is not impaired by expression of TECPR1$^{\Delta PH\text{-}2xFYVE}$.

Taken together, these results suggest that the PH domain of TECPR1 is important for its targeting to lysosomes by interacting with PtdIns(4)P. Furthermore, replacement of the PH domain by a tandem FYVE domain mistargets TECPR1 to PtdIns(3)P-rich compartments that are positive for early endosomal, late endosomal, and lysosomal markers. The data further suggest that TECPR1$^{\Delta PH\text{-}2xFYVE}$ localizes to both acidified and non-acidified compartments. Despite colocalizing with endosomal markers, the described TECPR1 constructs do not influence LC3B-II flux or lysosomal EGFR degradation, indicating that TECPR1 is not essential for canonical autophagy or endocytosis.

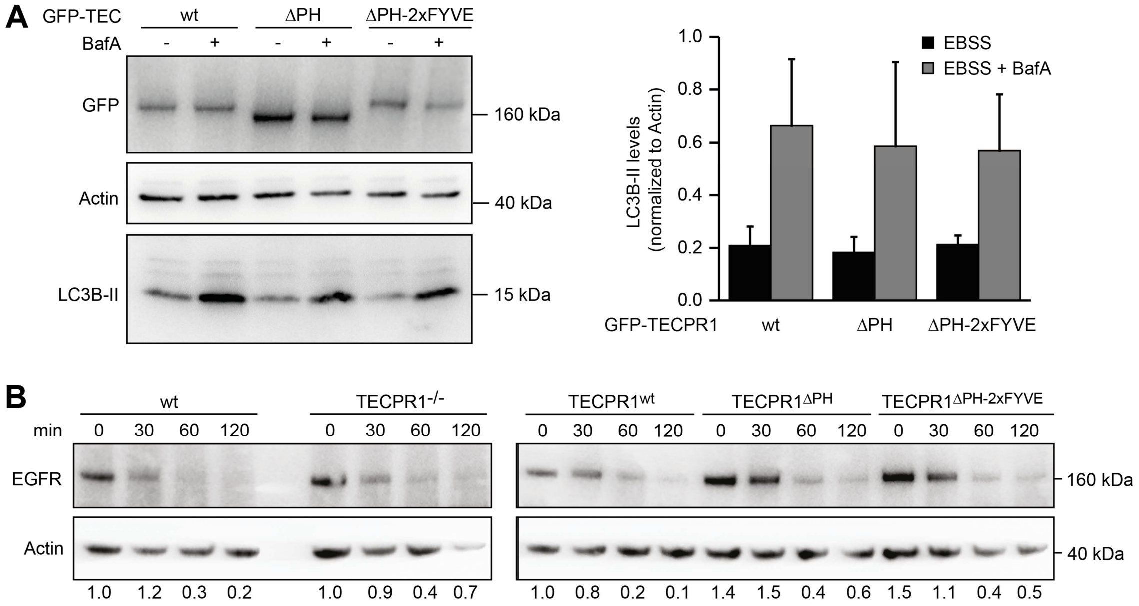

Figure 24: Effect of TECPR1 constructs on LC3B-II levels and EGFR degradation. **(A)** TECPR1$^{-\backslash-}$ cells were transfected with GFP-TECPR1 constructs and incubated for 2 hours in either EBSS or EBSS including BafA. Cell lysates were run on a 4-20% Mini-PROTEAN TGX gel and immunoblotted using antibodies against GFP, β-actin, and LC3B. LC3B-II levels were quantified from 3 independent experiments and normalized to β-actin. **(B)** EGFR degradation assay with HeLa wt, TECPR1$^{-/-}$, or TECPR1$^{-/-}$ cells transiently expressing TECPR1^{wt}, TECPR1$^{\Delta PH}$, or TECPR1$^{\Delta PH\text{-}2xFYVE}$. The time of EGF stimulation is indicated and EGFR levels were normalized to β-actin as indicated below.

3.5 Recruitment of LC3C to TECPR1$^{\Delta PH\text{-}2xFYVE}$ structures

To reveal whether TECPR1 is the dominant factor for the subcellular localization of hATG8s, the recruitment of hATG8 homologs was investigated using the mistargeting mutant TECPR1$^{\Delta PH\text{-}2xFYVE}$ that localizes to aberrant EEA1-positive structures. Therefore, RFP-TECPR1$^{\Delta PH\text{-}2xFYVE}$ was coexpressed with GFP-tagged hATG8s in TECPR1$^{-\backslash-}$ cells and the colocalization was quantified (**Figure 25**). A significant colocalization was only observed between RFP-TECPR1$^{\Delta PH\text{-}2xFYVE}$ and GFP-LC3C and not with other hATG8 family members, indicating that TECPR1$^{\Delta PH\text{-}2xFYVE}$ selectively recruits LC3C. Note that here again, bright GFP-LC3C puncta are juxtapositioned to large RFP-TECPR1$^{\Delta PH\text{-}2xFYVE}$ structures.

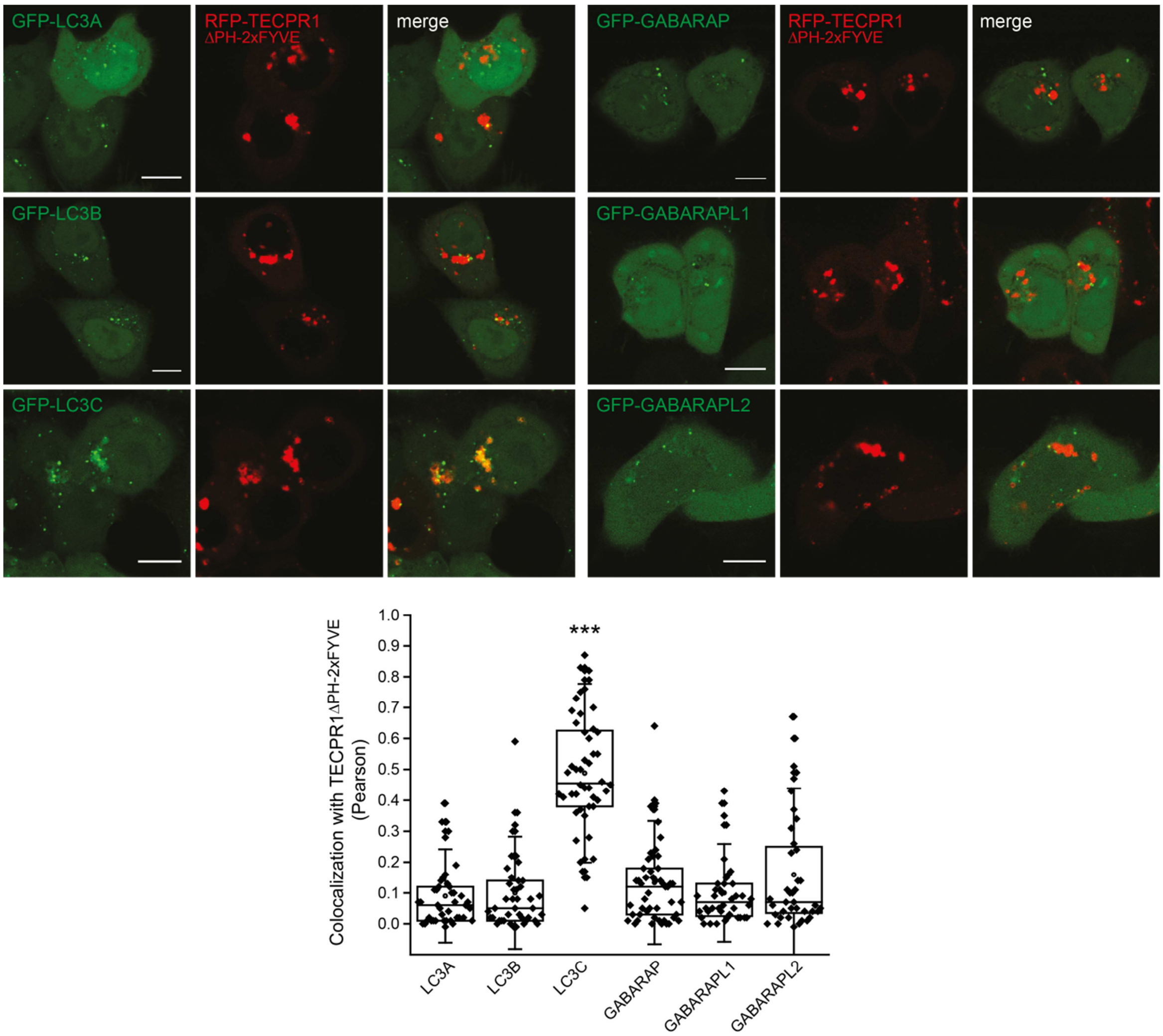
GFP-LC3A
RFP-TECPR1
ΔPH-2xFYVE
merge
GFP-GABARAP
RFP-TECPR1
ΔPH-2xFYVE
merge
GFP-LC3B
GFP-GABARAPL1
GFP-LC3C
GFP-GABARAPL2
Colocalization with TECPR1ΔPH-2xFYVE
(Pearson)
1.0
0.9
0.8
0.7
0.6
0.5
0.4
0.3
0.2
0.1
0.0
***
LC3A
LC3B
LC3C
GABARAP
GABARAPL1
GABARAPL2

Figure 25: Colocalization of hATG8s with TECPR1$^{\Delta PH\text{-}2xFYVE}$. HeLa TECPR1$^{-\backslash-}$ cells transiently expressing RFP-TECPR1$^{\Delta PH\text{-}2xFYVE}$ and GFP-tagged hATG8s were analyzed by live cell confocal microscopy. Colocalization was quantified using the Pearson coefficient (n > 40 cells). Scale bars, 10 µm.

To confirm that LC3C is indeed recruited to aberrant early endosomal structures by TECPR1$^{\Delta PH\text{-}2xFYVE}$, immunofluorescent staining for the early endosomal marker EEA1 was performed in TECPR1$^{-\backslash-}$ cells that were coexpressing GFP-LC3C and RFP-TECPR1 constructs (**Figure 26**). While GFP-LC3C did not colocalize with EEA1 in RFP-TECPR1^{wt}- or RFP-TECPR1$^{\Delta PH}$-expressing cells, colocalization with EEA1 was strongly increased when RFP-TECPR1$^{\Delta PH\text{-}2xFYVE}$ was expressed. This result confirms that LC3C is recruited to EEA1-positive structures by TECPR1$^{\Delta PH\text{-}2xFYVE}$. Note that again the distribution of EEA1 was drastically changed in RFP-TECPR1$^{\Delta PH\text{-}2xFYVE}$-expressing cells and only large EEA1 structures colocalized significantly with both RFP-TECPR1$^{\Delta PH\text{-}2xFYVE}$ and GFP-LC3C. Similar results were obtained in HEK293 cells, which excludes that the recruitment of LC3C by TECPR1$^{\Delta PH\text{-}2xFYVE}$ is a cell type-specific effect (**Figure 40 in the appendix**).

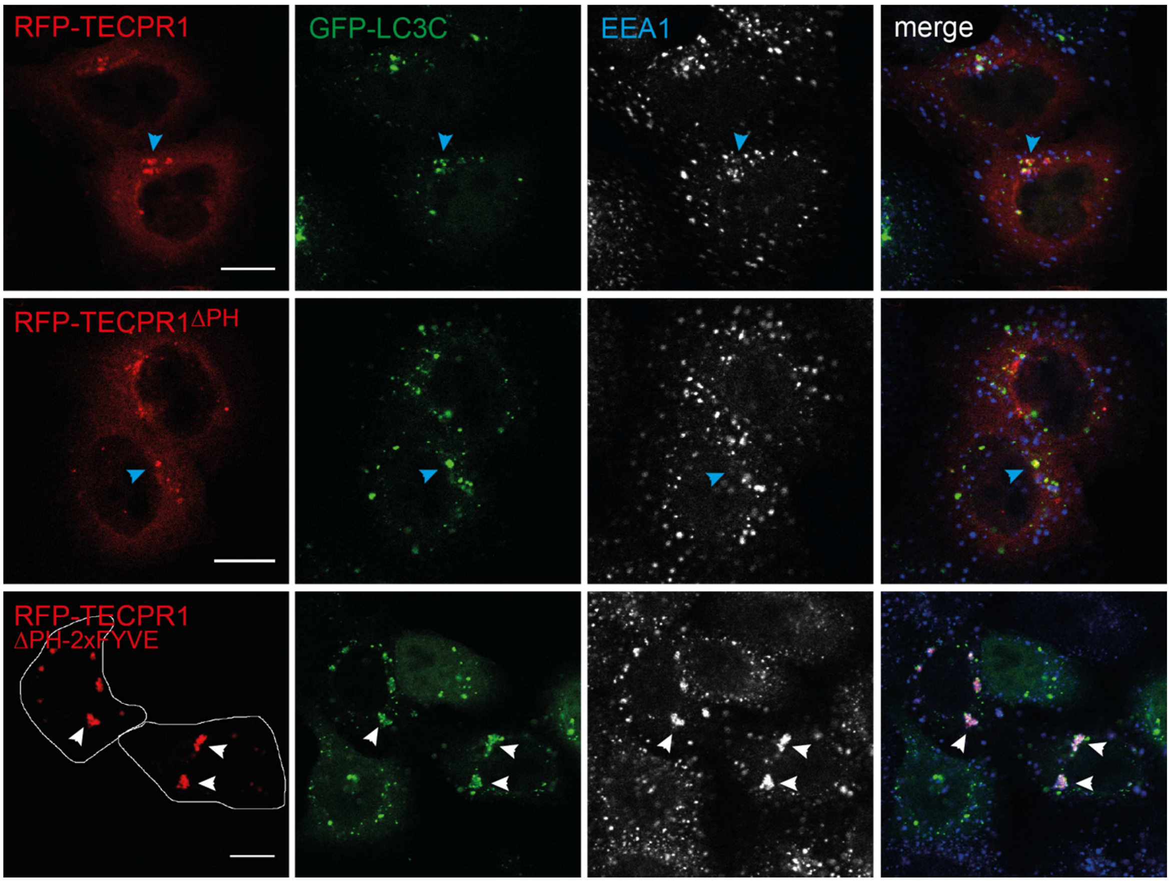

Figure 26: Recruitment of LC3C to EEA1-positive structures by TECPR1$^{\Delta PH\text{-}2xFYVE}$. Confocal images of HeLa TECPR1$^{-\backslash-}$ cells that were cotransfected with GFP-LC3C and RFP-TECPR1, RFP-TECPR1$^{\Delta PH}$, or RFP-TECPR1$^{\Delta PH\text{-}2xFYVE}$, starved for 2 hours and stained for EEA1 by immunofluorescence. Blue arrows indicate TECPR1 and LC3C structures that are not colocalizing with EEA1 and white arrows indicate colocalizing structures. Scale bars, 10 µm.

To reveal the nature of TECPR1$^{\Delta\text{PH-2xFYVE}}$-positive atypical endosomal compartments, which are positive for early and late endosomal markers, CLEM was performed to correlate GFP-TECPR1$^{\Delta\text{PH-2xFYVE}}$ fluorescence with organelles at an ultrastructural level (**Figure 27**). Strikingly, GFP-TECPR1$^{\Delta\text{PH-2xFYVE}}$ localized to the outer membrane of organelles that resemble MVBs. This strongly suggests that accumulated EEA1- and LAMP2-positive structures that were observed in immunofluorescent staining of TECPR1$^{\Delta\text{PH-2xFYVE}}$-expressing cells correspond to MVB-like compartments. Moreover, RFP-LC3C-positive electron-dense vesicles were observed in vicinity of TECPR1$^{\Delta\text{PH-2xFYVE}}$-positive MVBs. These LC3C-positive structures were often surrounded by either double membranes, typical for autophagosomes, or single membranes, which could correspond to amphisomes since they contain intraluminal vesicles.

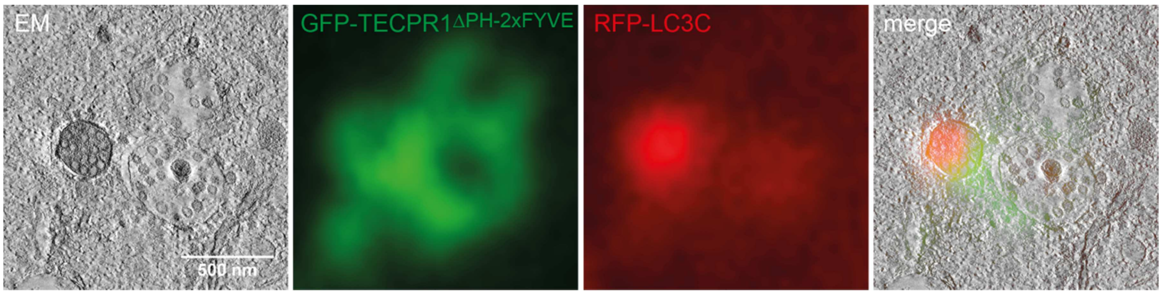

Figure 27: CLEM of HeLa TECPR1$^{-/-}$ cells transiently expressing GFP-TECPR1$^{\Delta\text{PH-2xFYVE}}$ and RFP-LC3C. Tomograms of 300 nm sections were acquired and one representative slice of the tomogram and the correlated fluorescent images are depicted here.

In this thesis, a LIR motif was identified and characterized in TECPR1 that is able to bind lipidated hATG8 proteins *in vitro* and is important for the recruitment of LC3C. To investigate whether mistargeting of LC3C by TECPR1$^{\Delta\text{PH-2xFYVE}}$ is influenced upon mutation of the LIR motif, the LIR mutants W175A, I178A, and W175A/I178A were analyzed for their ability to recruit LC3C to EEA1-positive structures. To exclude an effect of overexpression of fluorescently tagged LC3C, a non-selective LC3 antibody that recognizes all three LC3 subfamily members was used due to lack of a specific LC3C antibody. In TECPR1$^{-\backslash-}$ cells complemented with GFP-TECPR1$^{\Delta\text{PH-2xFYVE}}$, LC3 strongly colocalized with TECPR1$^{\Delta\text{PH-2xFYVE}}$ and EEA1, demonstrating that LC3-positive structures are recruited by TECPR1$^{\Delta\text{PH-2xFYVE}}$ to MVB-like compartments (**Figure 28**). Strikingly, the colocalization of LC3 with GFP-TECPR1$^{\Delta\text{PH-2xFYVE}}$ LIR mutants was significantly reduced, although these constructs still localized to EEA1-positive endosomes. This indicates that the W^{175}xxI^{178} LIR motif in TECPR1 is important for the recruitment of LC3 proteins. A similar observation was made with HA-tagged hATG8s that were coexpressed with a LIR mutant of GFP-TECPR1$^{\Delta\text{PH-2xFYVE}}$ in TECPR1$^{-/-}$ cells. None of the hATG8 homologs colocalized with the W175A/I178A LIR mutant (**Figure 41 in the appendix**). Notably, cells expressing TECPR1$^{\Delta\text{PH-2xFYVE}}$ LIR mutants exhibited smaller EEA1 structures compared to cells expressing TECPR1$^{\Delta\text{PH-2xFYVE}}$.

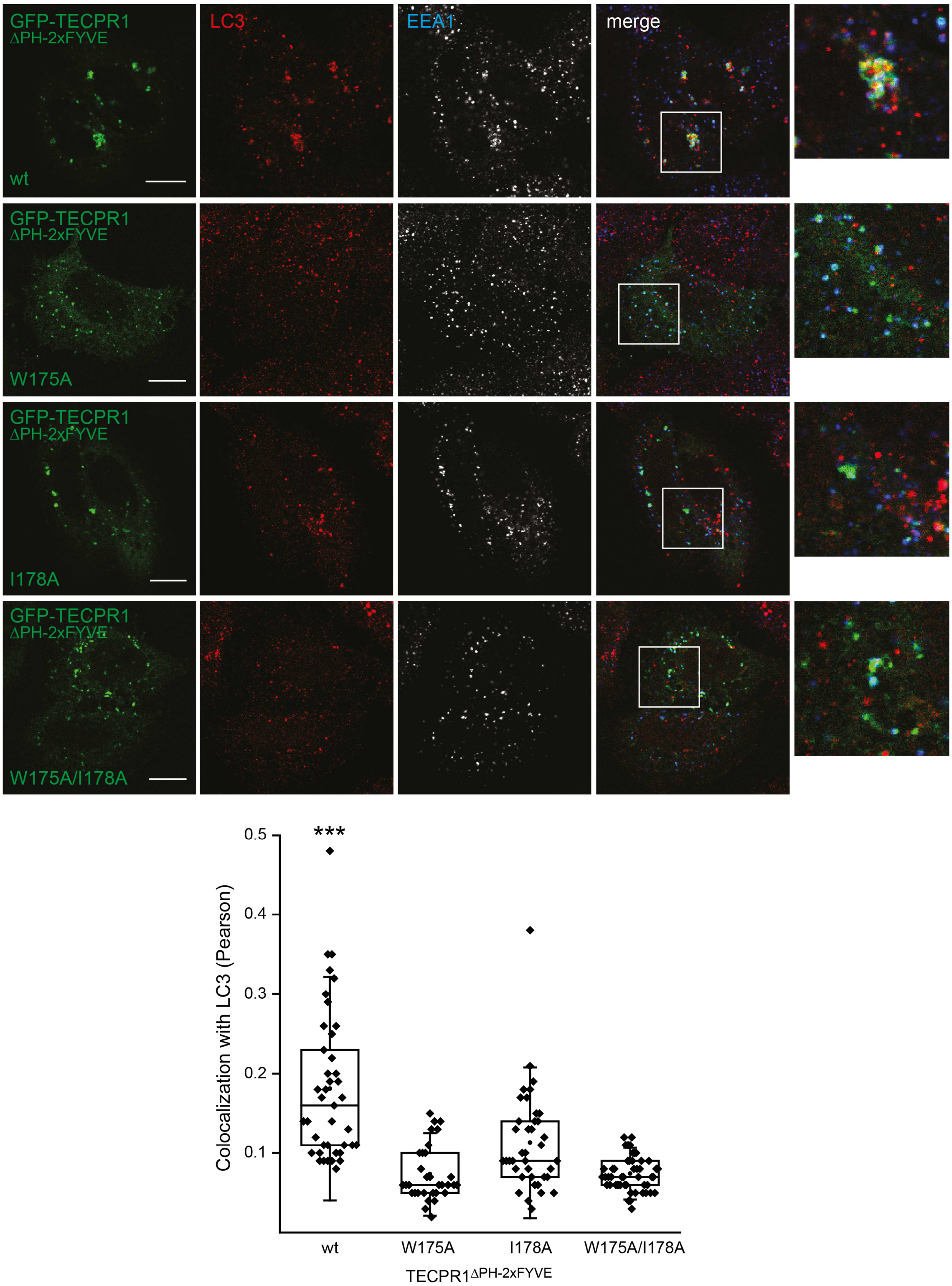
GFP-TECPR1
ΔPH-2xFYVE
LC3
EEA1
merge
wt
W175A
I178A
W175A/I178A
***
0.5
0.4
0.3
0.2
0.1
Colocalization with LC3 (Pearson)
wt
W175A
I178A
W175A/I178A
TECPR1ΔPH-2xFYVE

Figure 28: Recruitment of LC3 to TECPR1$^{\Delta PH\text{-}2xFYVE}$ LIR mutants. Confocal images of HeLa TECPR1$^{-/-}$ cells transiently expressing GFP-TECPR1$^{\Delta PH\text{-}2xFYVE}$ or the respective LIR mutants that were stained with anti-LC3 (M152-3) and anti-EEA1 by immunofluorescence. Selected regions of merged channels are cropped and enlarged. Colocalization between GFP-TECPR1$^{\Delta PH\text{-}2xFYVE}$ LIR mutants and endogenous LC3 was quantified using the Pearson coefficient (n > 30 cells). Scale bars, 10 µm.

Interestingly, GABARAPs were not observed to colocalize with or be in the vicinity of TECPR1$^{\Delta\text{PH-2xFYVE}}$ compartments. However, both TECPR1 and the GABARAPs are implemented in autophagosome-lysosome fusion. To investigate whether the GABARAPs are involved in the recruitment of LC3 to TECPR1$^{\Delta\text{PH-2xFYVE}}$-positive structures, an siRNA-mediated knockdown of the GABARAP subfamily (validation of siRNAs see **Figure 42 in the appendix**) was performed and colocalization of LC3 with GFP-TECPR1$^{\Delta\text{PH-2xFYVE}}$ was quantified (**Figure 29**). Notably, depletion of the GABARAPs resulted in increased colocalization, indicating that the GABARAPs are important in the turnover of LC3, likely by promoting autophagosome-lysosome fusion.

In summary, mistargeting of TECPR1 to EEA1- and LAMP2-positive MVBs selectively recruits LC3C-positive electron-dense autophagosome-, autolysosome-, and amphisome-like organelles to these structures. Furthermore, mutating the LIR motif W^{175}xxI^{178} in TECPR1$^{\Delta\text{PH-2xFYVE}}$ significantly reduces the recruitment of LC3, while depletion of the GABARAP subfamily increases colocalization between LC3 and TECPR1$^{\Delta\text{PH-2xFYVE}}$. These results strongly support the hypothesis that TECPR1 selectively recruits LC3C-positive autophagosomes to lysosomes.

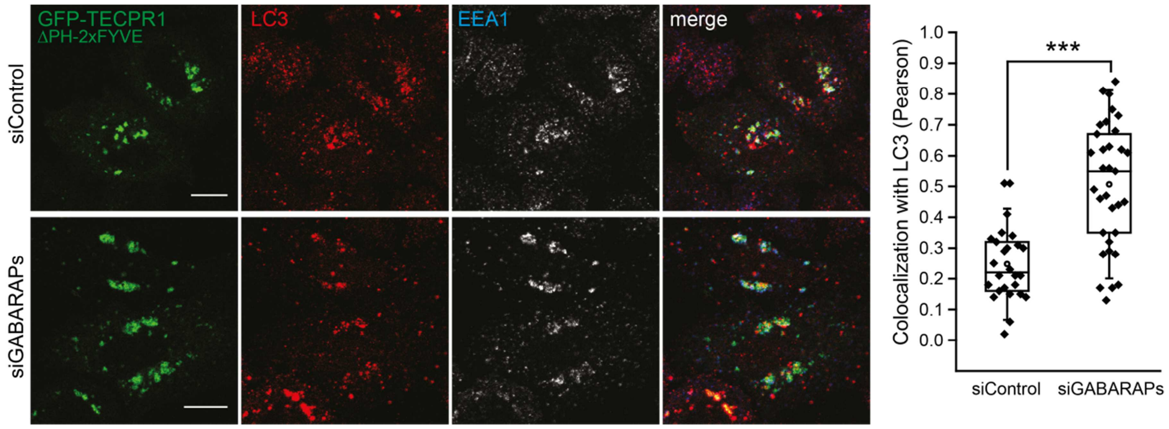

Figure 29: Involvement of GABARAPs in recruiting LC3 to EEA1-positive structures by TECPR1$^{\Delta\text{PH-2xFYVE}}$. HeLa TECPR1$^{-\backslash-}$ cells were transfected with indicated siRNAs and with GFP-TECPR1$^{\Delta\text{PH-2xFYVE}}$ and stained with anti-LC3 (M152-3) and anti-EEA1. Colocalization between GFP-TECPR1$^{\Delta\text{PH-2xFYVE}}$ and LC3 was quantified using the Pearson coefficient (n > 25 cells). Scale bars, 10 µm.

3.6 TECPR1 and hATG8 proteins in selective autophagy

TECPR1 has been implicated in selective types of autophagy, such as xenophagy, mitophagy, and aggrephagy (Ogawa et al., 2011). Additionally, the findings of this thesis suggest that TECPR1 functions in selective rather than non-selective autophagy since it was shown that TECPR1 selectively recruits LC3C-positive autophagosomes to lysosomes. To test whether the LC3C-positive compartments at TECPR1$^{\Delta\text{PH-2xFYVE}}$ structures contain specific autophagic cargo, such as mitochondria or peroxisomes, TECPR1$^{-\backslash-}$ cells coexpressing RFP-TECPR1$^{\Delta\text{PH-2xFYVE}}$ and GFP-LC3C were stained for the mitochondrial chaperonin Hsp60 or the peroxisomal membrane protein PMP70, respectively (**Figure 30A**). Both markers neither colocalized with GFP-LC3C nor with RFP-TECPR1$^{\Delta\text{PH-2xFYVE}}$, indicating that LC3C-positive autophagosomes do not enclose mitochondria or peroxisomes. The involvement of LC3C in PINK1/Parkin-mediated mitophagy was further excluded by monitoring the degradation of damaged mitochondria. Therefore, HEK293 cells were treated with CCCP, a reagent that depolarizes the inner mitochondrial membrane and thereby induces the degradation of damaged mitochondria via autophagy. Depletion of neither TECPR1 nor LC3C caused a significant accumulation of mitochondrial Hsp60, which is in agreement with the observation that LC3C-positive autophagosomes do not contain mitochondria (**Figure 30B**).

However, most LC3C puncta colocalized with ubiquitin (Ub) and the Ub-binding receptor p62. Although ubiquitin and p62 are markers for different kinds of autophagic cargo, the absence of mitochondrial or peroxisomal markers suggests that LC3C-positive structures contain ubiquitinated protein aggregates. This interpretation is further supported by CLEM experiments, which have shown that LC3C structures do not enclose mitochondria or peroxisomes, but electron-dense amorphous material, which likely corresponds to aggregated proteins (**Figure 13**). The same observation that GFP-LC3C puncta colocalize with p62 and ubiquitin was made in HEK293 cells (**Figure 40 in the appendix**) and confirms that LC3C-positive autophagosomes contain ubiquitinated cargo, which is independent of the used cell line.

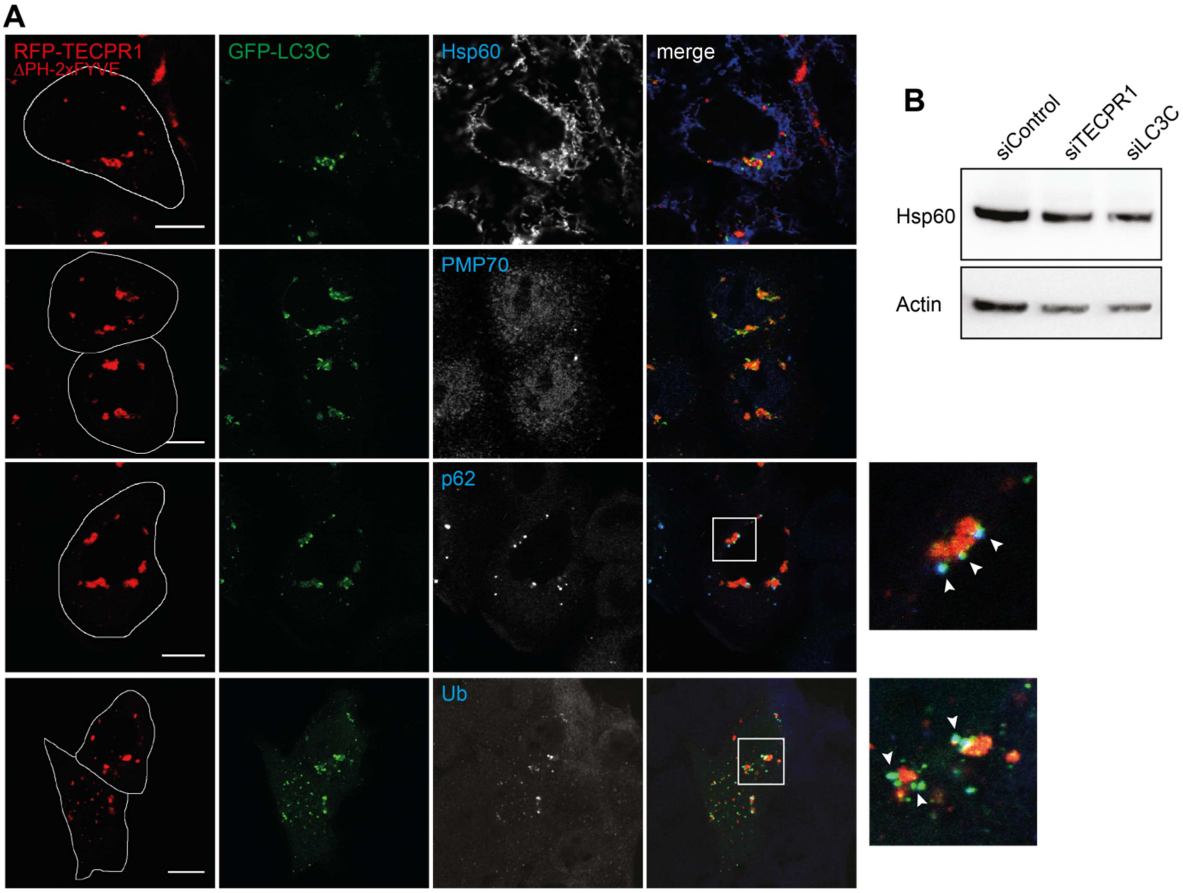

Figure 30: Colocalization of markers with LC3C at TECPR1$^{\Delta PH\text{-}2xFYVE}$ structures. **(A)** HeLa TECPR1$^{-\backslash-}$ cells were cotransfected with RFP-TECPR1$^{\Delta PH\text{-}2xFYVE}$ and GFP-LC3C and stained for Hsp60, PMP70, p62, and ubiquitin (Ub). Selected regions are cropped and enlarged. Arrows indicate GFP-LC3C puncta that colocalize with p62 or Ub at TECPR1$^{\Delta PH\text{-}2xFYVE}$ structures. Scale bars, 10 µm. **(B)** HEK293 cells were transfected with indicated siRNAs and treated with CCCP for 4 hours. Cell lysates were immunoblotted with anti-Hsp60 and anti-β-actin.

Recruitment of TECPR1 and hATG8s to protein aggregates

The ubiquitin-binding autophagy receptor p62 has been implicated in mitophagy, pexophagy, xenophagy, and aggrephagy (Rogov et al., 2014). The fact that LC3C-positive autophagosomes did not contain mitochondria or peroxisomes and the cells were not infected with pathogens suggests that LC3C-positive autophagosomes enclose protein aggregates. To test if TECPR1 and LC3C are involved in the formation or clearance of protein aggregates, TECPR1$^{-\backslash-}$ cells were cotransfected with RFP-TECPR1 and GFP-LC3C and protein aggregate formation was induced with puromycin, a translational inhibitor that leads to an accumulation of misfolded proteins. The immunofluorescent staining of these cells with anti-Ub and anti-p62 antibodies revealed that both TECPR1 and LC3C strongly colocalized with Ub- and p62-positive protein aggregates (**Figure 31**). While TECPR1 only localized to large Ub-positive aggregates, LC3C localized to almost all Ub-positive structures, suggesting that LC3C plays an important role in the autophagic clearance of aggregates. Interestingly, not only LC3C but all hATG8 homologs localized to protein aggregates and colocalized with TECPR1 at these structures (**Figure 43 in the appendix**). Hence, TECPR1, LC3C, and other hATG8 family members are recruited to protein aggregates.

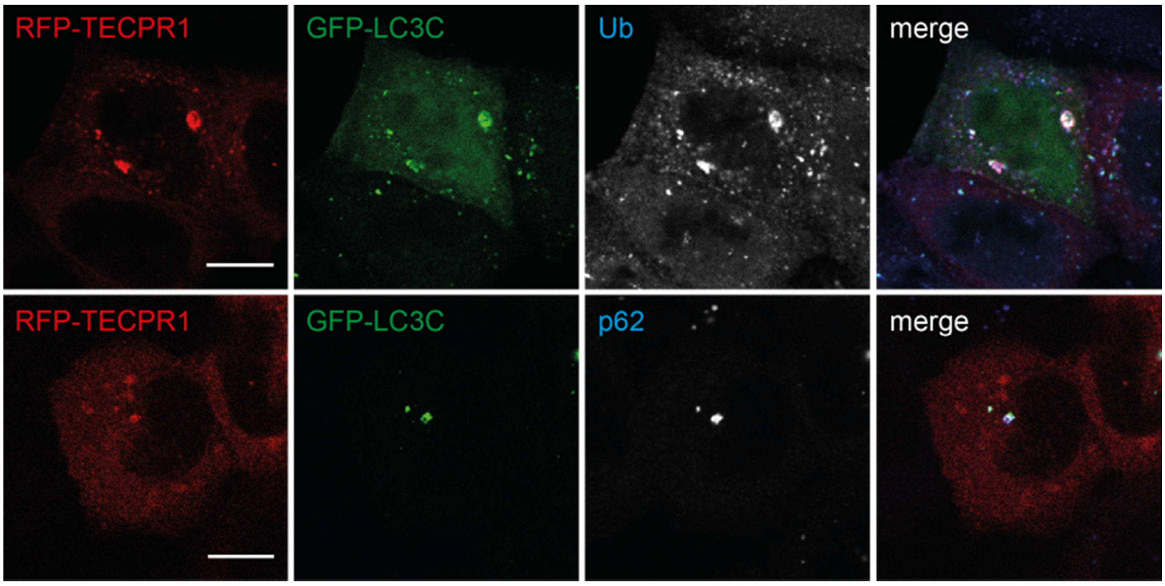

Figure 31: Recruitment of TECPR1 and LC3C to protein aggregates. HeLa TECPR1$^{-\backslash-}$ cells were cotransfected with RFP-TECPR1 and GFP-LC3C and aggregate formation was induced with puromycin for 2 hours. Cells were stained with anti-ubiquitin (Ub) and anti-p62 antibodies. Scale bars, 10 µm.

To test whether the recruitment of hATG8s and TECPR1 to protein aggregates depend on each other, either hATG8 proteins or TECPR1 were depleted and colocalization with protein aggregates was analyzed. When cells were treated with siRNAs against all hATG8 homologs simultaneously, GFP-tagged TECPR1 still localized to protein aggregates, indicating that TECPR1 recruitment to protein aggregates is independent of hATG8 proteins (**Figure 32A**). To examine whether the recruitment of LC3C and other hATG8 proteins depends on TECPR1, colocalization of GFP-tagged hATG8s with protein aggregates was analyzed in TECPR1 deficient cells (**Figure 32B**). Here again, the recruitment of hATG8s to cellular aggregates did not depend on TECPR1, since GFP-LC3B and GFP-LC3C colocalized strongly with ubiquitinated protein aggregates in TECPR1$^{-\backslash-}$ cells.

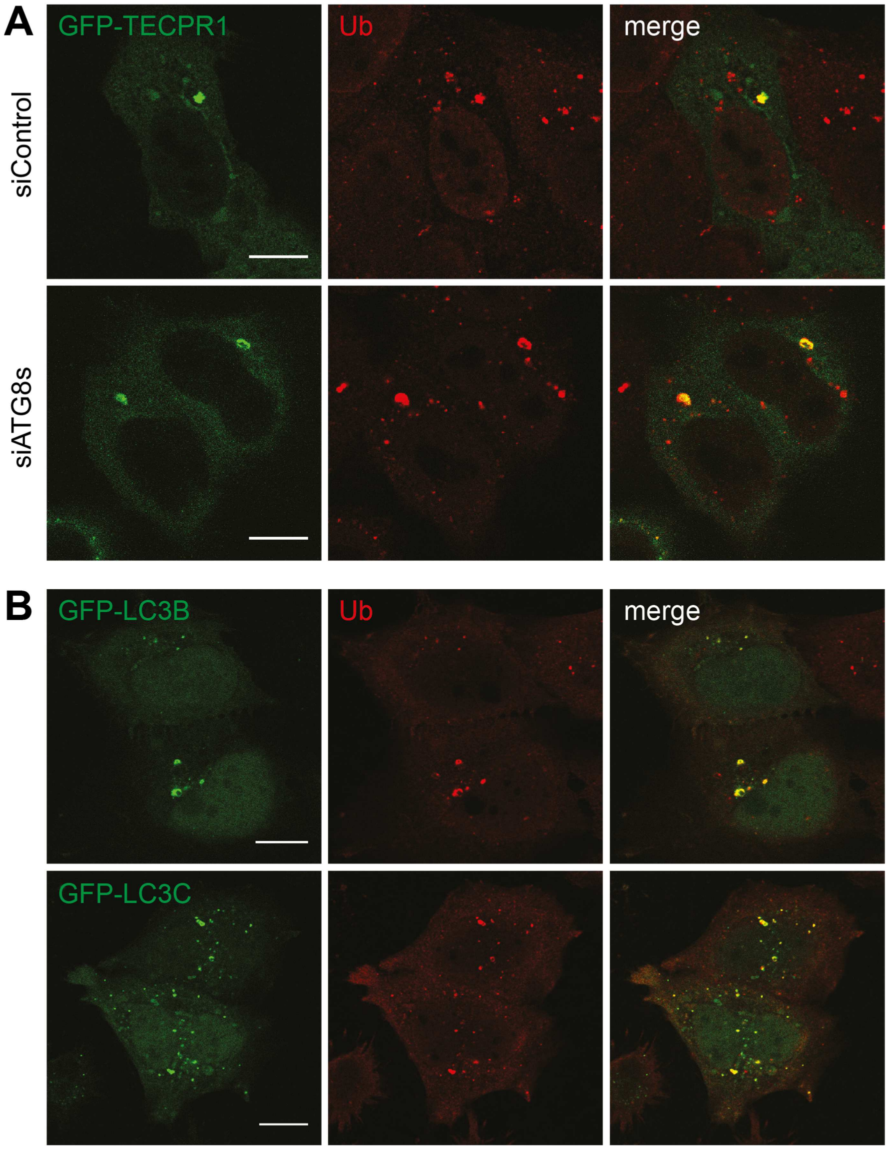

Figure 32: Recruitment of TECPR1 and hATG8 homologs to protein aggregates. **(A)** Confocal images of HeLa TECPR1$^{-\backslash-}$ cells that were transfected with indicated siRNAs and with GFP-TECPR1. Aggregate formation was induced with puromycin for 2 hours and cells were stained for ubiquitin (Ub) by immunofluorescence. **(B)** Confocal images of HeLa TECPR1$^{-\backslash-}$ cells that were transfected with GFP-LC3B or GFP-LC3C. Aggregate formation was induced with puromycin for 2 hours and cells were stained for ubiquitin (Ub) by immunofluorescence. Scale bars, 10 µm.

Autophagic clearance of protein aggregates involves targeting of misfolded proteins to lysosomes for their degradation. To analyze whether TECPR1-positive protein aggregates are targeted to lysosomes, TECPR1$^{-\backslash-}$ cells complemented with GFP-TECPR1 and induced with puromycin were stained for the lysosomal marker LAMP1. Strikingly, LAMP1 colocalized more with TECPR1-positive protein aggregates than with aggregates that were negative for GFP-TECPR1 (**Figure 33**). This suggests that TECPR1 is important for targeting of protein aggregates to lysosomes, thereby promoting autophagic removal of cellular aggregates.

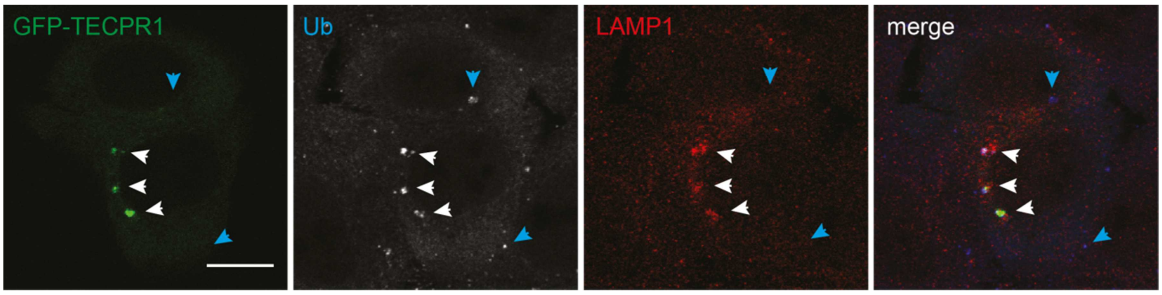

Figure 33: Colocalization of TECPR1 with protein aggregates and LAMP1. HeLa TECPR1$^{-\backslash-}$ cells were transfected with GFP-TECPR1. Formation of protein aggregates was induced with puromycin for 2 hours and cells were stained by immunofluorescence using anti-ubiquitin (Ub, Lys48 specific) and anti-LAMP1 antibodies. White arrows indicate Ub-aggregates that are positive for GFP-TECPR1 and LAMP1, while blue arrows indicate Ub-aggregates that are negative for GFP-TECPR1 and LAMP1. Scale bar, 10 µm.

Impact of TECPR1 and hATG8s on the clearance of protein aggregates

The recruitment of TECPR1 and hATG8 family members to protein aggregates suggests that they are involved in eliminating misfolded proteins. Thus, the impact of TECPR1, LC3C, and other hATG8 homologs on the clearance of protein aggregates was investigated. Protein aggregate formation was induced with puromycin and the clearance of protein aggregates was examined after removal of puromycin. In control wt cells, the number of protein aggregates was strongly reduced already four hours after puromycin withdrawal (**Figure 34A**). Knockdown of LC3A, LC3B, and LC3C simultaneously resulted in similar numbers of protein aggregates compared to control cells, indicating that LC3 subfamily members including LC3C are dispensable for the effective removal of protein aggregates (validation of siRNAs see **Figure 42 in the appendix**). Knockdown of the GABARAP subfamily, on the other hand, significantly increased the percent of cells containing large aggregates, immediately as well as four hours after removal of puromycin. This result indicates that the GABARAPs are essential for the elimination of protein aggregates and is consistent with observations of this thesis and of previous studies that suggested that GABARAP and not LC3 subfamily members are pivotal for autophagy, particularly for the fusion of autophagosomes with lysosomes (Szalai et al., 2015; Nguyen et al., 2016). Knockout of TECPR1 in HeLa cells, however, only slightly but not significantly increased the number of protein aggregates (**Figure 34B**). Moreover, there was no synergistic effect of hATG8 depletion and TECPR1 knockout, indicating that TECPR1 is not important for the clearance of protein aggregates under these conditions.

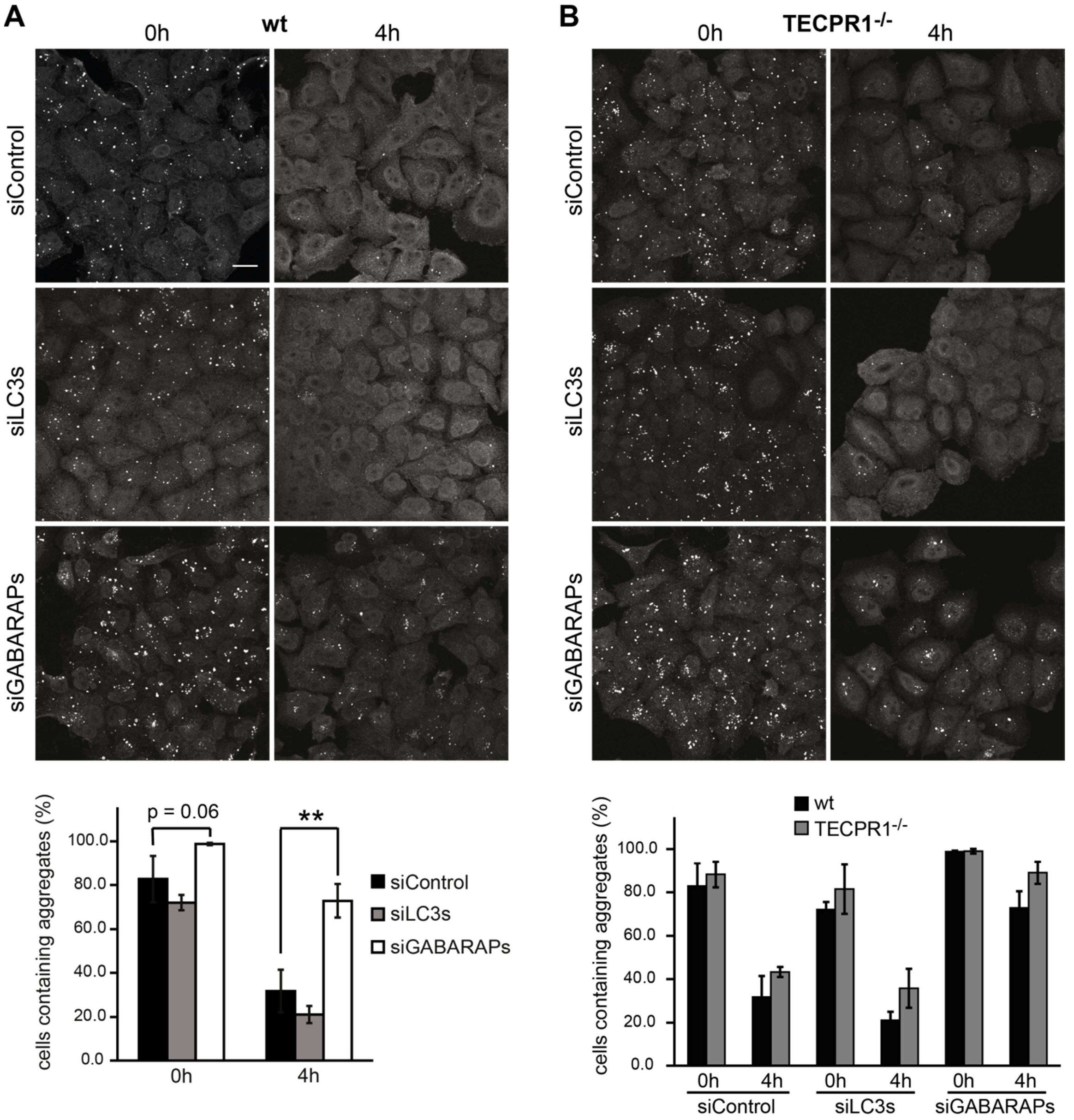

Figure 34: Effect of depletion of LC3 or GABARAP subfamilies on the clearance of protein aggregates in wt and TECPR1$^{-\backslash-}$ cells. HeLa wt **(A)** or TECPR1$^{-\backslash-}$ **(B)** cells were transfected with indicated siRNA pools and formation of protein aggregates was induced with puromycin for 4 hours. The time after removal of puromycin is indicated (0h and 4h). Cells were stained with anti-ubiquitin antibody by immunofluorescence, analyzed by confocal microscopy, and cells containing large aggregates were counted (n > 300 cells from 3 independent experiments). Scale bar, 20 µm.

The weak effect of TECPR1 knockout on the removal of aggregates suggests that either TECPR1 is not involved in aggregate clearance or there are mechanisms that compensate for its loss. To exclude that cells bypass TECPR1-mediated autophagic degradation of protein aggregates by enhanced proteasome activity, wt and TECPR1$^{-\backslash-}$ cells were incubated with the proteasome inhibitor MG132, which also leads to an accumulation of protein aggregates. Importantly, after eight hours of MG132 treatment, TECPR1$^{-\backslash-}$ cells contained more protein aggregates than wt cells, suggesting that TECPR1 plays a role in the clearance of protein aggregates via autophagy (**Figure 35**).

Collectively, these data show that TECPR1 and hATG8 proteins are recruited to protein aggregates and TECPR1 promotes targeting of these aggregates to lysosomes. Furthermore, aggregate clearance assays demonstrate that the GABARAPs are essential for eliminating protein aggregates in HeLa cells, whereas the LC3s as well as TECPR1 are less important. However, inhibition of the proteasome increases the impact of TECPR1 on the clearance of protein aggregates.

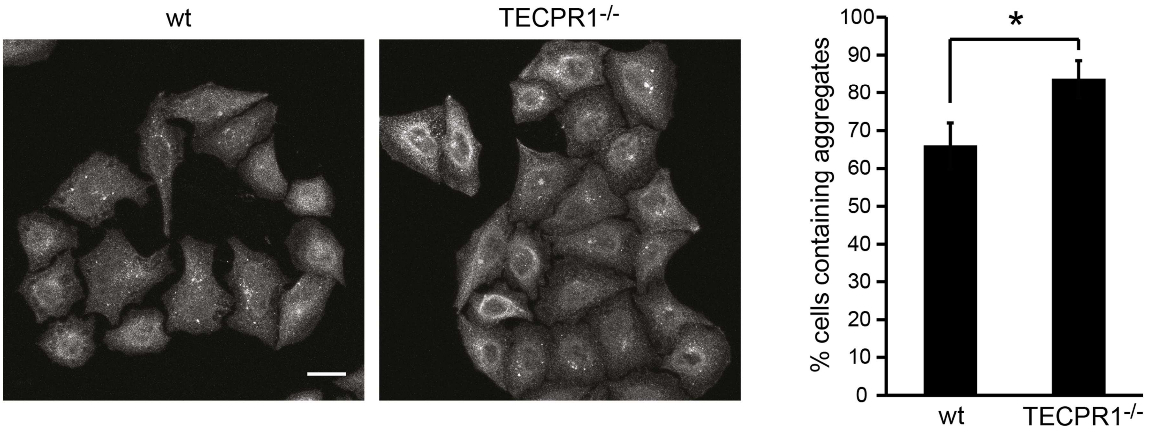

Figure 35: Aggregate formation with MG132 in wt and TECPR1$^{-\backslash-}$ cells. HeLa wt or TECPR1$^{-\backslash-}$ cells were incubated with MG132 for 8 hours, stained for ubiquitin by immunofluorescence, analyzed by confocal microscopy, and cells containing aggregates were counted (n > 250 cells from 3 independent experiments). Scale bar, 20 µm.

Interaction of TECPR1 with WDR81

The BEACH and WD40 repeat-containing protein WDR81 has recently been implicated in the removal of protein aggregates by interacting with p62 and LC3C (Liu et al., 2017). The study reported that loss of either WDR81 or LC3C causes an accumulation of ubiquitinated protein aggregates. Since it was shown here that TECPR1 recruits LC3C- and p62-positive structures, the question arose whether TECPR1 can interact and cooperate with WDR81 to eliminate misfolded proteins via autophagy. To answer this question, co-immunoprecipitation experiments were performed using TECPR1$^{-\backslash-}$ cells transiently expressing HA-tagged WDR81 and GFP-tagged TECPR1. HA-WDR81 indeed co-immunoprecipitated with GFP-TECPR1, suggesting that the two proteins interact (**Figure 36A**). In addition, GFP-tagged WDR81 colocalized strongly with RFP-tagged

TECPR1 and LC3C at ubiquitinated aggregates that were induced with puromycin (**Figure 36B**). This supports the finding that WDR81 interacts with TECPR1 and LC3C at protein aggregates and implies that WDR81, LC3C, and TECPR1 could cooperate to promote autophagic clearance of misfolded proteins.

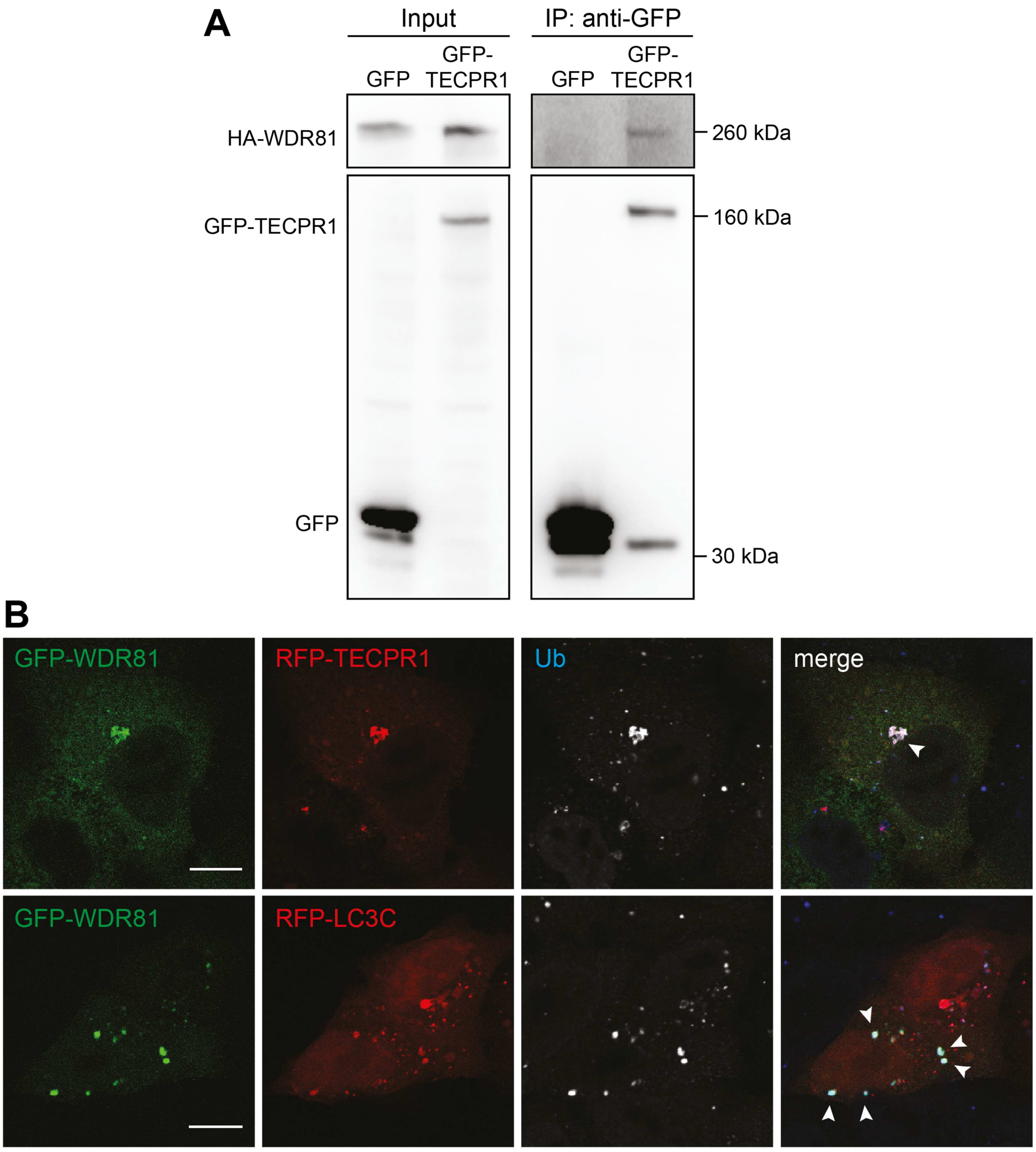
A
Input
IP: anti-GFP
GFP
GFP-TECPR1
GFP
GFP-TECPR1
HA-WDR81
GFP-TECPR1
GFP
260 kDa
160 kDa
30 kDa
B
GFP-WDR81
RFP-TECPR1
Ub
merge
GFP-WDR81
RFP-LC3C

Figure 36: Interaction of TECPR1 with WDR81. **(A)** Co-immunoprecipitation of HeLa TECPR1$^{-\backslash-}$ cells transiently expressing HA-WDR81 and GFP-TECPR1 or GFP, respectively, using a GFP-Trap. **(B)** Confocal images of HeLa cells that were transfected with GFP-WDR81 and RFP-TECPR1 or RFP-LC3C. Protein aggregates were induced with puromycin for 2 hours and cells were stained for ubiquitin (Ub) by immunofluorescence. Arrows indicate colocalizing structures. Scale bars, 10 µm.

4 DISCUSSION

Autophagy is a central recycling system of cells and thus essential to maintain cellular homeostasis and to respond to stress conditions. It prevents cells from accumulating damaged or dispensable material and protects organisms from diseases like cancer, infections, and neurodegeneration. Macroautophagy involves the formation of the autophagosome, a unique double-membraned compartment that encloses cytoplasmic material to deliver it to the lysosome (or the vacuole in yeast). During autophagosome formation, the ubiquitin-like conjugation of hATG8 proteins (Atg8 in yeast) to autophagosomal membranes plays an important role. The UBL conjugation cascade results in a covalent bond between hATG8 proteins and the lipid PE and its last step is catalyzed by the E3-like ATG12−ATG5 conjugate that can form complexes with either ATG16L1 or TECPR1. Although the mechanism of autophagosome biogenesis is well understood in yeast, the system in higher eukaryotes is more complex. Mammals often express multiple orthologs of yeast ATG proteins; for example there are six different hATG8 homologs that can be divided into LC3 and GABARAP subfamilies. Moreover, mammalian ATG proteins also exert autophagy-unrelated functions, like the GABARAPs, which are involved in intracellular trafficking. In addition, there is crosstalk between autophagy and other cellular pathways, which makes the mammalian system even more complex compared to yeast.

TECPR1 is a multidomain protein that lacks a yeast ortholog but has been implicated in mammalian autophagy. However, the function of TECPR1 in canonical autophagy is still unclear, since conflicting data have been published previously. One study reported that autophagosomes accumulate in absence of TECPR1, suggesting that TECPR1 is important for autophagosome maturation and fusion with lysosomes (Chen et al., 2012). On the contrary, another study observed the opposite effect of TECPR1 depletion on canonical autophagy, but found TECPR1 to be involved in selective types of autophagy (Ogawa et al., 2011). TECPR1 interacts with ATG12−ATG5 through a conserved AIR motif and the complex has been shown to be mutually exclusive from the ATG12−ATG5-ATG16L1 complex (Kim et al., 2015). However, the role of the ATG12−ATG5-TECPR1 complex remains largely unknown. One study suggested that the complex functions as tethering factor that joins autophagosomes with lysosomes (Chen et al., 2012), whereas another study speculated that it serves as adaptor for bacterial pathogens (Ogawa et al., 2011). Yet, the fact that ATG16L1 and TECPR1 bind to the same site in ATG5 through a conserved motif implies that TECPR1 plays a role in the hATG8 conjugation system, which has not been investigated in previous studies. Furthermore, the molecular mechanism of how TECPR1 promotes autophagosome-lysosome fusion, as well as autophagic degradation of selective cargo remains elusive.

To characterize the function of TECPR1 in autophagy, the following four questions were addressed in this thesis: (1) What is the impact of TECPR1 on the conjugation of the different hATG8 homologs compared to ATG16L1? (2) Does TECPR1 interact with specific hATG8 proteins? (3) What is the subcellular localization of TECPR1 and interacting hATG8 proteins and how are they targeted to the respective compartments? (4) What are the roles of TECPR1 and hATG8 proteins in selective types of autophagy, such as aggrephagy and mitophagy? To answer the first question, to what extent TECPR1 regulates the conjugation of the different hATG8 proteins to membranes, a combinatorial approach using *in vitro* reconstitution experiments and complementary *in vivo* studies was used. *In vitro* experiments required the production of recombinant ATG proteins and the lipidation reaction to be reconstituted on artificial membranes, while *in vivo* studies required CRISPR/Cas9-mediated knockout HeLa cell lines that are deficient for ATG16L1 or TECPR1. Based on these results, the second question, whether TECPR1 interacts with specific hATG8 homologs, was addressed. Potential interaction sites in TECPR1 were identified in *in vivo* colocalization experiments and *in vitro* binding assays using hATG8 proteins conjugated to artificial membranes. To answer the third question, what the subcellular localization of TECPR1 and interacting hATG8 proteins is, a combination of electron microscopy and immunofluorescence methods was used. In addition, mutagenesis of single TECPR1 domains was performed to reveal how TECPR1 is targeted to specific cellular membranes and compartments. Finally, the role of TECPR1 and hATG8 proteins in selective types of autophagy was defined by analyzing the colocalization of TECPR1 and hATG8s with selective cargo markers. Moreover, the influence of depletion of TECPR1 and hATG8 proteins on the clearance of aggregated proteins and damaged mitochondria was investigated.

4.1 The role of TECPR1 in the hATG8 conjugation system

Knockout of TECPR1 leads to an accumulation of LC3C and GABARAPL2 puncta

The interaction of TECPR1 with ATG5 has been confirmed by independent labs and has been further demonstrated to be mutually exclusive from the interaction of ATG16L1 with ATG5 (Ogawa et al., 2011; Chen et al., 2012; Kim et al., 2015). This implies that in addition to ATG16L1, TECPR1 is also involved in the UBL conjugation of hATG8 proteins. To test whether TECPR1 promotes lipidation of hATG8 proteins, hATG8 puncta formation was systematically analyzed in HeLa cells that are deficient for either TECPR1 (TECPR1$^{-/-}$) or ATG16L1 (ATG16L1$^{-/-}$). As expected, the number of GFP-tagged LC3A, LC3B, and LC3C puncta is drastically reduced in ATG16L1$^{-/-}$ cells. Moreover, the number of GFP-tagged GABARAP and GABARAPL1 puncta is also decreased, suggesting that ATG16L1 is essential for the recruitment of hATG8s to isolation membranes. Consistent with the reduction in hATG8 puncta, lipidation of LC3 family members is blocked in ATG16L1$^{-/-}$ cells, indicating that ATG16L1 is also essential for the lipidation of hATG8 proteins. In contrast to ATG16L1, knockout of TECPR1 does not influence the lipidation of hATG8 proteins. However, the number of GFP-LC3C and GFP-GABARAPL2 puncta are significantly increased in TECPR1$^{-/-}$ cells, while the number of other hATG8 proteins stays unchanged compared to wt cells. This indicates that either expression of LC3C and

GABARAPL2 is increased, or that the turnover of LC3C- and GABARAPL2-positive membranes is impaired upon knockout of TECPR1. Since TECPR1 has been implicated in later steps in autophagosome formation, particularly in fusion of autophagosomes with lysosomes (Chen et al., 2012; Kim et al., 2015), it appears likely that LC3C and GABARAPL2 puncta correspond to late autophagosomes that accumulate upon a block of fusion by knockout of TECPR1.

TECPR1 promotes conjugation of LC3C and GABARAP family members to artificial membranes

The selective accumulation of LC3C- and GABARAPL2-positive structures upon depletion of TECPR1 indicates that TECPR1 can interact with specific hATG8 proteins. To test whether TECPR1 indeed interacts with specific hATG8 proteins and to further investigate its function in the UBL conjugation system, the entire UBL conjugation cascade was reconstituted *in vitro* using recombinant proteins and artificial membranes. Previously, it has been shown that the E3-like ATG12−ATG5 conjugate needs to be activated by ATG16L1 to efficiently catalyze conjugation of hATG8s to PE on GUV membranes (Kaufmann, 2015). Here, it was further demonstrated that TECPR1 is also able to activate ATG12−ATG5 and, in contrast to ATG16L1, selectively promotes the lipidation of LC3C and the GABARAPs. This indicates that TECPR1 selectively recruits these hATG8 proteins to the membrane, thereby facilitating their conjugation to the membrane. However, depletion of TECPR1 in HeLa cells does not affect the lipidation of hATG8s but leads to a selective accumulation of LC3C and GABARAPL2 puncta. This discrepancy between *in vitro* and *in vivo* data implies that although TECPR1 does not promote hATG8 conjugation, TECPR1 can specifically interact with these hATG8 homologs.

Deletion of the ATG5 interaction site in TECPR1 does not alter its subcellular distribution

The fact that TECPR1 is dispensable for hATG8 lipidation raises the question: What is the function of the ATG12−ATG5-TECPR1 complex? The complex has been suggested to tether autophagosomes to lysosomes to regulate their fusion (Kim et al., 2015; Chen et al., 2012). Strikingly, it was shown in this thesis that deletion of the ATG5 interaction site in TECPR1 (TECPR1$^{\Delta AIR}$) does not change its subcellular localization. Instead, TECPR1$^{\Delta AIR}$ still localizes to lysosomes and colocalizes with LC3C, which excludes the possibility that the ability of TECPR1 to bind to lysosomal as well as LC3C-positive membranes depends on the interaction with ATG12−ATG5. Therefore, the physiological role of this interaction needs to be clarified in future experiments.

Taken together, the function of the interaction of TECPR1 with ATG12−ATG5 is still not completely understood. It was demonstrated in this thesis that TECPR1 can activate the E3-like ATG12−ATG5 conjugate, similarly to ATG16L1, and therefore promote the lipidation of LC3C and GABARAP proteins *in vitro*. The specificity of TECPR1 towards LC3C and GABARAP proteins strongly suggests that TECPR1 interacts with these hATG8 homologs and is consistent with the finding that TECPR1 is important for the turnover of LC3C- and GABARAPL2-positive membranes *in vivo*.

4.2 Interaction of TECPR1 with hATG8 proteins

TECPR1 interacts with lipidated LC3C and dynamically interacts with LC3C-positive compartments

The selective *in vitro* lipidation of LC3C by TECPR1 as well as the accumulation of LC3C puncta in TECPR1 depleted cells suggests that TECPR1 interacts with LC3C-positive compartments. However, an interaction between LC3C and TECPR1 could not be observed in pull-down or other *in vitro* assays, which raises the possibility that TECPR1 is recognizing only lipidated, and not soluble, LC3C. Indeed, PE-conjugated LC3C is recruited to TECPR1-positive artificial membranes, indicating that TECPR1 specifically recognizes LC3C in its lipidated form. Based on differential binding of antibodies to the lipidated versus unlipidated form, it has been suggested that Atg8 changes its conformation upon PE-conjugation (Nakatogawa et al., 2007). As a consequence, Atg8/hATG8 interaction partners are believed to have a preference for either the lipidated or unlipidated form and this hypothesis is supported by the data shown here. However, the mechanism of how exactly the lipidation state is recognized is still unclear and needs to be investigated in future studies.

Further evidence for the interaction of TECPR1 with LC3C is provided by the fact that LC3C puncta are often found in close proximity to TECPR1 structures. However, TECPR1 was not observed to co-immunoprecipitate with LC3C, indicating that this interaction may be transient. Moreover, some LC3C puncta dynamically contact TECPR1 structures or lysotracker-stained compartments, suggesting that there might be docking events between LC3C- and TECPR1-positive compartments that do not result in complete fusions of these vesicles. Alternatively, there might be kiss-and-run fusions of LC3C-positive autophagosomes with TECPR1-positive lysosomes, which result in a transfer of autophagosomal content to the lysosome while maintaining two separate vesicles. This kiss-and-run mechanism has been previously suggested to play a role in autophagosome-lysosome fusion (Jahreiss et al., 2008). Therefore, the data presented here propose that TECPR1-positive lysosomes and LC3C-positive compartments dynamically interact with each other.

TECPR1 possesses a LIR motif

TECPR1 possesses multiple domains, including two WD-repeat domains composed of β-propeller repeats (TR1 and TR2), two dysferlin motifs, a disordered DR domain, and a PH domain. In contrast to the DR domain and the C-terminal TR2 domain, the N-terminal TR1 domain, which contains four β-propeller repeats, colocalizes with lysosomal markers as well as with LC3C. Therefore, it appears likely that the TR1 domain can interact with LC3C and indeed a LIR motif was found in the N-terminal domain that binds to lipidated hATG8 homologs in floatation assays. Although *in vivo* TECPR1 is mainly found associated with LC3C and not with other hATG8 homologs, the isolated TECPR1 peptide containing the $W^{175}xxI^{178}$ LIR motif interacts with all hATG8 homologs to a similar extent. This suggests that TECPR1 recognizes additional regions in LC3C that provide specificity, a possibility that should be addressed in future experiments. Moreover, mutations in the LIR motif affect not only the colocalization with hATG8 proteins but also the cellular distribution of TECPR1, which implies that either the LIR mutant of TECPR1 is not functional or that TECPR1 needs to interact with LC3C or other hATG8 proteins to be targeted to the correct compartments.

In conclusion, this work shows that TECPR1 can interact with lipidated LC3C through a canonical LIR motif in the N-terminal domain of TECPR1. Furthermore, LC3C-positive compartments dynamically interact with TECPR1-positive structures, indicating that the interaction between TECPR1 and LC3C is transient.

4.3 Subcellular localization of TECPR1 and LC3C

TECPR1 localizes to (auto-)lysosomes

A previous study reported that TECPR1 localizes to early autophagosomal structures to target bacteria to autophagosomal membranes (Ogawa et al., 2011), while another study suggested that TECPR1 localizes to autolysosomes (Chen et al., 2012). To clarify the subcellular localization of TECPR1, CLEM was performed and revealed that large GFP-TECPR1 structures correspond to lysosomes or autolysosomes. Consistent with that finding, large GFP-TECPR1 structures colocalize with late endosomal and lysosomal markers in IF experiments. However, smaller TECPR1 puncta, which are negative for endosomal markers, are occasionally observed. In immuno-EM experiments, TECPR1 was found to localize to clusters of small vesicles, which could correspond to the small TECPR1 puncta observed in IF. TECPR1 has been reported to interact with the human TRAPPIII tethering complex (Behrends et al., 2010), which was recently shown to be important in ATG9 trafficking and in promoting autophagy (Lamb et al., 2016; Imai et al., 2016). Moreover, it was shown here that TECPR1 colocalizes with ATG9 and partially with the TGN marker TGN46 and the recycling endosomal marker Rab11A, which both have been associated with ATG9 vesicles (Young et al., 2006; Orsi et al., 2012). Hence, small TECPR1 puncta that are negative for endosomal markers could be involved in trafficking of ATG9 vesicles.

The PH domain binds to PtdIns(4)P and targets TECPR1 to lysosomal membranes

The interaction with ATG12–ATG5 has been suggested to allow TECPR1 to bind to the lipid PtdIns(3)P (Chen et al., 2012). Here, however, TECPR1 was not found associated with PtdIns(3)P, neither at PtdIns(3)P-positive artificial membranes, nor at PtdIns(3)P-rich membranes in HeLa cells. Instead, TECPR1 exhibits a strong affinity for PtdIns(4)P-positive membranes both, *in vitro* and *in vivo*. This observation is in agreement with the localization of TECPR1 to lysosomes, which have been reported to be rich in PtdIns(4)P but not PtdIns(3)P (Jeschke et al., 2015). PtdIns(4)P is essential to preserve lysosomal identity, since the absence of the PtdIns(4)P-generating PI4KIIIβ results in abnormal formation of lysosomal tubules and unwanted lysosomal efflux (Sridhar et al., 2013). Moreover, the conversion of PtdIns(4)P to PtdIns(4,5)P_2 regulates autophagic lysosome reformation and is therefore important to maintain lysosome homeostasis (Rong et al., 2012). In addition, the generation of PtdIns(4)P on autophagosomes has been suggested to be important for the fusion of autophagosomes with lysosomes (Wang et al., 2015). Therefore, the localization of TECPR1 to PtdIns(4)P on lysosomal membranes might play a role in fusion and fission events that involve lysosomal membranes. Furthermore, it was shown in this thesis that, to a certain extent, the phosphoinositide-binding PH domain targets TECPR1 to PtdIns(4)P-positive and lysosomal membranes. However, TECPR1$^{\Delta PH}$ is still partly colocalizing with PtdIns(4)P and lysosomal markers. Moreover, the N-terminal TR1 domain that lacks the PH domain is, like full-length TECPR1, strongly colocalizing with lysosomal and late endosomal markers. Thus, the interaction of the PH domain with PtdIns(4)P cannot be the only mechanism through which TECPR1 is targeted to lysosomes. The involvement of the TR1 domain in targeting TECPR1 to lysosomal membranes should therefore be investigated further.

Replacing the PH domain of TECPR1 by a tandem FYVE domain mistargets TECPR1 to MVBs

To investigate the impact of the PtdIns(4)P-binding PH domain on the localization of TECPR1 further, the PH domain was replaced by two repeats of the PtdIns(3)P-binding FYVE domain to generate TECPR1$^{\Delta PH\text{-}2xFYVE}$. The replacement of these phosphoinositide-binding domains results in mistargeting of TECPR1 to the outer membrane of MVB-like organelles. Surprisingly, these compartments are positive for all tested endosomal markers, from early endosomal markers EEA1 and Rab5 to late endosomal and lysosomal markers Rab7 and LAMP2, respectively. Moreover, TECPR1$^{\Delta PH\text{-}2xFYVE}$ colocalizes with PtdIns(3)P and PtdIns(4)P as well as with lysotracker, which labels acidified compartments. Thus, the conventional transition from Rab5- to Rab7-positive endosomes is not observed in TECPR1$^{\Delta PH\text{-}2xFYVE}$-expressing cells, suggesting that maturation and sorting of MVBs is impaired. This would in turn imply that TECPR1$^{\Delta PH\text{-}2xFYVE}$ dramatically interferes with the endocytic pathway. Therefore, the effect of TECPR1$^{\Delta PH\text{-}2xFYVE}$ expression in TECPR1$^{-/-}$ cells on the degradation of EGFR was investigated. Strikingly, EGFR degradation is not affected in TECPR1$^{\Delta PH\text{-}2xFYVE}$-expressing cells, which indicates that the endocytic system is still functional. Thus, it appears likely that functional endosomes coexist with TECPR1$^{\Delta PH\text{-}2xFYVE}$-induced aberrant MVBs. Importantly, it was demonstrated in this work that expression of TECPR1$^{\Delta PH\text{-}2xFYVE}$ also recruits LC3C-positive compartments to these aberrant EEA1-positive endosomes. The selectivity of this recruitment demonstrates that TECPR1 dictates the subcellular localization of LC3C and strongly suggests that TECPR1 directly interacts with LC3C.

LC3C localizes to a large number of electron-dense structures and colocalizes with STX17 and ubiquitin

Since LC3C-positive compartments are selectively recruited by TECPR1$^{\Delta PH\text{-}2xFYVE}$, it was of eminent importance to reveal the nature of these LC3C-positive structures. Interestingly, the number of GFP-LC3C puncta in HeLa cells exceeds the number of GFP-LC3B or GFP-LC3A puncta by more than two fold. Since LC3C has been mainly implicated in selective types of autophagy, such as xenophagy, mitophagy, and aggrephagy (von Muhlinen et al., 2012; Liu et al., 2017; Le Guerroué et al., 2017) as well as in maintaining functional ER exit sites (Stadel et al., 2015), many LC3C puncta do not correspond to canonical autophagosomes. Surprisingly, although LC3C has been reported to play a role in basal PINK1/Parkin-independent mitophagy, the majority of LC3C puncta does not colocalize with mitochondrial markers in HeLa cells. Instead, most LC3C structures are positive for ubiquitin and the ubiquitin-binding autophagy receptor p62 as well as for the late autophagosomal marker STX17, the SNARE that localizes to the outer membrane of completed autophagosomes and promotes fusion with lysosomes (Itakura et al., 2012). The colocalization of LC3C with these marker proteins suggests that LC3C-positive structures correspond to late autophagosomes that contain ubiquitinated cargo. Importantly, CLEM experiments revealed that LC3C almost exclusively localizes to electron-dense structures, many of which resemble autophagosomes, amphisomes, and autolysosomes. This indicates that LC3C-positive compartments contain aggregated proteins and therefore strongly supports the hypothesis that LC3C plays a role in aggrephagy.

The specific localization of LC3C to protein aggregates would further suggest that LC3C is mediating the selective engulfment of protein aggregates by autophagosomal membranes. Similar to this theory, LC3C has been reported to be involved in the selective targeting of intracellular bacteria into autophagosomes by binding to the autophagy receptor NDP52 (von Muhlinen et al., 2012). If LC3C was mediating the selective engulfment of protein aggregates, LC3C would have to be conjugated to the inner membrane of the autophagosome to bind to selective receptors. However, it was shown here that, using an RFP-GFP-hATG8 reporter in absence of intracellular pathogens, the majority of LC3C, GABARAP and GABARAPL2 is not transported into lysosomes, suggesting that these proteins are mainly attached to the outer membrane of autophagosomes. Since only a small fraction of LC3C puncta colocalizes with lysosomal markers, the majority of LC3C does not remain on the membrane of autolysosomes after fusion. This implies that LC3C could be recycled by ATG4 proteins before LC3C-positive autophagosomes fuse with lysosomes, a possibility that should be analyzed in future studies. Importantly, LC3C and other hATG8 homologs that are present at the outer membrane of autophagosomes can potentially interact with proteins on other membrane compartments, which could be important for the recruitment of autophagosomes to lysosomes. Thus, the precise mechanism of how aggregated proteins are selectively targeted into the lumen of LC3C-positive autophagosomes remains elusive and needs to be investigated in future studies.

4.4 The role of TECPR1 and LC3C in selective autophagy

TECPR1 is involved in the clearance of protein aggregates

The role of TECPR1 in canonical autophagy, which involves the lipidation and turnover of LC3B, is still a matter of debate. On the one hand, it was reported that autophagosomes accumulate in TECPR1 depleted cells (Chen et al., 2012), while on the other hand, it was published that LC3B-II levels are slightly decreased when TECPR1 is depleted (Ogawa et al., 2011). Consistent with the latter study, it was shown here that the level of LC3B-II is slightly but not significantly reduced in HeLa TECPR1$^{-\backslash-}$ cells in absence and presence of Bafilomycin A1, suggesting that TECPR1 is dispensable for canonical autophagy.

Both TECPR1 and LC3C have been implicated in various types of selective autophagy. It was shown that the removal of intracellular bacteria, damaged mitochondria, and protein aggregates was reduced in TECPR1$^{-/-}$ mouse embryonic fibroblasts (Ogawa et al., 2011). Furthermore, LC3C has been shown to be important for the clearance of intracellular bacteria (von Muhlinen et al., 2012), mitochondria (Le Guerroué et al., 2017), as well as protein aggregates (Liu et al., 2017). However, in this thesis it was demonstrated that depletion of LC3C or TECPR1 has at most a minor effect on the degradation of damaged mitochondria and protein aggregates. Consistent with a previous study that suggested that the GABARAPs and not the LC3s are important for autophagosome maturation and fusion with lysosomes (Nguyen et al., 2016), it was observed in this thesis that knockdown of the GABARAP subfamily but not of the LC3 subfamily results in impaired clearance of protein aggregates. This suggests that the GABARAPs can compensate for the loss of LC3 subfamily members. Moreover, depletion of the GABARAP subfamily increases the colocalization between LC3 and TECPR1$^{\Delta PH\text{-}2xFYVE}$, which indicates that the turnover of LC3 proteins is impaired and is consistent with the assumption that GABARAP proteins are essential for autophagosome-lysosome fusion.

Only when TECPR1$^{-/-}$ HeLa cells are treated with the proteasome inhibitor MG132 do protein aggregates significantly accumulate compared to wt cells, indicating that the cells can compensate for the loss of TECPR1-mediated autophagic clearance of aggregates by proteasomal activity. Generally, fusion of autophagosomes with lysosomes requires the Rab7 effector and tethering complex HOPS, as well as SNARE proteins. Therefore, knockout of TECPR1 might be compensated by other tethering factors like the HOPS complex. However, LC3C and TECPR1 both localize to puromycin-induced protein aggregates, which strongly implies that they function in the removal of these aggregates. Moreover, LC3C-positive autophagosomes that contain electron-dense material are recruited by TECPR1 variants, supporting the hypothesis that TECPR1 and LC3C are involved in the clearance of protein aggregates through autophagy.

A recent study has reported that the BEACH and WD40 repeat-containing protein WDR81 is involved in the elimination of aggregated proteins by interacting with p62 and LC3C (Liu et al., 2017). Since TECPR1 is also found associated with LC3C- and p62-positive autophagosomes, its interaction and colocalization with WDR81 was investigated. Strikingly, TECPR1 and LC3C colocalize with WDR81 at protein aggregates and TECPR1 interacts with WDR81 in co-immunoprecipitations. WDR81 could therefore mediate the recruitment of TECPR1 to p62-positive protein aggregates. This further suggests that TECPR1 could cooperate with WDR81 in an LC3C-dependent manner to promote clearance of protein aggregates, which should be further analyzed.

Collectively, the results obtained in this thesis suggest a new model for the role of TECPR1 in autophagic clearance of protein aggregates (**Figure 37**). TECPR1 resides on lysosomal membranes, where it binds to PtdIns(4)P via its PH domain and selectively recruits LC3C-positive autophagosomes via a canonical LIR motif. LC3C-positive autophagosomes contain ubiquitin- and p62-positive protein aggregates that are delivered to the lysosome after being recruited by TECPR1. Therefore, TECPR1 and LC3C cooperate to promote clearance of protein aggregates through autophagy.

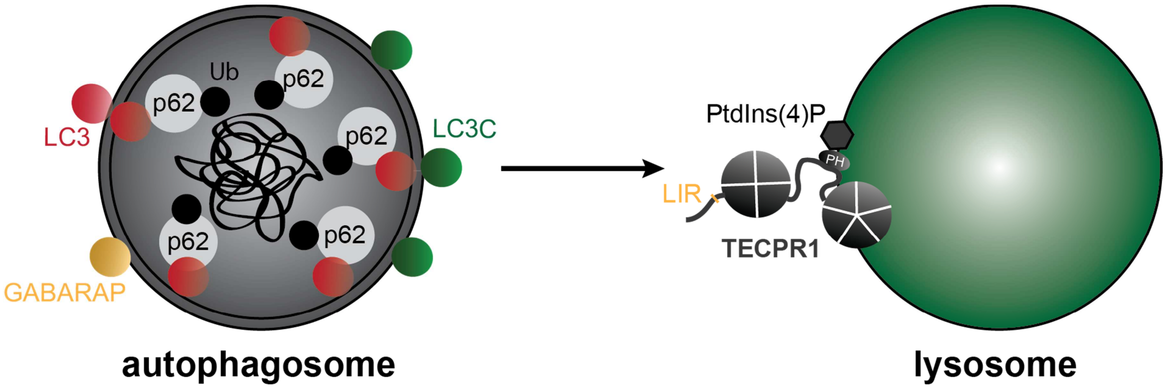

Figure 37: Proposed model for the role of TECPR1 in autophagic clearance of protein aggregates. TECPR1 binds to PtdIns(4)P at the lysosomal membrane and specifically recruits LC3C-positive autophagosomes to lysosomes via a LIR motif in TECPR1. The recruitment of these LC3C-positive autophagosomes that contain ubiquitin (Ub)- and p62-positive protein aggregates by TECPR1 thus promotes clearance of protein aggregates.

5 OUTLOOK

This thesis provided evidence of a novel role of TECPR1 in the clearance of protein aggregates through autophagy. TECPR1 closely cooperates with LC3C to recruit selective autophagosomes that enclose aggregated proteins to lysosomes and therefore promotes their degradation. Despite the provided details about the molecular mechanism of TECPR1- and LC3C-mediated aggrephagy, there are open questions that need to be addressed in the future.

The nature of large and bright structures of fluorescently tagged TECPR1 has been well described in this thesis. However, smaller TECPR1 puncta are occasionally observed that do not colocalize with endosomal markers and could not be detected in CLEM, probably due to their limited fluorescent intensity. Thus, these small TECPR1 structures should be characterized in further studies. To identify more interaction partners of TECPR1 and its domains, MS analysis could be performed and for example reveal how the N-terminal TR1 domain targets TECPR1 to lysosomal membranes. In addition, interactions between TECPR1 and previously reported TECPR1-binding proteins, like the human TRAPPIII tethering complex (Behrends et al., 2010), need to be validated and characterized.

It was demonstrated in this thesis that TECPR1 selectively recruits LC3C, which depends on the LIR motif in TECPR1. However, a direct interaction was not observed, likely due to a transient interaction between the two proteins as well as the membrane anchoring of LC3C, which makes interactions difficult to study. Therefore, alternative methods should be used that can detect transient interactions and be applied to insoluble proteins. One of these methods is BioID, which is based on biotinylation of neighboring proteins by a biotin ligase fused to the protein of interest. Moreover, the interaction between TECPR1 and LC3C should be further characterized by mapping the binding site in LC3C, for example by mutational analysis. This could also reveal the molecular details of how TECPR1 selectively recognizes LC3C.

To investigate the function of TECPR1 and the hATG8 proteins *in vivo*, they were cloned together with fluorescent or affinity tags into mammalian expression vectors harboring a CMV promoter and transfected into HeLa or HEK293 cells. However, fusion of proteins with large tags as well as overexpression of the proteins can dramatically change their biochemical properties. Therefore, specific antibodies should be used to analyze the subcellular localization as well as the levels of endogenous proteins. Yet, there are no antibodies available that reliably distinguish between the homologs of the LC3 subfamily or specifically recognize TECPR1. A solution to this issue would be to genetically tag the proteins of interest by using CRISPR/Cas9 gene editing, which allows for the expression of proteins at their physiological levels.

It is still unclear how exactly protein aggregates are recognized by the autophagic machinery. Although autophagy receptors, including p62 and OPTN, are involved in aggrephagy, they are also known to recognize other ubiquitinated autophagic substrates, like outer mitochondrial membrane proteins (Rogov et al., 2014). Thus, the selective engulfment of aggregated proteins by autophagosomal membranes cannot be explained by the presence of currently identified autophagy receptors. Moreover, although LC3C almost exclusively localizes to electron-dense structures, the majority of LC3C is not transported into the lysosome, suggesting that it does not mediate tethering of protein aggregates to autophagosomal membranes. Therefore, it is important to identify the factors that recognize and target protein aggregates into the autophagosomal lumen, for example by MS analysis, which allows for detection of the interactome of aggregated proteins.

The model system used in this thesis is adequate for investigating principle mechanisms in autophagy. However, cell lines that are more relevant for diseases should be used in the future to analyze how toxic protein aggregates are recognized and cleared through autophagy. Since aggrephagy is mainly related to neurodegenerative diseases, such as amyotrophic lateral sclerosis (ALS) or Huntington's disease, neuronal cell lines, patient cells, or mouse models should be used to investigate the removal of physiological relevant protein aggregates. Moreover, different aggregate-prone proteins cause different neurodegenerative diseases, for example amyloid beta is involved in Altzheimer's disease and alpha-synuclein in Parkinson's disease. It would be of peculiar interest whether the here identified TECPR1- and LC3C-mediated mechanism also plays a role in the clearance of disease-related protein aggregates. Therefore, the recruitment of TECPR1 and LC3C to specific protein aggregates of cells derived from patients and the effect on the elimination of these aggregates should be investigated. Furthermore, the identification of additional factors that recognize and target specific protein aggregates to autophagosomes could provide new therapeutic targets.

6 APPENDIX

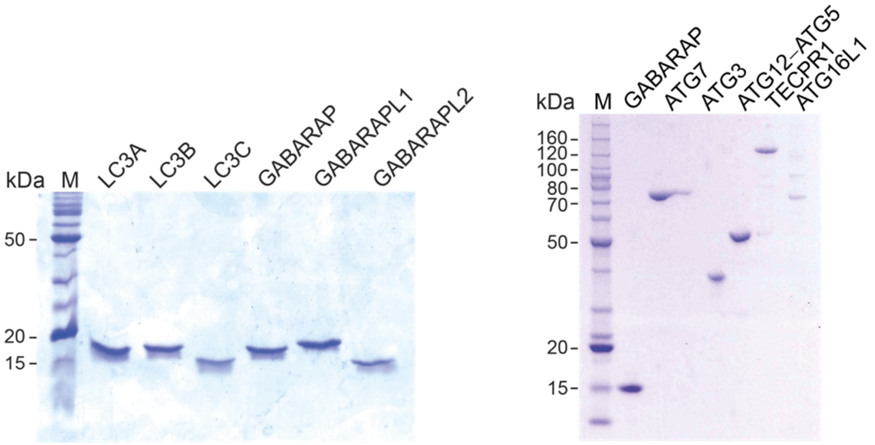
kDa
M
LC3A
LC3B
LC3C
GABARAP
GABARAPL1
GABARAPL2
50
20
15
kDa
M
GABARAP
ATG7
ATG3
ATG12–ATG5
TECPR1
ATG16L1
160
120
100
80
70
50
20
15

Figure 38: Recombinant proteins used for *in vitro* experiments.

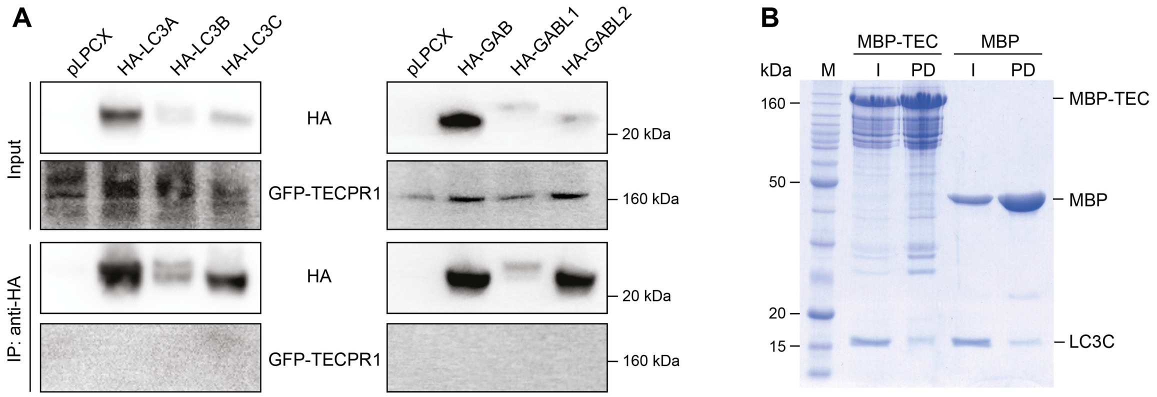
A
pLPCX
HA-LC3A
HA-LC3B
HA-LC3C
pLPCX
HA-GAB
HA-GABL1
HA-GABL2
Input
IP: anti-HA
HA
GFP-TECPR1
HA
GFP-TECPR1
20 kDa
160 kDa
20 kDa
160 kDa
B
MBP-TEC
MBP
kDa
M
I
PD
I
PD
160
50
20
15
MBP-TEC
MBP
LC3C

Figure 39: Co-immunoprecipitation and *in vitro* pull-down assay with TECPR1 and hATG8 proteins. **(A)** HeLa TECPR1$^{-/-}$ cells were cotransfected with GFP-TECPR1 and HA-tagged hATG8s or the empty pLPCX vector, respectively. Co-immunoprecipitation was performed using anti-HA affinity matrix and samples were immunoblotted with anti-HA and anti-GFP antibodies. **(B)** His$_6$-MBP-tagged TECPR1 (MBP-TEC) or His$_6$-MBP (MBP) was incubated together with LC3C and Ni-NTA agarose beads. Input (I) and pull-down (PD) samples were subjected to SDS-PAGE and stained with coomassie staining solution.

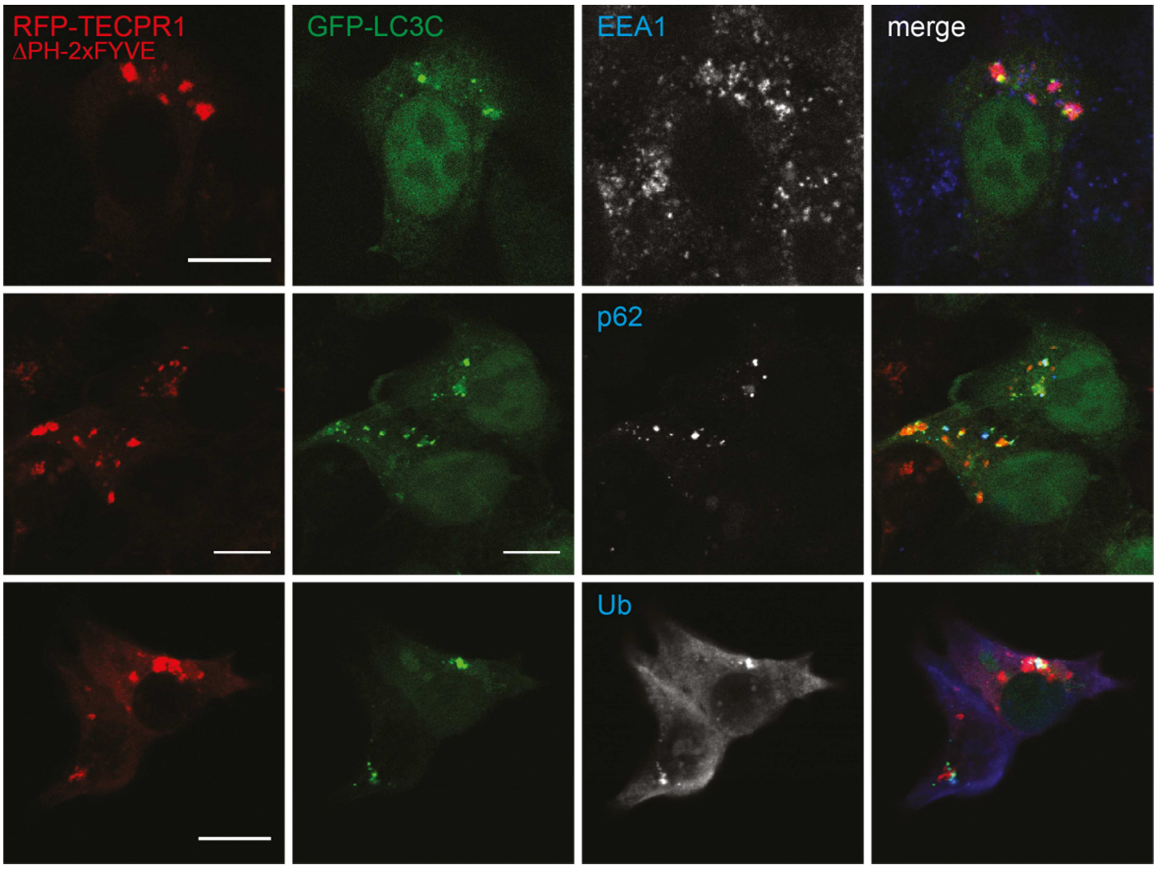
RFP-TECPR1
ΔPH-2xFYVE
GFP-LC3C
EEA1
merge
p62
Ub

Figure 40: Colocalization of markers with LC3C at TECPR1$^{\Delta PH\text{-}2xFYVE}$ structures in HEK293 cells. Confocal images of HEK293 cells that were cotransfected with RFP-TECPR1$^{\Delta PH\text{-}2xFYVE}$ and GFP-LC3C and stained for EEA1, p62, and ubiquitin (Ub) by immunofluorescence. Scale bars, 10 µm.

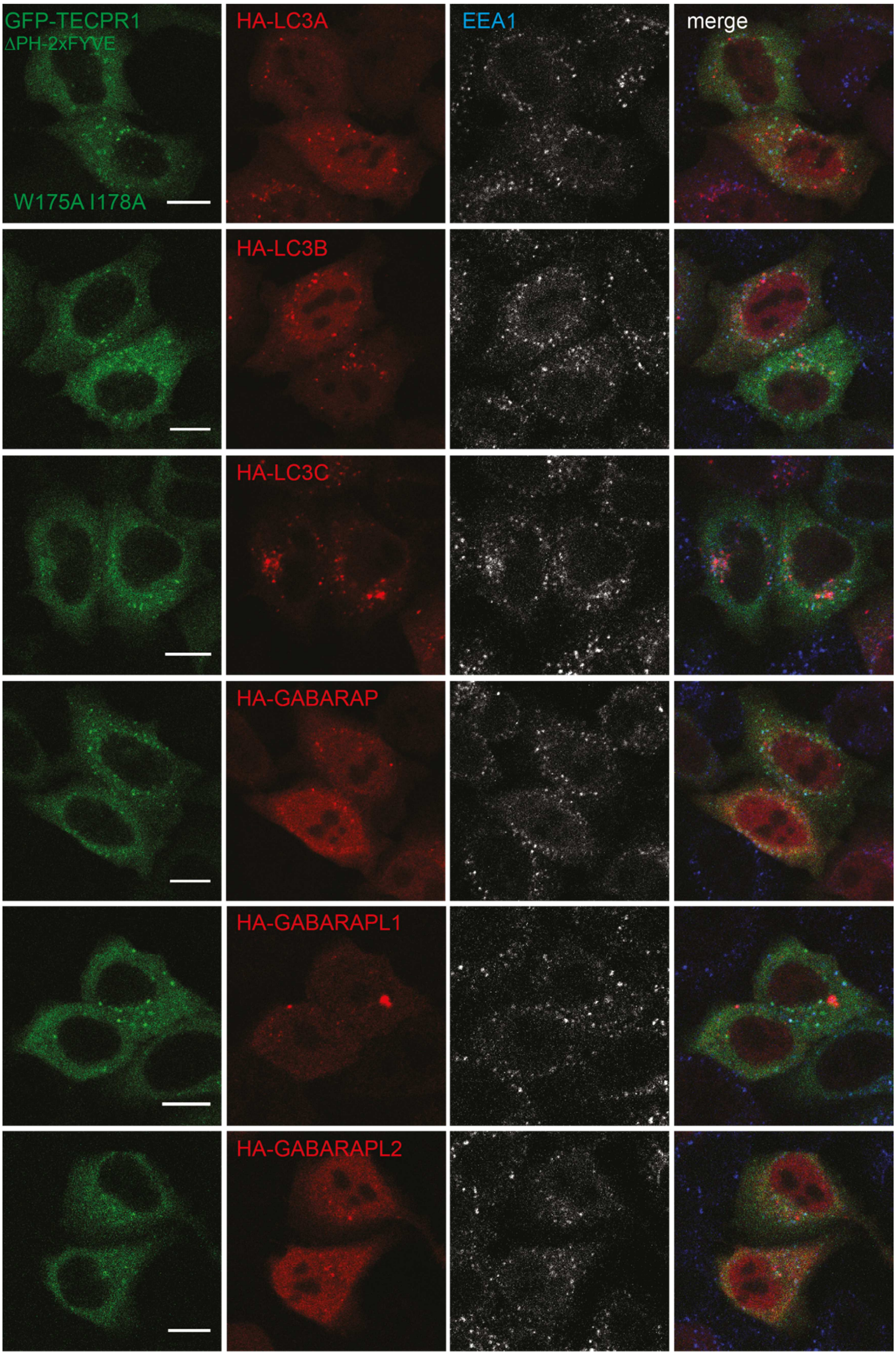
GFP-TECPR1
ΔPH-2xFYVE
W175A I178A
HA-LC3A
EEA1
merge
HA-LC3B
HA-LC3C
HA-GABARAP
HA-GABARAPL1
HA-GABARAPL2

Figure 41: Colocalization of hATG8s with TECPR1$^{\Delta PH\text{-}2xFYVE}$ W175A/I178A LIR mutant and EEA1. Confocal images of HeLa TECPR1$^{-/-}$ cells that were cotransfected with HA-tagged hATG8s and TECPR1$^{\Delta PH\text{-}2xFYVE}$ W175A/I178A and stained for EEA1 by immunofluorescence. Scale bars, 10 µm.

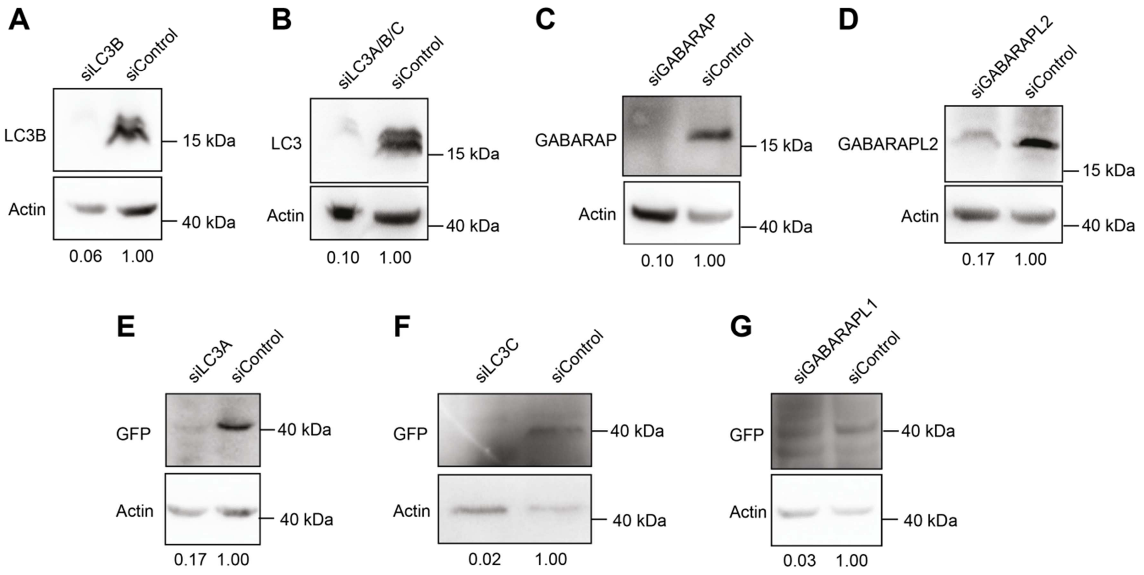
A
siLC3B
siControl
LC3B
15 kDa
Actin
40 kDa
0.06 1.00
B
siLC3A/B/C
siControl
LC3
15 kDa
Actin
40 kDa
0.10 1.00
C
siGABARAP
siControl
GABARAP
15 kDa
Actin
40 kDa
0.10 1.00
D
siGABARAPL2
siControl
GABARAPL2
15 kDa
Actin
40 kDa
0.17 1.00
E
siLC3A
siControl
GFP
40 kDa
Actin
40 kDa
0.17 1.00
F
siLC3C
siControl
GFP
40 kDa
Actin
40 kDa
0.02 1.00
G
siGABARAPL1
siControl
GFP
40 kDa
Actin
40 kDa
0.03 1.00

Figure 42: Validation of used siRNAs. **(A-D)** HeLa cells were transfected with indicated siRNAs (10 nM each), incubated for 72 hours, and immunoblotted with indicated antibodies. HeLa cells stably expressing GFP-tagged LC3A **(E)**, LC3C **(F)**, or GABARAPL1 **(G)** were transfected with indicated siRNAs (10 nM each), incubated for 72 hours, and immunoblotted with anti-GFP and anti-β-actin antibodies. hATG8 levels were normalized to β-actin as indicated below.

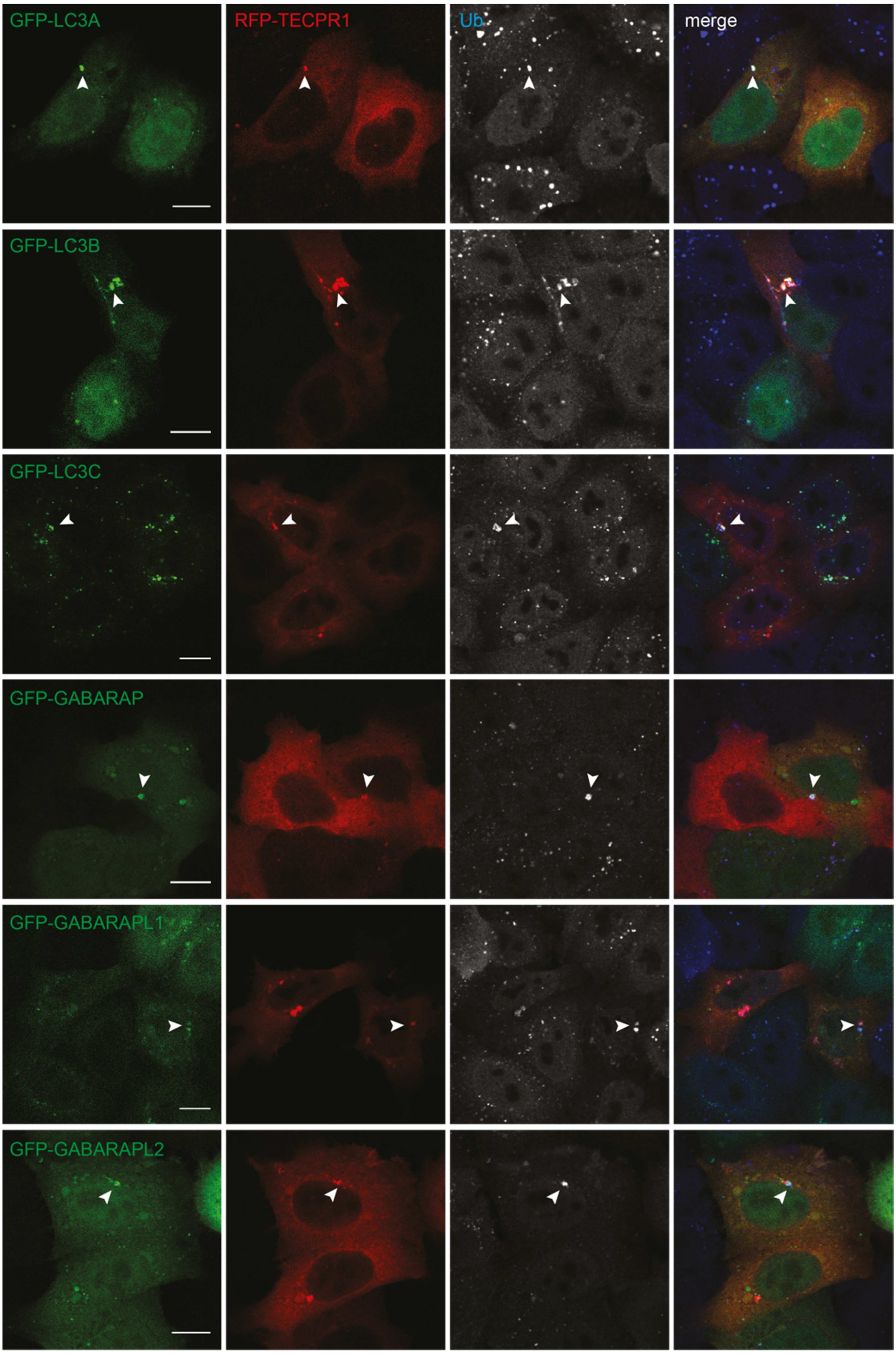
GFP-LC3A
RFP-TECPR1
Ub
merge
GFP-LC3B
GFP-LC3C
GFP-GABARAP
GFP-GABARAPL1
GFP-GABARAPL2

Figure 43: Colocalization of TECPR1 and hATG8s at protein aggregates. Confocal images of HeLa TECPR1$^{-/-}$ cells that were cotransfected with RFP-TECPR1 and GFP-tagged hATG8s. Aggregate formation was induced with puromycin for 2 hours and cells were stained for ubiquitin (Ub) by immunofluorescence. Arrows indicate colocalization of both RFP-TECPR1 and GFP-hATG8s with ubiquitin. Scale bars, 10 µm.

7 REFERENCES

Axe, E. L., Walker, S. A., Manifava, M., Chandra, P., Roderick, H. L., Habermann, A., Griffiths, G. & Ktistakis, N. T. (2008). Autophagosome formation from membrane compartments enriched in phosphatidylinositol 3-phosphate and dynamically connected to the endoplasmic reticulum. *The Journal of Cell Biology,* 182**,** 685-701.

Balderhaar, H. J. & Ungermann, C. (2013). CORVET and HOPS tethering complexes - coordinators of endosome and lysosome fusion. *J Cell Sci,* 126**,** 1307-16.

Bandyopadhyay, U., Kaushik, S., Varticovski, L. & Cuervo, A. M. (2008). The chaperone-mediated autophagy receptor organizes in dynamic protein complexes at the lysosomal membrane. *Mol Cell Biol,* 28**,** 5747-63.

Behrends, C., Sowa, M. E., Gygi, S. P. & Harper, J. W. (2010). Network organization of the human autophagy system. *Nature,* 466**,** 68-76.

Bjørkøy, G., Lamark, T., Brech, A., Outzen, H., Perander, M., Øvervatn, A., Stenmark, H. & Johansen, T. (2005). p62/SQSTM1 forms protein aggregates degraded by autophagy and has a protective effect on huntingtin-induced cell death. *The Journal of Cell Biology,* 171**,** 603-614.

Chen, D., Fan, W., Lu, Y., Ding, X., Chen, S. & Zhong, Q. (2012). A mammalian autophagosome maturation mechanism mediated by TECPR1 and the Atg12-Atg5 conjugate. *Mol Cell,* 45**,** 629-41.

Chen, Y. A. & Scheller, R. H. (2001). SNARE-mediated membrane fusion. *Nat Rev Mol Cell Biol,* 2**,** 98-106.

Cherra, S. J., Kulich, S. M., Uechi, G., Balasubramani, M., Mountzouris, J., Day, B. W. & Chu, C. T. (2010). Regulation of the autophagy protein LC3 by phosphorylation. *The Journal of Cell Biology,* 190**,** 533-539.

Coyle, J. E., Qamar, S., Rajashankar, K. R. & Nikolov, D. B. (2002). Structure of GABARAP in two conformations: implications for GABA(A) receptor localization and tubulin binding. *Neuron,* 33**,** 63-74.

Dall'armi, C., Devereaux, K. A. & Di Paolo, G. (2013). The role of lipids in the control of autophagy. *Curr Biol,* 23**,** R33-45.

David J.Gillooly, I. C. M., Margaret Lindsay, Robert Gould, Nia J.Bryant, Jean-Michel Gaullier, Robert G.Parton and Harald Stenmark (2000). Localization of phosphatidylinositol 3-phosphate in yeast and mammalian cells. *The EMBO Journal,* 19**,** 4577±4588.

Dempfle, L. (2014). Analyzing the Function of TECPR1 in Autophagy by In Vitro Reconstitution.

Diao, J., Liu, R., Rong, Y., Zhao, M., Zhang, J., Lai, Y., Zhou, Q., Wilz, L. M., Li, J., Vivona, S., Pfuetzner, R. A., Brunger, A. T. & Zhong, Q. (2015). ATG14 promotes membrane tethering and fusion of autophagosomes to endolysosomes. *Nature,* 520**,** 563-6.

Dice, J. F. (1990). Peptide sequences that target cytosolic proteins for lysosomal proteolysis. *Trends Biochem Sci,* 15**,** 305-9.

Dooley, H. C., Razi, M., Polson, H. E., Girardin, S. E., Wilson, M. I. & Tooze, S. A. (2014). WIPI2 links LC3 conjugation with PI3P, autophagosome formation, and pathogen clearance by recruiting Atg12-5-16L1. *Mol Cell,* 55**,** 238-52.

Elkin, S. R., Lakoduk, A. M. & Schmid, S. L. (2016). Endocytic pathways and endosomal trafficking: a primer. *Wien Med Wochenschr,* 166**,** 196-204.

Farre, J. C. & Subramani, S. (2004). Peroxisome turnover by micropexophagy: an autophagy-related process. *Trends Cell Biol,* 14**,** 515-23.

Fujita, N., Itoh, T., Omori, H., Fukuda, M., Noda, T. & Yoshimori, T. (2008). The Atg16L complex specifies the site of LC3 lipidation for membrane biogenesis in autophagy. *Mol Biol Cell,* 19**,** 2092-100.

Ganley, I. G., Wong, P. M., Gammoh, N. & Jiang, X. (2011). Distinct autophagosomal-lysosomal fusion mechanism revealed by thapsigargin-induced autophagy arrest. *Mol Cell,* 42**,** 731-43.

Ge, L., Melville, D., Zhang, M. & Schekman, R. (2013). The ER-Golgi intermediate compartment is a key membrane source for the LC3 lipidation step of autophagosome biogenesis. *Elife,* 2**,** e00947.

Gillooly, D. J., Raiborg, C. & Stenmark, H. (2003). Phosphatidylinositol 3-phosphate is found in microdomains of early endosomes. *Histochem Cell Biol,* 120**,** 445-53.

Hammond, G. R., Machner, M. P. & Balla, T. (2014). A novel probe for phosphatidylinositol 4-phosphate reveals multiple pools beyond the Golgi. *J Cell Biol,* 205**,** 113-26.

Hammond, G. R., Schiavo, G. & Irvine, R. F. (2009). Immunocytochemical techniques reveal multiple, distinct cellular pools of PtdIns4P and PtdIns(4,5)P(2). *Biochem J,* 422**,** 23-35.

Hanada, T., Noda, N. N., Satomi, Y., Ichimura, Y., Fujioka, Y., Takao, T., Inagaki, F. & Ohsumi, Y. (2007). The Atg12-Atg5 conjugate has a novel E3-like activity for protein lipidation in autophagy. *J Biol Chem,* 282**,** 37298-302.

Harding, T. M., Morano, K. A., Scott, S. V. & Klionsky, D. J. (1995). Isolation and characterization of yeast mutants in the cytoplasm to vacuole protein targeting pathway. *The Journal of Cell Biology,* 131**,** 591-602.

He, H., Dang, Y., Dai, F., Guo, Z., Wu, J., She, X., Pei, Y., Chen, Y., Ling, W., Wu, C., Zhao, S., Liu, J. O. & Yu, L. (2003). Post-translational modifications of three members of the human MAP1LC3 family and detection of a novel type of modification for MAP1LC3B. *J Biol Chem,* 278**,** 29278-87.

Hosokawa, N., Hara, T., Kaizuka, T., Kishi, C., Takamura, A., Miura, Y., Iemura, S., Natsume, T., Takehana, K., Yamada, N., Guan, J. L., Oshiro, N. & Mizushima, N. (2009). Nutrient-dependent mTORC1 association with the ULK1-Atg13-FIP200 complex required for autophagy. *Mol Biol Cell,* 20**,** 1981-91.

Ichimura, Y., Imamura, Y., Emoto, K., Umeda, M., Noda, T. & Ohsumi, Y. (2004). In vivo and in vitro reconstitution of Atg8 conjugation essential for autophagy. *J Biol Chem,* 279**,** 40584-92.

Ichimura, Y., Kirisako, T., Takao, T., Satomi, Y., Shimonishi, Y., Ishihara, N., Mizushima, N., Tanida, I., Kominami, E., Ohsumi, M., Noda, T. & Ohsumi, Y. (2000). A ubiquitin-like system mediates protein lipidation. *Nature,* 408**,** 488-92.

Imai, K., Hao, F., Fujita, N., Tsuji, Y., Oe, Y., Araki, Y., Hamasaki, M., Noda, T. & Yoshimori, T. (2016). Atg9A trafficking through the recycling endosomes is required for autophagosome formation. *J Cell Sci,* 129**,** 3781-3791.

Itakura, E., Kishi-Itakura, C. & Mizushima, N. (2012). The hairpin-type tail-anchored SNARE syntaxin 17 targets to autophagosomes for fusion with endosomes/lysosomes. *Cell,* 151**,** 1256-69.

Itakura, E., Kishi, C., Inoue, K. & Mizushima, N. (2008). Beclin 1 forms two distinct phosphatidylinositol 3-kinase complexes with mammalian Atg14 and UVRAG. *Mol Biol Cell,* 19**,** 5360-72.

Itakura, E. & Mizushima, N. (2010). Characterization of autophagosome formation site by a hierarchical analysis of mammalian Atg proteins. *Autophagy,* 6**,** 764-76.

Jager, S., Bucci, C., Tanida, I., Ueno, T., Kominami, E., Saftig, P. & Eskelinen, E. L. (2004). Role for Rab7 in maturation of late autophagic vacuoles. *J Cell Sci,* 117**,** 4837-48.

Jahreiss, L., Menzies, F. M. & Rubinsztein, D. C. (2008). The itinerary of autophagosomes: from peripheral formation to kiss-and-run fusion with lysosomes. *Traffic,* 9**,** 574-87.

Jeschke, A., Zehethofer, N., Lindner, B., Krupp, J., Schwudke, D., Haneburger, I., Jovic, M., Backer, J. M., Balla, T., Hilbi, H. & Haas, A. (2015). Phosphatidylinositol 4-phosphate and phosphatidylinositol 3-phosphate regulate phagolysosome biogenesis. *Proc Natl Acad Sci U S A,* 112**,** 4636-41.

Jiang, P., Nishimura, T., Sakamaki, Y., Itakura, E., Hatta, T., Natsume, T. & Mizushima, N. (2014). The HOPS complex mediates autophagosome–lysosome fusion through interaction with syntaxin 17. *Molecular Biology of the Cell,* 25**,** 1327-1337.

Joachim, J., Jefferies, H. B., Razi, M., Frith, D., Snijders, A. P., Chakravarty, P., Judith, D. & Tooze, S. A. (2015). Activation of ULK Kinase and Autophagy by GABARAP Trafficking from the Centrosome Is Regulated by WAC and GM130. *Mol Cell,* 60**,** 899-913.

Joachim, J., Razi, M., Judith, D., Wirth, M., Calamita, E., Encheva, V., Dynlacht, B. D., Snijders, A. P., O'reilly, N., Jefferies, H. B. J. & Tooze, S. A. (2017). Centriolar Satellites Control GABARAP Ubiquitination and GABARAP-Mediated Autophagy. *Curr Biol,* 27**,** 2123-2136 e7.

Juhasz, G. & Neufeld, T. P. (2006). Autophagy: A Forty-Year Search for a Missing Membrane Source. *PLOS Biology,* 4**,** e36.

Jung, C. H., Jun, C. B., Ro, S. H., Kim, Y. M., Otto, N. M., Cao, J., Kundu, M. & Kim, D. H. (2009). ULK-Atg13-FIP200 complexes mediate mTOR signaling to the autophagy machinery. *Mol Biol Cell,* 20**,** 1992-2003.

Kabeya, Y., Mizushima, N., Ueno, T., Yamamoto, A., Kirisako, T., Noda, T., Kominami, E., Ohsumi, Y. & Yoshimori, T. (2000). LC3, a mammalian homologue of yeast Apg8p, is localized in autophagosome membranes after processing. *The EMBO Journal,* 19**,** 5720-5728.

Kabeya, Y., Mizushima, N., Yamamoto, A., Oshitani-Okamoto, S., Ohsumi, Y. & Yoshimori, T. (2004). LC3, GABARAP and GATE16 localize to autophagosomal membrane depending on form-II formation. *J Cell Sci,* 117**,** 2805-12.

Kaufmann, A. (2015). In vitro reconstitution of the autophagic membrane scaffold.

Kaufmann, A., Beier, V., Franquelim, H. G. & Wollert, T. (2014). Molecular mechanism of autophagic membrane-scaffold assembly and disassembly. *Cell,* 156**,** 469-81.

Kihara, A., Kabeya, Y., Ohsumi, Y. & Yoshimori, T. (2001). Beclin-phosphatidylinositol 3-kinase complex functions at the trans-Golgi network. *EMBO Rep,* 2**,** 330-5.

Kim, J., Kundu, M., Viollet, B. & Guan, K. L. (2011). AMPK and mTOR regulate autophagy through direct phosphorylation of Ulk1. *Nat Cell Biol,* 13**,** 132-41.

Kim, J. H., Hong, S. B., Lee, J. K., Han, S., Roh, K. H., Lee, K. E., Kim, Y. K., Choi, E. J. & Song, H. K. (2015). Insights into autophagosome maturation revealed by the structures of ATG5 with its interacting partners. *Autophagy,* 11**,** 75-87.

Kimura, S., Noda, T. & Yoshimori, T. (2014). Dissection of the Autophagosome Maturation Process by a Novel Reporter Protein, Tandem Fluorescent-Tagged LC3. *Autophagy,* 3**,** 452-460.

Kirisako, T., Ichimura, Y., Okada, H., Kabeya, Y., Mizushima, N., Yoshimori, T., Ohsumi, M., Takao, T., Noda, T. & Ohsumi, Y. (2000). The reversible modification regulates the membrane-binding state of Apg8/Aut7 essential for autophagy and the cytoplasm to vacuole targeting pathway. *J Cell Biol,* 151**,** 263-76.

Klionsky, D. J. (2008). Autophagy revisited: A conversation with Christian de Duve. *Autophagy,* 4**,** 740-743.

Klionsky, D. J., Abdelmohsen, K., Abe, A., Abedin, M. J., Abeliovich, H., Acevedo Arozena, A., Adachi, H., Adams, C. M., Adams, P. D., Adeli, K., Adhihetty, P. J., Adler, S. G., Agam, G., Agarwal, R., Aghi, M. K., Agnello, M., Agostinis, P., Aguilar, P. V., Aguirre-Ghiso, J., Airoldi, E. M., Ait-Si-Ali, S., Akematsu, T., Akporiaye, E. T., Al-Rubeai, M., Albaiceta, G. M., Albanese, C., Albani, D., Albert, M. L., Aldudo, J., Algul, H., Alirezaei, M., Alloza, I., Almasan, A., Almonte-Beceril, M., Alnemri, E. S., Alonso, C., Altan-Bonnet, N., Altieri, D. C., Alvarez, S., Alvarez-Erviti, L., Alves, S., Amadoro, G., Amano, A., Amantini, C., Ambrosio, S., Amelio, I., Amer, A. O., Amessou, M., Amon, A., An, Z., Anania, F. A., Andersen, S. U., Andley, U. P., Andreadi, C. K., Andrieu-Abadie, N., Anel, A., Ann, D. K., Anoopkumar-Dukie, S., Antonioli, M., Aoki, H., Apostolova, N., Aquila, S., Aquilano, K., Araki, K., Arama, E., Aranda, A., Araya, J., Arcaro, A., Arias, E., Arimoto, H., Ariosa, A. R., Armstrong, J. L., Arnould, T., Arsov, I., Asanuma, K., Askanas, V., Asselin, E., Atarashi, R., Atherton, S. S., Atkin, J. D., Attardi, L. D., Auberger, P., Auburger, G., Aurelian, L., Autelli, R., Avagliano, L., Avantaggiati, M. L., Avrahami, L., Awale, S., Azad, N., Bachetti, T., Backer, J. M., Bae, D. H., Bae, J. S., Bae, O. N., Bae, S. H., Baehrecke, E. H., Baek, S. H., Baghdiguian, S., Bagniewska-Zadworna, A., et al. (2016). Guidelines for the use and interpretation of assays for monitoring autophagy (3rd edition). *Autophagy,* 12**,** 1-222.

Komatsu, M., Waguri, S., Ueno, T., Iwata, J., Murata, S., Tanida, I., Ezaki, J., Mizushima, N., Ohsumi, Y., Uchiyama, Y., Kominami, E., Tanaka, K. & Chiba, T. (2005). Impairment of starvation-induced and constitutive autophagy in Atg7-deficient mice. *J Cell Biol,* 169**,** 425-34.

Kremer, J. R., Mastronarde, D. N. & Mcintosh, J. R. (1996). Computer visualization of three-dimensional image data using IMOD. *J Struct Biol,* 116**,** 71-6.

Kukulski, W., Schorb, M., Welsch, S., Picco, A., Kaksonen, M. & Briggs, J. A. (2012). Precise, correlated fluorescence microscopy and electron tomography of lowicryl sections using fluorescent fiducial markers. *Methods Cell Biol,* 111**,** 235-57.

Kuma, A., Hatano, M., Matsui, M., Yamamoto, A., Nakaya, H., Yoshimori, T., Ohsumi, Y., Tokuhisa, T. & Mizushima, N. (2004). The role of autophagy during the early neonatal starvation period. *Nature,* 432**,** 1032-6.

Kuznetsov, S. A. & Gelfand, V. I. (1987). 18 kDa microtubule-associated protein: identification as a new light chain (LC-3) of microtubule-associated protein 1 (MAP-1). *FEBS Lett,* 212**,** 145-8.

Lamb, C. A., Nuhlen, S., Judith, D., Frith, D., Snijders, A. P., Behrends, C. & Tooze, S. A. (2016). TBC1D14 regulates autophagy via the TRAPP complex and ATG9 traffic. *EMBO J,* 35**,** 281-301.

Landajuela, A., Hervas, J. H., Anton, Z., Montes, L. R., Gil, D., Valle, M., Rodriguez, J. F., Goni, F. M. & Alonso, A. (2016). Lipid Geometry and Bilayer Curvature Modulate LC3/GABARAP-Mediated Model Autophagosomal Elongation. *Biophys J,* 110**,** 411-22.

Le Guerroué, F., Eck, F., Jung, J., Starzetz, T., Mittelbronn, M., Kaulich, M. & Behrends, C. (2017). Autophagosomal Content Profiling Reveals an LC3C-Dependent Piecemeal Mitophagy Pathway. *Molecular Cell,* 68**,** 786-796.e6.

Legesse-Miller, A., Sagiv, Y., Porat, A. & Elazar, Z. (1998). Isolation and characterization of a novel low molecular weight protein involved in intra-Golgi traffic. *J Biol Chem,* 273**,** 3105-9.

Li, M., Hou, Y., Wang, J., Chen, X., Shao, Z. M. & Yin, X. M. (2011). Kinetics comparisons of mammalian Atg4 homologues indicate selective preferences toward diverse Atg8 substrates. *J Biol Chem,* 286**,** 7327-38.

Liu, X., Li, Y., Wang, X., Xing, R., Liu, K., Gan, Q., Tang, C., Gao, Z., Jian, Y., Luo, S., Guo, W. & Yang, C. (2017). The BEACH-containing protein WDR81 coordinates p62 and LC3C to promote aggrephagy. *J Cell Biol*.

Longatti, A., Lamb, C. A., Razi, M., Yoshimura, S., Barr, F. A. & Tooze, S. A. (2012). TBC1D14 regulates autophagosome formation via Rab11- and ULK1-positive recycling endosomes. *J Cell Biol,* 197**,** 659-75.

Madjo, U., Leymarie, O., Fremont, S., Kuster, A., Nehlich, M., Gallois-Montbrun, S., Janvier, K. & Berlioz-Torrent, C. (2016). LC3C Contributes to Vpu-Mediated Antagonism of BST2/Tetherin Restriction on HIV-1 Release through a Non-canonical Autophagy Pathway. *Cell Rep,* 17**,** 2221-2233.

Mancias, J. D. & Kimmelman, A. C. (2016). Mechanisms of Selective Autophagy in Normal Physiology and Cancer. *J Mol Biol,* 428**,** 1659-80.

Mann, S. S. & Hammarback, J. A. (1994). Molecular characterization of light chain 3. A microtubule binding subunit of MAP1A and MAP1B. *J Biol Chem,* 269**,** 11492-7.

Mcewan, D. G., Popovic, D., Gubas, A., Terawaki, S., Suzuki, H., Stadel, D., Coxon, F. P., Miranda De Stegmann, D., Bhogaraju, S., Maddi, K., Kirchof, A., Gatti, E., Helfrich, M. H., Wakatsuki, S., Behrends, C., Pierre, P. & Dikic, I. (2015). PLEKHM1 regulates autophagosome-lysosome fusion through HOPS complex and LC3/GABARAP proteins. *Mol Cell,* 57**,** 39-54.

Mizushima, N., Kuma, A., Kobayashi, Y., Yamamoto, A., Matsubae, M., Takao, T., Natsume, T., Ohsumi, Y. & Yoshimori, T. (2003). Mouse Apg16L, a novel WD-repeat protein, targets to the autophagic isolation membrane with the Apg12-Apg5 conjugate. *J Cell Sci,* 116**,** 1679-88.

Mizushima, N., Levine, B., Cuervo, A. M. & Klionsky, D. J. (2008). Autophagy fights disease through cellular self-digestion. *Nature,* 451**,** 1069-75.

Mizushima, N., Noda, T., Yoshimori, T., Tanaka, Y., Ishii, T., George, M. D., Klionsky, D. J., Ohsumi, M. & Ohsumi, Y. (1998). A protein conjugation system essential for autophagy. *Nature,* 395**,** 395-8.

Mizushima, N., Yamamoto, A., Matsui, M., Yoshimori, T. & Ohsumi, Y. (2004). In vivo analysis of autophagy in response to nutrient starvation using transgenic mice expressing a fluorescent autophagosome marker. *Mol Biol Cell,* 15**,** 1101-11.

Moreau, K., Ravikumar, B., Renna, M., Puri, C. & Rubinsztein, D. C. (2011). Autophagosome precursor maturation requires homotypic fusion. *Cell,* 146**,** 303-17.

Nair, U., Yen, W. L., Mari, M., Cao, Y., Xie, Z., Baba, M., Reggiori, F. & Klionsky, D. J. (2012). A role for Atg8-PE deconjugation in autophagosome biogenesis. *Autophagy,* 8**,** 780-93.

Nakatogawa, H., Ichimura, Y. & Ohsumi, Y. (2007). Atg8, a ubiquitin-like protein required for autophagosome formation, mediates membrane tethering and hemifusion. *Cell,* 130**,** 165-78.

Nakatogawa, H. & Ohsumi, Y. (2012). SDS-PAGE techniques to study ubiquitin-like conjugation systems in yeast autophagy. *Methods Mol Biol,* 832**,** 519-29.

Nemos, C., Mansuy, V., Vernier-Magnin, S., Fraichard, A., Jouvenot, M. & Delage-Mourroux, R. (2003). Expression of gec1/GABARAPL1 versus GABARAP mRNAs in human: predominance of gec1/GABARAPL1 in the central nervous system. *Brain Res Mol Brain Res,* 119**,** 216-9.

Nguyen, T. N., Padman, B. S., Usher, J., Oorschot, V., Ramm, G. & Lazarou, M. (2016). Atg8 family LC3/GABARAP proteins are crucial for autophagosome-lysosome fusion but not autophagosome formation during PINK1/Parkin mitophagy and starvation. *J Cell Biol*.

Nishimura, T., Tamura, N., Kono, N., Shimanaka, Y., Arai, H., Yamamoto, H. & Mizushima, N. (2017). Autophagosome formation is initiated at phosphatidylinositol synthase-enriched ER subdomains. *EMBO J*.

Noda, N. N., Kumeta, H., Nakatogawa, H., Satoo, K., Adachi, W., Ishii, J., Fujioka, Y., Ohsumi, Y. & Inagaki, F. (2008). Structural basis of target recognition by Atg8/LC3 during selective autophagy. *Genes Cells,* 13**,** 1211-8.

Ogawa, M., Yoshikawa, Y., Kobayashi, T., Mimuro, H., Fukumatsu, M., Kiga, K., Piao, Z., Ashida, H., Yoshida, M., Kakuta, S., Koyama, T., Goto, Y., Nagatake, T., Nagai, S., Kiyono, H., Kawalec, M., Reichhart, J. M. & Sasakawa, C. (2011). A Tecpr1-dependent selective autophagy pathway targets bacterial pathogens. *Cell Host Microbe,* 9**,** 376-89.

Orsi, A., Razi, M., Dooley, H. C., Robinson, D., Weston, A. E., Collinson, L. M. & Tooze, S. A. (2012). Dynamic and transient interactions of Atg9 with autophagosomes, but not membrane integration, are required for autophagy. *Mol Biol Cell,* 23**,** 1860-73.

Otomo, C., Metlagel, Z., Takaesu, G. & Otomo, T. (2013). Structure of the human ATG12~ATG5 conjugate required for LC3 lipidation in autophagy. *Nat Struct Mol Biol,* 20**,** 59-66.

Pankiv, S., Clausen, T. H., Lamark, T., Brech, A., Bruun, J. A., Outzen, H., Overvatn, A., Bjorkoy, G. & Johansen, T. (2007). p62/SQSTM1 binds directly to Atg8/LC3 to facilitate degradation of ubiquitinated protein aggregates by autophagy. *J Biol Chem,* 282**,** 24131-45.

Paul-Gilloteaux, P., Heiligenstein, X., Belle, M., Domart, M.-C., Larijani, B., Collinson, L., Raposo, G. & Salamero, J. (2017). eC-CLEM: flexible multidimensional registration software for correlative microscopies. *Nat Meth,* 14**,** 102-103.

Pengo, N., Agrotis, A., Prak, K., Jones, J. & Ketteler, R. (2017). A reversible phospho-switch mediated by ULK1 regulates the activity of autophagy protease ATG4B. *Nat Commun,* 8**,** 294.

Pfisterer, S. G., Bakula, D., Frickey, T., Cezanne, A., Brigger, D., Tschan, M. P., Robenek, H. & Proikas-Cezanne, T. (2014). Lipid droplet and early autophagosomal membrane targeting of Atg2A and Atg14L in human tumor cells. *Journal of Lipid Research,* 55**,** 1267-1278.

Pickart, C. M. (2001). Mechanisms underlying ubiquitination. *Annu Rev Biochem,* 70**,** 503-33.

Ran, F. A., Hsu, P. D., Wright, J., Agarwala, V., Scott, D. A. & Zhang, F. (2013). Genome engineering using the CRISPR-Cas9 system. *Nat Protoc,* 8**,** 2281-308.

Ravikumar, B., Moreau, K., Jahreiss, L., Puri, C. & Rubinsztein, D. C. (2010). Plasma membrane contributes to the formation of pre-autophagosomal structures. *Nat Cell Biol,* 12**,** 747-57.

Rogov, V., Dotsch, V., Johansen, T. & Kirkin, V. (2014). Interactions between autophagy receptors and ubiquitin-like proteins form the molecular basis for selective autophagy. *Mol Cell,* 53**,** 167-78.

Rong, Y., Liu, M., Ma, L., Du, W., Zhang, H., Tian, Y., Cao, Z., Li, Y., Ren, H., Zhang, C., Li, L., Chen, S., Xi, J. & Yu, L. (2012). Clathrin and phosphatidylinositol-4,5-bisphosphate regulate autophagic lysosome reformation. *Nat Cell Biol,* 14**,** 924-34.

Russell, R. C., Tian, Y., Yuan, H., Park, H. W., Chang, Y.-Y., Kim, J., Kim, H., Neufeld, T. P., Dillin, A. & Guan, K.-L. (2013). ULK1 induces autophagy by phosphorylating Beclin-1 and activating VPS34 lipid kinase. *Nat Cell Biol,* 15**,** 741-750.

Saftig, P. & Klumperman, J. (2009). Lysosome biogenesis and lysosomal membrane proteins: trafficking meets function. *Nat Rev Mol Cell Biol,* 10**,** 623-35.

Sanchez-Wandelmer, J., Kriegenburg, F., Rohringer, S., Schuschnig, M., Gomez-Sanchez, R., Zens, B., Abreu, S., Hardenberg, R., Hollenstein, D., Gao, J., Ungermann, C., Martens, S., Kraft, C. & Reggiori, F. (2017). Atg4 proteolytic activity can be inhibited by Atg1 phosphorylation. *Nat Commun,* 8**,** 295.

Schindelin, J., Arganda-Carreras, I., Frise, E., Kaynig, V., Longair, M., Pietzsch, T., Preibisch, S., Rueden, C., Saalfeld, S., Schmid, B., Tinevez, J. Y., White, D. J., Hartenstein, V., Eliceiri, K., Tomancak, P. & Cardona, A. (2012). Fiji: an open-source platform for biological-image analysis. *Nat Methods,* 9**,** 676-82.

Scholz, J., Besir, H., Strasser, C. & Suppmann, S. (2013). A new method to customize protein expression vectors for fast, efficient and background free parallel cloning. *BMC Biotechnol,* 13**,** 12.

Sengupta, S., Peterson, T. R. & Sabatini, D. M. (2010). Regulation of the mTOR complex 1 pathway by nutrients, growth factors, and stress. *Molecular cell,* 40**,** 310-322.

Shpilka, T. W., H.; Pietrokovski, S.; Elazar, Z. (2011). Atg8: an autophagy-related ubiquitin-like protein family. *Genome Biology*.

Shvets, E., Abada, A., Weidberg, H. & Elazar, Z. (2011). Dissecting the involvement of LC3B and GATE-16 in p62 recruitment into autophagosomes. *Autophagy,* 7**,** 683-688.

Sou, Y. S., Waguri, S., Iwata, J., Ueno, T., Fujimura, T., Hara, T., Sawada, N., Yamada, A., Mizushima, N., Uchiyama, Y., Kominami, E., Tanaka, K. & Komatsu, M. (2008). The Atg8 conjugation system is indispensable for proper development of autophagic isolation membranes in mice. *Mol Biol Cell,* 19**,** 4762-75.

Sridhar, S., Patel, B., Aphkhazava, D., Macian, F., Santambrogio, L., Shields, D. & Cuervo, A. M. (2013). The lipid kinase PI4KIIIbeta preserves lysosomal identity. *EMBO J,* 32**,** 324-39.

Stadel, D., Millarte, V., Tillmann, K. D., Huber, J., Tamin-Yecheskel, B. C., Akutsu, M., Demishtein, A., Ben-Zeev, B., Anikster, Y., Perez, F., Dotsch, V., Elazar, Z., Rogov, V., Farhan, H. &

Behrends, C. (2015). TECPR2 Cooperates with LC3C to Regulate COPII-Dependent ER Export. *Mol Cell,* 60**,** 89-104.

Suzuki, K., Kubota, Y., Sekito, T. & Ohsumi, Y. (2007). Hierarchy of Atg proteins in pre-autophagosomal structure organization. *Genes Cells,* 12**,** 209-18.

Szalai, P., Hagen, L. K., Saetre, F., Luhr, M., Sponheim, M., Overbye, A., Mills, I. G., Seglen, P. O. & Engedal, N. (2015). Autophagic bulk sequestration of cytosolic cargo is independent of LC3, but requires GABARAPs. *Exp Cell Res,* 333**,** 21-38.

Thumm, M., Egner, R., Koch, B., Schlumpberger, M., Straub, M., Veenhuis, M. & Wolf, D. H. (1994). Isolation of autophagocytosis mutants of Saccharomyces cerevisiae. *FEBS Letters,* 349**,** 275-280.

Tokuyasu, K. T. (1973). A TECHNIQUE FOR ULTRACRYOTOMY OF CELL SUSPENSIONS AND TISSUES. *The Journal of Cell Biology,* 57**,** 551-565.

Tsukada, M. & Ohsumi, Y. (1993). Isolation and characterization of autophagy-defective mutants of Saccharomyces cerevisiae. *FEBS Letters,* 333**,** 169-174.

Verlhac, P., Gregoire, I. P., Azocar, O., Petkova, D. S., Baguet, J., Viret, C. & Faure, M. (2015). Autophagy receptor NDP52 regulates pathogen-containing autophagosome maturation. *Cell Host Microbe,* 17**,** 515-25.

Vicinanza, M., Korolchuk, V. I., Ashkenazi, A., Puri, C., Menzies, F. M., Clarke, J. H. & Rubinsztein, D. C. (2015). PI(5)P regulates autophagosome biogenesis. *Mol Cell,* 57**,** 219-34.

Von Muhlinen, N., Akutsu, M., Ravenhill, B. J., Foeglein, A., Bloor, S., Rutherford, T. J., Freund, S. M., Komander, D. & Randow, F. (2012). LC3C, bound selectively by a noncanonical LIR motif in NDP52, is required for antibacterial autophagy. *Mol Cell,* 48**,** 329-42.

Wang, H., Bedford, F. K., Brandon, N. J., Moss, S. J. & Olsen, R. W. (1999). GABA(A)-receptor-associated protein links GABA(A) receptors and the cytoskeleton. *Nature,* 397**,** 69-72.

Wang, H., Sun, H. Q., Zhu, X., Zhang, L., Albanesi, J., Levine, B. & Yin, H. (2015). GABARAPs regulate PI4P-dependent autophagosome:lysosome fusion. *Proc Natl Acad Sci U S A,* 112**,** 7015-20.

Weidberg, H., Shpilka, T., Shvets, E., Abada, A., Shimron, F. & Elazar, Z. (2011). LC3 and GATE-16 N termini mediate membrane fusion processes required for autophagosome biogenesis. *Dev Cell,* 20**,** 444-54.

Weidberg, H., Shvets, E., Shpilka, T., Shimron, F., Shinder, V. & Elazar, Z. (2010). LC3 and GATE-16/GABARAP subfamilies are both essential yet act differently in autophagosome biogenesis. *The EMBO Journal,* 29**,** 1792-1802.

Wild, P., Farhan, H., Mcewan, D. G., Wagner, S., Rogov, V. V., Brady, N. R., Richter, B., Korac, J., Waidmann, O., Choudhary, C., Dötsch, V., Bumann, D. & Dikic, I. (2011). Phosphorylation of the Autophagy Receptor Optineurin Restricts Salmonella Growth. *Science,* 333**,** 228-233.

Wild, P., Mcewan, D. G. & Dikic, I. (2014). The LC3 interactome at a glance. *J Cell Sci,* 127**,** 3-9.

Wilkinson, D. S., Jariwala, J. S., Anderson, E., Mitra, K., Meisenhelder, J., Chang, J. T., Ideker, T., Hunter, T., Nizet, V., Dillin, A. & Hansen, M. (2015). Phosphorylation of LC3 by the Hippo kinases STK3/STK4 is essential for autophagy. *Mol Cell,* 57**,** 55-68.

Yamamoto, H., Kakuta, S., Watanabe, T. M., Kitamura, A., Sekito, T., Kondo-Kakuta, C., Ichikawa, R., Kinjo, M. & Ohsumi, Y. (2012). Atg9 vesicles are an important membrane source during early steps of autophagosome formation. *J Cell Biol,* 198**,** 219-33.

Young, A. R., Chan, E. Y., Hu, X. W., Kochl, R., Crawshaw, S. G., High, S., Hailey, D. W., Lippincott-Schwartz, J. & Tooze, S. A. (2006). Starvation and ULK1-dependent cycling of mammalian Atg9 between the TGN and endosomes. *J Cell Sci,* 119**,** 3888-900.

Yu, L., Mcphee, C. K., Zheng, L., Mardones, G. A., Rong, Y., Peng, J., Mi, N., Zhao, Y., Liu, Z., Wan, F., Hailey, D. W., Oorschot, V., Klumperman, J., Baehrecke, E. H. & Lenardo, M. J. (2010). Termination of autophagy and reformation of lysosomes regulated by mTOR. *Nature,* 465**,** 942-6.

8 ACKNOWLEDGEMENTS

I would like to thank everyone who made this thesis possible and successful.

First of all, I want to thank my supervisor Dr. Thomas Wollert for his exceptional support during my PhD. Particularly, I want to thank him for providing me challenges I would have probably not taken of my own accord, like presenting my work at a symposium already in my first year or undergo a 3-month training at the EMBL, Heidelberg. Moreover, I enjoyed the scientific discussions with him, which usually ended in constructive ideas.

I also want to thank Prof. Stefan Jentsch, who at the beginning of my PhD kindly agreed to be my official supervisor before he sadly passed away too soon. In addition, I want to thank Prof. Ulrich Hartl for being second reviewer of this thesis. Thanks also to my TAC members, especially Julia von Blume and Christian Behrends, who showed great interest in my project, gave useful advice, and were always willing to collaborate with our lab.

Furthermore, I would like to thank my (former) lab members for the scientific exchange as well as for their company during lunch breaks and other work-(un)related activities. Particularly, I want to thank Viola Beier, who lightened my workload, so that I had more time to analyze data and plan experiments. Moreover, I want to thank Anna Kaufmann for her excellent supervision during my master thesis, which made a smooth transition into my PhD possible.

I would also like to thank the Biochemistry Core and Imaging Facility of the Max Planck Institute of Biochemistry in Martinsried as well as the Electron Microscopy Core Facility of the EMBL in Heidelberg for providing their equipment and scientific services.

Finally, I am grateful to my family and friends who always supported me, with special thanks to Andi, who always encouraged me with his positive attitude.